Home Institution: Università degli Studi di Padova

Department of Pharmaceutical and Pharmacological Sciences

Ph.D. COURSE IN: PHARMACOLOGICAL SCIENCES
CURRICULUM: PHARMACOLOGY, TOXICOLOGY AND THERAPEUTICS
XXXII SERIES

Endoplasmic reticulum homeostasis, lipid droplets biogenesis and autophagy in *Drosophila* models of Hereditary Spastic Paraplegia

Thesis written with the financial contribution of Associazione La Nostra Famiglia - IRCCS Eugenio Medea.

Coordinator: Prof. Nicola Ferri
Supervisor: Dott.ssa Genny Orso

Ph.D. student: Barbara Napoli

1. INDEX

ABSTRACT

Mutations in the *SPG4* gene (*Spastin*), *SPG31* gene (*REEP1*) and SPG3A gene (*Atlastin*) are the most common causes of autosomal dominant Hereditary Spastic Paraplegia (HSP), a complex genetic disorder characterized by the axonal degeneration of corticospinal tracts. Interactions between REEP1, Atlastin and Spastin, have a crucial role in modifying ER architecture and lipid metabolism, two important emerging cellular aspects potentially underlying HSP pathological mechanism. The role of lipid droplets (LDs) in HSP has been highlighted by recent evidence that proteins such as Seipin/SPG17, Erlin2/SPG18, Atlastin/SPG3A, Spartin/SPG20, REEP1/SPG31 and Spastin/SPG4 affect cellular LD turnover. Moreover, the authophagy/lysosomes degradative pathway is another important process that crosses LD and ER homeostasis. Different studies have shown that Spastin modulates the endosomal tubule fission and has a crucial role in the tethering of cellular organelles such as LDs, endosomes and peroxisomes. The depletion of spastin alters the ER-endosome contacts, impairs endosomal tubule fission and induces lysosome abnormalities. Furthermore, spastin reduces the LD-peroxisome contacts and affects the fatty acid (FA) trafficking from LDs to peroxisomes. In spite of these findings, the relationship between ER homeostasis and the lipid pathway, with the related implications for neuronal dysfunction in HSP, still remains unknown.

In this work we used the common fruit fly, *Drosophila melanogaster,* as model organism to perform *in vivo* studies aimed at describing ReepA function in endoplasmic reticulum homeostasis and morphology and, establishing the role of ReepA and Dspastin in LD biogenesis and autophagy. In order to investigate these pathways, we manipulated the expression of *Drosophila* REEPA and Spastin by using loss of function alleles and RNA interference approaches. Since immunostaining experiments have shown that loss of ReepA function modifies ER morphology. We investigated the role of ReepA in ER homeostasis, quantifying the mRNA levels of the main genes involved in unfolded protein response (UPR). The results indicate that absence of ReepA triggers a selective activation of the Ire1 and Atf6 branches of UPR. *Drosophila* lacking ReepA exhibit locomotor dysfunction and shortened lifespan and display a decrease in LD number and size in nerves and muscles phenotypes reminiscent of those caused by Dspastin-RNAi. In order to understand the link between ER homeostasis and LD turnover, we quantified the relative mRNA expression of genes (*Mino* and *Mdy*) involved in lipid metabolism. Both HSP models displayed a reduction of *Mino* and *Mdy* mRNA levels suggesting a role for Spastin and ReepA in LD biogenesis. Moreover, we investigated the formation of early and late autophagosomes, lysosomes and autolysosomes using fluorescent monomeric tandem constructs that allow the visualization of autophagosomes and

lysosomes *in vivo*. Loss of ReepA and Spastin function impaired the autophagic flux, increasing the number of early/immature and late autophagosomes. Moreover, we showed that loss of DSpastin and ReepA function produces larger lysosomes, consistent with the studies in mammalian models. We also found that naringenin, a flavonoid that possesses strong antioxidant activity and is considered a neuroprotective phytochemical, is able to rescue the cellular phenotypes, the lifespan and locomotor disability associated with loss of ReepA and Dspastin-RNAi. Our data highlight the importance of ER homeostasis in nervous system functionality and in HSP neurodegenerative mechanisms opening new avenues for HSP treatment.

RIASSUNTO

Mutazioni dei geni SPG4 (Spastin), SPG31 (REEP1) e SPG3A (Atlastin) rappresentano le cause più comuni di forma autosomica dominante di Paraplegia Spastica Ereditaria (HSP), un disturbo genetico complesso caratterizzato dalla degenerazione degli assoni delle vie corticospinali. Le interazioni tra le proteine REEP1, Atlastina e Spastina hanno un ruolo cruciale nella modulazione della struttura del reticolo endoplasmatico (RE) e nel metabolismo lipidico, due importanti aspetti cellulari implicati nel meccanismo patologico delle HSP. Studi recenti suggeriscono un ruolo dei lipid droplets (LDs) nelle HSP e mostrano che le proteine Seipin / SPG17, Erlin2 / SPG18, Atlastin/ SPG3A, Spartin / SPG20, REEP1 / SPG31 e Spastin / SPG4 influenzano il turnover cellulare degli LDs. L'autofagia potrebbe essere un meccanismo di interconnessione tra il metabolismo lipidico e l'omeostasi del RE. Recentemente alcuni studi hanno dimostrato che Spastina modula la fissione dei tubuli endosomiali e i contatti tra i vari organelli cellulari come LDs, endosomi e perossisomi. L'assenza della proteina spastina, infatti, diminuisce il contatto tra endosomi-RE e LDs-perossisomi, altera il processo di fissione endosomiale, induce alterazioni morfologiche nei lisosomi ed altera il trasporto degli acidi grassi dai LDs ai perossisomi e viceversa. Tuttavia, la precisa correlazione tra l'omeostasi del RE ed il metabolismo lipidico e il ruolo nella disfunzione neuronale nelle HSP è ancora sconosciuta.

In questo lavoro, abbiamo usato come organismo modello *Drosophila melanogaster* ed eseguito studi *in vivo* per descrivere la funzione della proteina ReepA nella morfologia e funzione del RE e per stabilire il ruolo di ReepA e Dspastina nella biogenesi dei LDs e nell'autofagia. Al fine di investigare questi meccanismi abbiamo manipolato geneticamente l'espressione delle due proteine di *Drosophila* tramite l'interference dell'RNA e loss of function della proteina. Gli esperimenti hanno mostrato che l'assenza di ReepA modifica la morfologia del RE. Successivamente abbiamo investigato il ruolo di ReepA nell'omeostasi del RE quantificando i livelli di mRNA dei principali geni coinvolti nella risposta allo stress del RE (UPR). I risultati mostrano che l'assenza della proteina ReepA innesca una risposta selettiva attivando solo due vie dell'UPR rispettivamente Ire1 e Atf6. Nel modello di *Drosophila* l'assenza di ReepA causa disfunzioni locomotorie, una diminuzione della vita media e una riduzione del numero e della dimensione dei LDs sia nel tessuto nervoso che in quello muscolare. Questi fenotipi sono simili a quelli già dimostrati nel modello di Dspastina-RNAi. Per comprendere la correlazione tra l'omeostasi del RE e turnover degli LD, abbiamo quantificato i livelli di mRNA di Mino e Mdy, principali geni coinvolti nel metabolismo lipidico. Entrambi i modelli di HSP mostrano una riduzione della loro espressione suggerendo un ruolo di spastina e ReepA nella biogenesi dei LDs.

Inoltre, abbiamo valutato il processo autofagico in dettaglio analizzando la formazione degli autofagosomi, lisosomi e autolisosomi tramite l'utilizzo di linee transgeniche che marcano queste strutture autofagiche. L'assenza di ReepA e Spastina induce un'alterazione dell'autofagia causando un aumento del numero di autofagosomi immaturi e tardivi. La down-regolazione di DSpastina e ReepA produce lisosomi più grandi, come sui modelli di mammiferi. Abbiamo anche osservato che la naringenina, un flavonoide che possiede una forte attività antiossidante e neuroprotettiva, prolunga la vita media, migliora l'attività locomotoria e reverte i fenotipi cellulari nei due modelli di loss of function di ReepA e Dspastina. I nostri dati evidenziano l'importanza dell'omeostasi del RE nella funzionalità del sistema nervoso e nei meccanismi neurodegenerativi dell'HSP ed aprono così nuove strategie per il trattamento delle paraplegie spastiche ereditarie.

1. INTRODUCTION

1.1 Hereditary Spastic Paraplegia (HSP)

Hereditary Spastic Paraplegia (HSP) is a genetically heterogeneous group of neurodegenerative diseases characterized by progressive spasticity and weakness at the lower limbs. Clinically the HSP has been classified as “pure” (or “uncomplicated”) and “complex” (or “complicated”) forms. The main clinical features of pure HSP are hyperreflexia, hypertonicity or bilateral spasticity of the legs, bladder dysfunction and vibratory sense impairment. Complicated forms show also additional neurological or extraneurological symptoms: mental retardation, cerebellar ataxia, peripheral neuropathy, epilepsy, retinopathy, optic atrophy, dystonia and parkinsonism (Boutry et al., 2019; Lavie et al., 2017; McDermott and Shaw, 2002). Genetically, the HSP can be divided in autosomal dominant (AD), autosomal recessive (AR), and X-linked forms. To date, 76 loci have been mapped on different chromosomes and 64 corresponding genes (the Spastic Gene or SPG genes) (Parodi et al., 2017) (Table 1).

The common pathological feature of HSP is the retrograde axonal degeneration of the distal portions of corticospinal and spinocerebellar tracts, corresponding to the longest motor and sensor axons of the central nervous system (CNS). Although we still know little about the mechanisms related to neurodegeneration in complicated forms, the functional studies carried out in recent years on HSP-linked genes have suggested that alterations to intracellular trafficking may be a common element. The affected functions include lipid metabolism, active axonal transport, organelle shaping and the activities of the endolysosomal system (Boutry et al., 2019; Salinas et al., 2008) (Figure 1). Although the progress made in deciphering the pathological process underling HSP, there is still no specific cure to prevent or slow down neuronal degeneration or dysfunction. To date, the treatments for HSP are based on antispastic drugs, botulinum toxin and physiotherapy (Bellofatto et al., 2019; Fink, 2013).

Table I. Genetic classification of Hereditary Spastic Paraplegia

Locus	Chromosome	Gene	Inheritance	Phenotype	Locus	Chromosome	Gene	Inheritance	Phenotype
SPG1	Xq28	L1CAM	X-linked	Complicated	SPG42	3q25.31	SLC33A1	AD	Pure
SPG2	Xq22.2	PLP1	X-linked	Complicated	SPG43	19q12	C19orf12	AR	Complicated
SPG3A	14q22.1	ATL1	AD /AH	Both	SPG44	1q42.13	GJC2	AR	Complicated
SPG4	2p22.3	SPAST	AD	Both	SPG45/SPG65	10q24.33	NT5C2	AR	Complicated
SPG5A	8q21.3	CYP7B1	AR	Both	SPG46	9p13.3	GBA2	AR	Complicated
SPG6	15q11.1	NIPA1	AD	Both	SPG47	1p13.2	AP4B1	AR	Complicated
SPG7	16q24.3	paraplegin	AD/AH	Both	SPG48	7p22.1	AP5Z1	AR	Complicated
SPG8	8q24.13	WASHC5	AD	Both	SPG49	14q32.31	TECPR2	AR	Complicated
SPG9	10q24.1	ALDH18A1	AD/AH	Both	SPG50	7q22.1	AP4M1	AR	Complicated
SPG10	12q13	KIF5A	AD	Both	SPG51	15q21.2	AP4E1	AR	Complicated
SPG11	15q21.1	Spactasin	AR	Both	SPG52	14q12	AP4S1	AR	Complicated
SPG12	19q13.32	RTN2	AD	Pure	SPG53	8p22	VPS37A	AR	Complicated
SPG13	2q33.1	HSPD1	AD	Pure	SPG54	8p11.23	DDHD2	AR	Complicated
SPG14	3q27-q28	Unknown	AR	Complicated	SPG55	12q24.31	C12orf65	AR	Complicated
SPG15	14q24.1	ZFYVE26	AR	Both	SPG56	4q25	CYP2U1	AR	Both
SPG16	Xq11.2	Unknown	X-linked	Both	SPG57	3q12.2	TFG	AR	Both
SPG17	11q13	BSCL2	AD	Complicated	SPG58	17p13.2	KIF1C	AR	Both
SPG18/37	8p11.2	ERLIN2	AD/AH	Complicated	SPG59	15q21.2	USP8	AR	Complicated
SPG19	9q33-q34	Unknown	AD	Pure	SPG60	3p22.2	WDR48	AR	Complicated
SPG20	13q12.3	SPART	AR	Complicated	SPG61	16p12.3	ARL6IP1	AR	Pure
SPG21	15q22.31	masparadin	AR	Complicated	SPG62	10q24.31	ERLIN1	AR	Complicated
SPG22	Xq13.2	SLC16A2	X-linked	Complicated	SPG63	1p13.3	AMPD2	AR	Complicated
SPG23	1q32.1	DSTYK	AR	Complicated	SPG64	10q24.1	ENTPD1	AR	Complicated
SPG24	13q14	Unknown	AR	Pure	SPG66	5q32	ARSI	AR	Complicated
SPG25	6q23-24.1	Unknown	AR	Complicated	SPG67	2q33.1	PGAP1	AR	Complicated
SPG26	12p13.3	B4GALNT1	AR	Complicated	SPG68	11q13.1	FLRT1	AR	Complicated
SPG27	10q22.1-q2	Unknown	AR	Both	SPG69	1q41	RAB3GAP2	AR	Complicated
SPG28	14q22.	DDHD1	AR	Both	SPG70	12q13.3	MARS	AR	Complicated
SPG29	1p31.1-p21.1	Unknown	AD	Complicated	SPG71	5p13.3	ZFR	AR	Complicated
SPG30	2q37.3	KIF1A	AD/AH	Complicated	SPG72	5q31.2	REEP2	AD and AR	Pure
SPG31	2p11.2	REEP1	AD	Pure	SPG73	19q13.33	CPT1C	AD	Complicated
SPG32	14q12-q21	Unknown	AR	Complicated	SPG74	1q42.13	IBA57	AR	Complicated
SPG34	Xq24-q25	Unknown	X-linked	Pure	SPG75	19q13.12	MAG	AR	Complicated
SPG35	16q23.1	FA2H	AR	Complicated	SPG76	11q13.1	CAPN1	AR	Both
SPG36	12q23-q24	Unknown	AD	Complicated	SPG77	6p25.1	FARS2	AR	Both
SPG38	4p16-p15	Unknown	AD	Complicated	SPG78	1p36.13	ATP13A2	AR	Complicated
SPG39	19p13.2	PNPLA6	AR	Complicated	SPG79	4p13	UCHL1	AR	Complicated
SPG41	11p14.1-p11.2	Unknown	AD	Pure	SPOAN	11q13,2	KLC2	AR	Complicated

AD= autosomal dominant; AR= autosomal recessive; ALDH18A1= Aldehyde dehydrogenase 18 family member A1; AMPD2= Adenosine Monophosphate Deaminase 2; AP= Adaptor-Related Protein Complex; ARL6IP1=ADP Ribosylation factor like GTPase 6 Interacting Protein 1, ARSI= Arylsulfatase family member; Atl1= Atlastin-1; ATP13A2= ATPase cation transporting 13A2; B4GALNT1= Beta-1,4-N-Acetyl-Galactosaminyltransferase 1; BSCL2= Berardinelli-Seip Congenital Lipodystrophy 2; CAPN1= Calpain 1; C12orf65= Chromosome 12 Open Reading Frame 65; C19orf2= Chromosome 19 Open Reading Frame 2; CPT1C= Carnitine Palmitoyltransferase 1C; CYP7B1= Cytochrome P450 family 7 subfamily B member 1; CYP2U1= Cytochrome P450 family 2 subfamily U member 1; DDHD1/2= Domain-Containing Protein 1/2; DSTYK= Dual Serine/Threonine and Tyrosine Protein Kinase; ENTPD1= Ectonucleoside TriPhosphate Diphosphohydrolase 1; ERLIN= Endoplasmic Reticulum Lipid Raft Associated Protein; FA2H= Fatty acid 2-hydroxylase; FARS2=

Phenylalanyl-tRNA Synthetase 2; FLRT1= Fibronectin Leucine Rich Transmembrane protein 1; GBA= Glucosylceramidase Beta; GJC2= Gap Junction Protein Gamma 2 HSPD1= Heat-Shock 60-KD Protein 1; IBA57= Iron-Sulfur cluster assembly factor IBA57; KIF= kinesin heavy chain family; KLC2= Kinesin Light Chain 2; L1CAM= L1 cell adhesion molecule; MAG= Myelin associated glycoprotein; MARS= Methionyl-tRNA synthethase 1; NIPA1= Non Imprintend in Prader-Willi/Angelman syndrome 1; NT5C2= 5'-nucleotidase cytosolic II; PGAP1= Post-GPI Attachment Proteins 1; PLP= proteolipid protein; PNPLA6=patatin-like phospholipase domain containing 6; RAB3GAP2= RAB3 GTPase activating non-catalytic protein subunit 2; REEP1/2= Receptor Enhancing Expression Protein 1/; RTN2= Reticulon 2; SLC16A2= Solute Carrier Family 16 Member 2; SLC33A1= Solute Carrier Family 33 Member 1;SPART= Spartin; SPAST=Spastin; TECPR2: Tectonin Bea-Propeller Repeat Containing 2; TFG= Trafficking from Endoplasmic Reticulum to Golgi regulator; UCHL1= Ubiquitin C-terminal Hydrolase L1; USP8= Ubiquitin Specific Peptidase 8; VP37A= Vacuolar Protein Sorting 37 A; WASHc5= WASH complex subunit 5; WDR= WD repeat domain; ZFYVE26= Zinc Finger Fyve Domain containing protein 26 (Spastizin); ZFR= Zinc Finger RNA binding protein

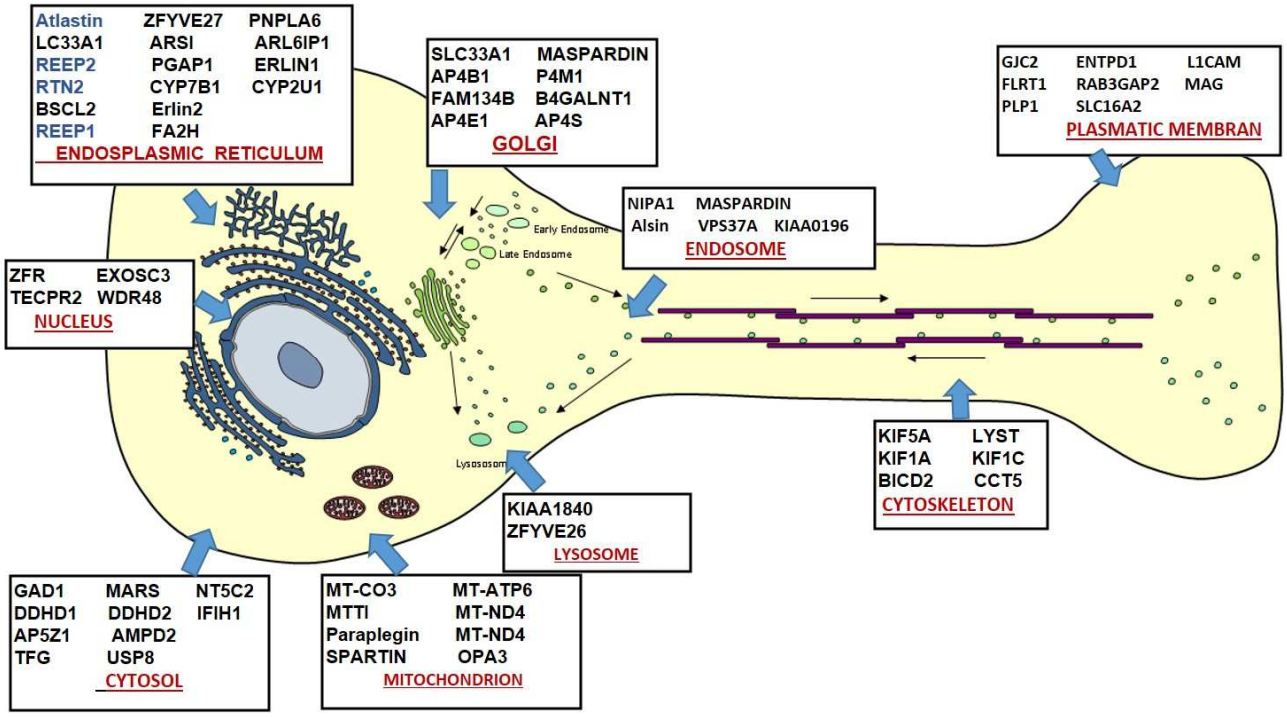

Figure 1. The Hereditary Spastic Paraplegia proteins. HSP proteins are involved in different cellular processes.

1.1.1 Receptor expression enhancing protein (REEP1) and Spastin

REEP1/SPG31, codifies for REEP1 (Receptor enhancing protein 1) and mutation in this gene is the third most common cause of autosomal dominant HSP, responsible for 6.5% of the HSP cases (Renvoisé et al., 2016; Züchner et al., 2006). Classical SPG31 variants include missense mutations and little insertions or deletions that cause a reading frameshift and produce premature stop codons. Splice site mutations and 3'-URT sequence modifications have been also reported (Beetz et al., 2008, 2013; Renvoisé et al., 2016; Richard et al., 2017b; Züchner et al., 2006). REEP1 protein belongs to the REEP/DP1/YOP1 superfamily and it is a member of endoplasmic reticulum (ER) shaping proteins family comprising six members in humans, divided structurally and functionally into

two main subgroups REEP1-4 and REEP5-6, with REEP1-4 proteins implicated in microtubule interactions with ER tubules (Figure 2).

Mutations in the *SPAST*/SPG4 gene, that encodes for spastin, are the most common cause of the disease and account for 40% of all HSP cases (Solowska and Baas, 2015). To date, spastin mutations identified include missense, nonsense and splice site mutations in different exons (Allison et al., 2017; Errico et al., 2004; Reid et al., 1999). Spastin belongs to ATPases associated with various cellular activities (AAA) protein family (Figure 3) and has two isoforms: M1 and M87. Spastin M1, is a 616 amino acid protein, spastin M87 lacks N-terminal 86 amino acids and M1 isoform is located to ER (Claudiani et al., 2005). The AAA proteins are involved in several cellular processes such as membrane trafficking, proteasome function, organelle biogenesis, and microtubule regulation (Errico et al., 2004; Salinas et al., 2007). The AAA proteins are characterized by 240 amino acid conserved P-loop NTPase domain containing Walker A and B motifs (Errico et al., 2004; Orso et al., 2005). Spastin belongs to the ATPase subfamily 7, which is characterized by p60 katanin, a microtubule-severing protein and SKD1, an endosome trafficking regulator (Errico et al., 2004). All AAA proteins show a conserved structure, one domain is located in the C-terminal part of the protein, the N-terminal is unwell characterized but encompasses the MIT (microtubule-interacting and trafficking molecules) (Errico et al., 2004).

The main function of spastin is the modulation of microtubules (MTs) dynamics by MTs severing, whereas REEP1 is an ER membrane protein primarily involved in ER shaping. REEP1 together with atlastin-1 and membrane-bound M1 isoform of spastin interact through hydrophobic hairpin domains within the tubular ER to coordinate ER shaping and microtubule interactions (Lavie et al., 2017). Mutations of REEP1 and spastin, or their absence, cause similar phenotypes such as dysregulation of lipid droplet (LD) biogenesis and aberrant lysosomal morphology. Their presence and interaction with ER membranes seem to be important to maintain a correct ER morphology and function and regulate the contact with other organelles.

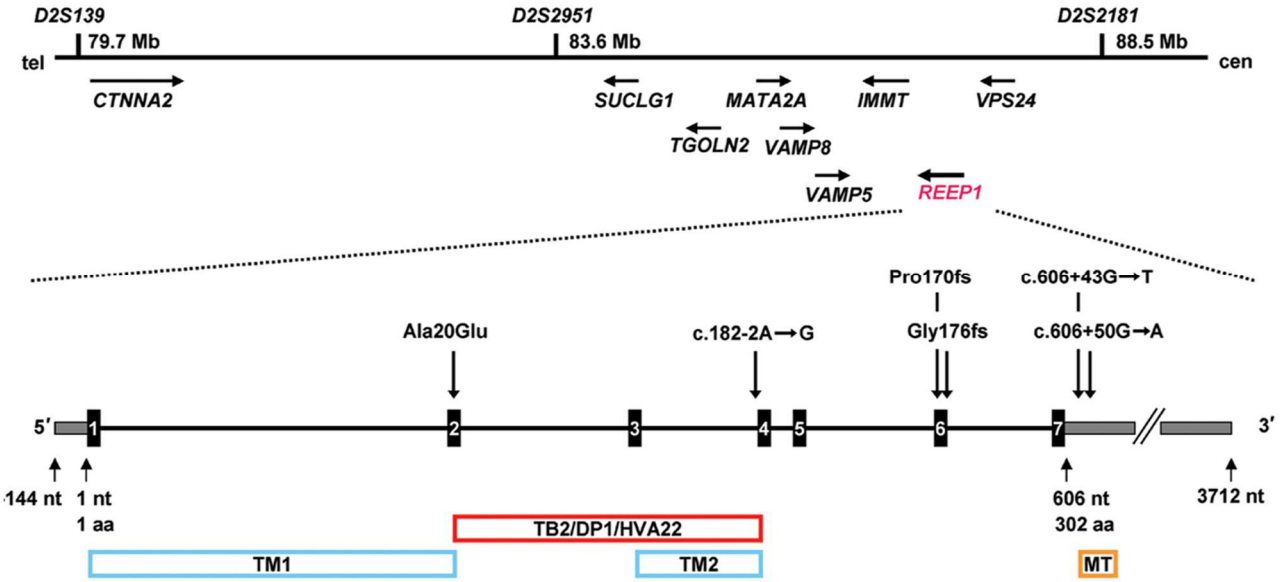

Figure 2. A schematic representation of Human REEP1(Züchner et al., 2006, image modified)

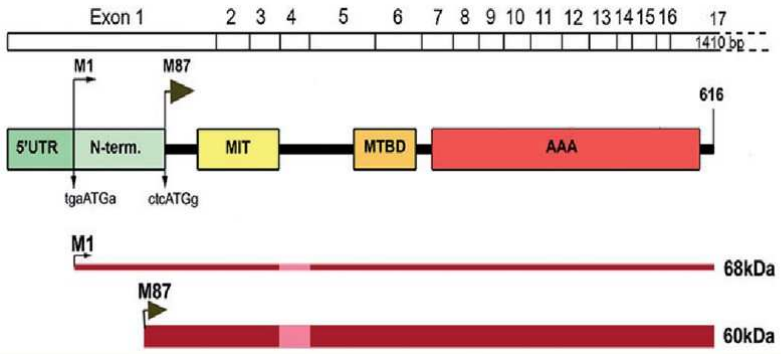

Figure 3. A schematic representation of Human Spastin (Solowska et al., 2014b, image modified)

1.2 Endoplasmic reticulum and HSP

1.2.1 ER structure and organization

The endoplasmic reticulum (ER) is a single membrane-bound organelle involved in many cellular processes including protein synthesis and transport, protein folding, lipid and steroid synthesis, carbohydrate metabolism, regulation of calcium homeostasis, detoxification, storage and action of enzymes, lipid droplet formation, and lipid metabolism (Grumati et al., 2017; Schwarz and Blower,

2016). ER can be divided in sub-compartments, each of them with specific structural and biochemical properties: the nuclear envelope (NE), a highly regulated membrane barrier that separates the nucleus from the cytoplasm, a system of flattened cisternae deputed to protein synthesis, and a peripheral tubular structure extending in to the cytoplasm to connect the cortical ER to the NE (English et al., 2009; English and Voeltz, 2013). Despite the lipid continuity between these compartments, the different composition of proteins and lipid species gives rise to specific functions for each sub domain (Figure 4) (Puhka et al., 2007, 2012; Shibata et al., 2010).

ER sheets are flat structures consisting of two lipid bilayers, covered with ribosomes involved in the synthesis and folding of membrane, luminal, and secreted proteins, whereas ER tubules are cylindrical structures (diameter ~30 nm in yeast and ~50 nm) with high membrane curvature at their cross-section. The tubular network is dynamic, and it is characterized by three-way junctions that connect individual tubules. The relative abundance of sheets or tubules changes in different cell types and is correlated to different functions of these cells (Schwarz and Blower, 2016). Pancreatic or adrenal cells that produce high levels of proteins and sterols display a peripheral ER with increased sheets, conversely neurons, muscle and epithelial cells that secrete few proteins show high level of ER tubules (Shibata et al., 2010; Terasaki et al., 2013).

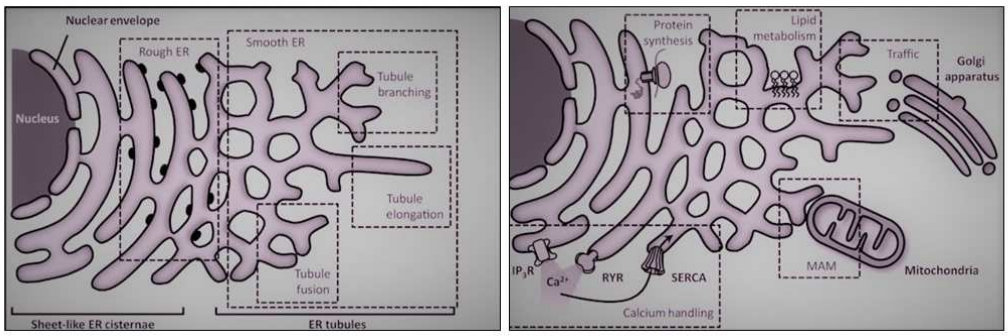

Figure 4. Image of ER structure and function (Bravo et al., 2013, image modified)

1.2.2 ER-shaping proteins in HSP

The structural organization of ER is created and maintained thanks to a continuous process of membrane remodeling governed by homotypic fusion events, tubulation and curvature rearrangements as well as cytoskeletal transport (Chen et al., 2013; Goyal and Blackstone, 2013). Some of the main players of this process are also involved in HSP. Mutations in the receptor expression-enhancing protein REEP1/SPG31 and reticulon2/SPG12, two of the main ER shaping proteins, cause autosomal dominant form of HSP. Due to their topology, these two proteins are supposed to induce high membrane curvature of the ER. It is postulated that the insertion of the two large hydrophobic domains of REEP1 and reticulon2 into the outer leaflet of the bilayer forms a

wedge that produces membrane curvature (Tolley et al., 2010; Voeltz et al., 2002; Zurek et al., 2011). In *Drosophila* the loss of reticulon and REEP1 caused expansion of ER sheets (O'Sullivan et al., 2012; Yalçın et al., 2017). Instead, to generate the three-way junctions of ER network, atlastin1, a transmembrane protein with GTPase activity which causes a dominant form of HSP (SPG3a), is required (Hu et al., 2008; Orso et al., 2009; Pendin et al., 2011). Several studies, conducted by independent research groups, contributed to clarify the mechanism by which atlastin1 is able to modify the ER morphology by homotypic membrane fusion. The current model proposes that two atlastin molecules, residing in opposite membranes, after dimerization can fuse the lipid bilayer by the hydrolysis of GTP (Liu et al., 2012; Pendin et al., 2011). This fine process of ER remodeling is dependent on cytoskeleton driving force. In addition to these HSP proteins participating to membrane shaping, spastin has been found to disassembly and remodel neuronal microtubules and participate to maintain the structure integrity of ER (Figure 5) (Evans et al., 2006; Liu et al., 2012; Orso et al., 2005; Pendin et al., 2011; Sanderson et al., 2006).

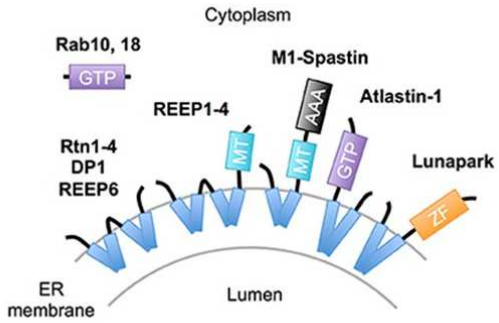

Figure 5. Proteins involved in ER network maintenance (Yamanaka and Nukina, 2018, image modified).

1.2.3 ER stress and ER morphology

The ER plays a crucial role in quality control of newly synthesized proteins of secretory pathway by two interconnected pathways: the unfolded protein response (UPR) and the ER-associated protein degradation (ERAD) path. UPR activation increases the folding capacity of ER, while ERAD system promotes terminally the misfolded proteins identification and their retro-translocation into the cytoplasm where they are degraded by the ubiquitin-proteasome system. In this way the ER maintains the flow of protein synthesis, folding and clearance. A condition referred to ER stress is activated by various stimuli including those of cellular redox regulation or by the accumulation of unfolded proteins in the ER, triggering the evolutionarily conserved pathway UPR (Gumeni et al., 2017). UPR is activated through three signaling cascades by ER transmembranes sensor proteins

PERK (PEKR-like endoplasmatic reticulum kinase), IRE1 (inositol requiring enzyme 1), and ATF6 (activating transcription factor 6 (Inagi et al., 2014). During regular physiological conditions, all three effectors bind to the ER chaperone 78 kDa glucose-regulated protein/binding immunoglobulin protein (GRP78/BIP) on their luminal domains (Moreno and Tiffany-Castiglioni, 2015). Upon ER stress, ATF6 dissociates from BIP, transfers to the Golgi and undergoes proteolytic processing to release the cytosolic domain and produces the active form ATF6f. Cytosolic ATF6f is then imported into the nucleus to induce the expression of protein quality control genes (Voeltz et al., 2002). The second pathway of the UPR is guided by PERK. During ER stress, PERK is activated by autophosphorylation and activates the ubiquitous translation initiation factor eIF2α, then indirectly inactivates eIF2. The eIF2α phosphorylation allows the specific translation of activing transcription factor 4 (ATF4), which upregulates many important genes involved in the redox control, metabolism and folding, causing a transient inhibition of most protein synthesis (Scheper and Hoozemans, 2015; Yamamoto et al., 2017). The ATF4 is involved in regulation of different glycolytic enzymes such as lactate dehydrogenase (Ldh). During ER stress Ldh expression is up-regulated with the consequent production of more lactate. ATF4 intermediates a shift from a metabolism based on oxidative phosphorylation to one more heavily reliant on glycolysis, reminiscent of aerobic glycolysis or the Warburg effect observed in cancer and other proliferative cells (Lee et al., 2015).

The UPR also activates the third UPR sensor, IRE1, which alternatively splices inactive X box-binding protein 1 (XBP1) mRNA, making active spliced XBP1 (sp-XBP1) (Tsaytler et al. 2011). The IRE1 pathway is one of the most studied branches of the UPR. Unfolded proteins induce activation of the IRE1 ribonuclease activity upon oligomerization on the ER membrane. The XBP1 activated form controls the expression of genes with X-box elements in their promoters, genes encoding ER chaperones and folding catalysts, as well as genes involved in the ERAD (Calfon et al., 2002; Credle et al., 2005; Yoshida et al., 2001).

The increase of protein synthesis requires the expansion of the ER membrane network, thus associating UPR with ER membrane extension (Mandl et al., 2013). However, another study also indicates that ER membrane expansion and generation of new ER sheets could act as a stress alleviating response independently on UPR activation, suggesting that ER expansion is an integral part of an effective UPR (Schuck et al., 2009).

The UPR activation is also connected to lipid droplet biogenesis. In yeast models, the absence of enzymes required to the biosynthesis of triacylglycerol and sterol esters induced the UPR activation (Olzmann and Carvalho, 2019; Velázquez et al., 2016a). In mammalian cells, the disruption of triacylglycerol synthesis and lipid droplet biogenesis also caused the UPR activation (Chitraju et al., 2017). In preadipocytes, the ablation of Rab18, an ER protein, induced an increase of UPR activation upon oleate treatment (Xu et al., 2018). Moreover, modulation of UPR after the disruption of optimal membrane rearrangements has already been reported: in *Drosophila*, downregulation of the ER-shaping protein Rtln1, causes partial loss of tubular ER and a significant increase of the ER stress

response in epidermal cells and neurons (O'Sullivan et al., 2012); the expression of *RTN3,* a specific receptor involved in the degradation of ER tubules, is upregulated by ER stress and its loss shows attenuated basal ER stress (Chen et al., 2011; Grumati et al., 2017); the *Arabidopsis* mutants of the atlastin GTPase homologue *RHD3*, which have long unbranched ER tubular structures, lack the ability to invoke UPR interfering with IRE1 function (Lai et al., 2014). Although the mechanism by which these ER-shaping proteins regulate UPR is still not clear, a link between tubular ER structure and ER stress exists.

1.3 Lipid droplet biogenesis and function in HSP

The lipid droplets (LDs) are cellular specialized organelles that store neutral lipids in all living organisms. They are composed by a core, containing mainly triacylglycerides (TAG) and sterol esters (SE), enclosed by a single phospholipid and proteins layer (Li et al., 2019; Tan et al., 2014; Wang, 2016).

Unlike most other organelles, LDs are not formed by growth and fission of existing droplets, but they are likely formed *de novo.* Several hypotheses have been proposed for describing the process of LD formation. The most accepted hypothesis postulates that lipids accumulate between the cytoplasmic leaflet of the ER membrane, and as the volume increases the leaflet swells as a globular mass until is pinched off from the membrane to become an independent LD (Suzuki et al., 2011).

LDs emerge from the endoplasmic reticulum leaflets/membranes, where two enzymes diacylglycerol acyltransferase 1 e 2 (DGAT1 e DGAT2) synthesize triglycerides. In mammals, the LD synthesis is characterized by three main steps: neutral lipid synthesis, LD formation and growth. The neutral lipid synthesis requires free fatty acid (FA) activation. De novo TAG synthesis occurs in a four-step pathway involving glycerol-3-phosphate O-acyltransferase (GPAT), 1-acylglycerol-3-phosphate O-acyltransferase (AGPAT), phosphatidic acid phosphatase (PAP) (or lipin), and diacylglycerol acyltransferase (DGAT) enzymes. At the last step of the pathway, FAs, firstly activated to acyl-CoA, are converted to TAGs through DGAT1 and DGAT2 enzymes (Figure 6) (Onal et al., 2017).

The importance of the LD in HSP mechanism is highlighted by recent evidences that proteins as Seipin/SPG17, Erlin2/SPG18, atlastin/SPG3a, spartin/SPG20 and REEP1/SPG31 have been found to localize or affect the LD turnover in cells (Belzil and Rouleau, 2012; Tan et al., 2014). Seipin, responsible of Silver syndrome (SPG17), is a critical regulator of human adipose tissue development. Spartin interacts with the surface lipid monolayer of LDs through its C-terminal region and plays a role in LD regulation by binding to TIP47 and E3 ubiquitin ligases, leading to degradation of LD-associated proteins (Alberts and Rotin, 2010; Falk et al., 2014; Hooper et al., 2010). Atlastin GTPases have been shown to regulate LD size in *C. elegans* and *D. melanogaster* and induce the formation of larger LDs after co-expression with REEP1 in mammalian cells (Klemm et al., 2013).

Moreover, mutated forms of human REEP1 are found to locate in LDs in cell cultures (Falk et al., 2014). Finally, spastin M1 isoform regulates the contact between LDs and peroxisomes, facilitating fatty acid trafficking (Chang et al., 2019).

The LDs are particularly important in tissues specialized for energy storage or lipid turnover, such as the adipose tissue, the liver, and the intestine, and accumulate in skeletal muscles and nervous system (Fujimoto et al., 2008; Ito et al., 2017; Morales et al., 2017; Onal et al., 2017; Walther and Farese Jr, 2012). LDs not only provide substrates for energy metabolism and building blocks for membranes, but also play a pivotal role in various cellular pathways, such as protein trafficking, protein degradation, and modulation of nuclear receptors (Onal et al., 2017). Moreover, LDs exhibit a protective function against oxidative damages caused by different stimuli leading to endoplasmic reticulum stress (Chitraju et al., 2017; Lee et al., 2017; Nguyen et al., 2017; Zheng et al., 2017).

In animal cells, the LDs are degraded through a selective autophagy process called lipophagy (Figure 7). The lipophagy process varies in different cell types, from fast degradation of large amount of lipids in liver cells during nutrient deprivation (Ward et al., 2016) to the regulation of protein levels by increased quantities of endogenous free fatty acid in neurons (Kaushik et al., 2011). *In vitro* studies have shown that the pharmacological inhibition of autophagy by 3-methyladenin induced an increase of TAG levels; moreover in embryonic fibroblasts of mice and *in vitro* cultured hepatocyte cells the ablation of Atg5 caused an increase in size and number of LDs (Singh et al., 2009).

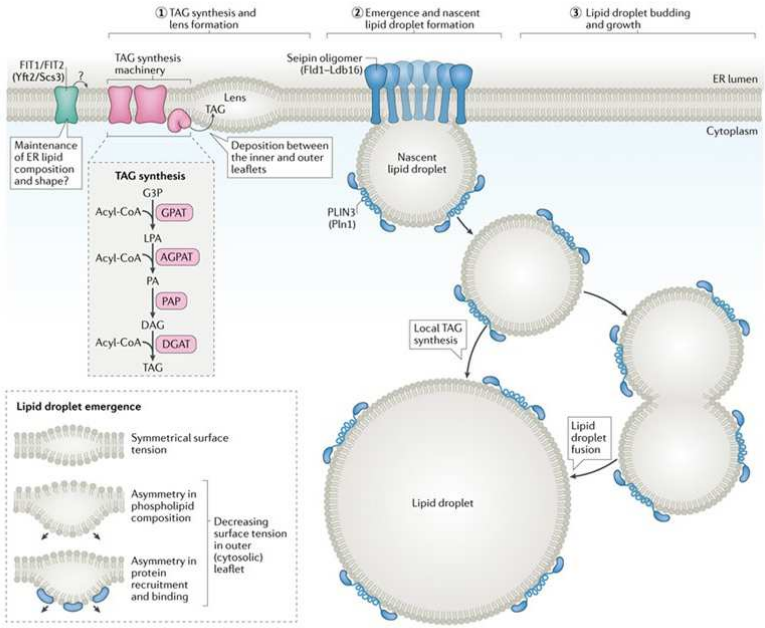

Figure 6. Synthesis of lipid droplets (Olzmann and Carvalho, 2019, image modified).

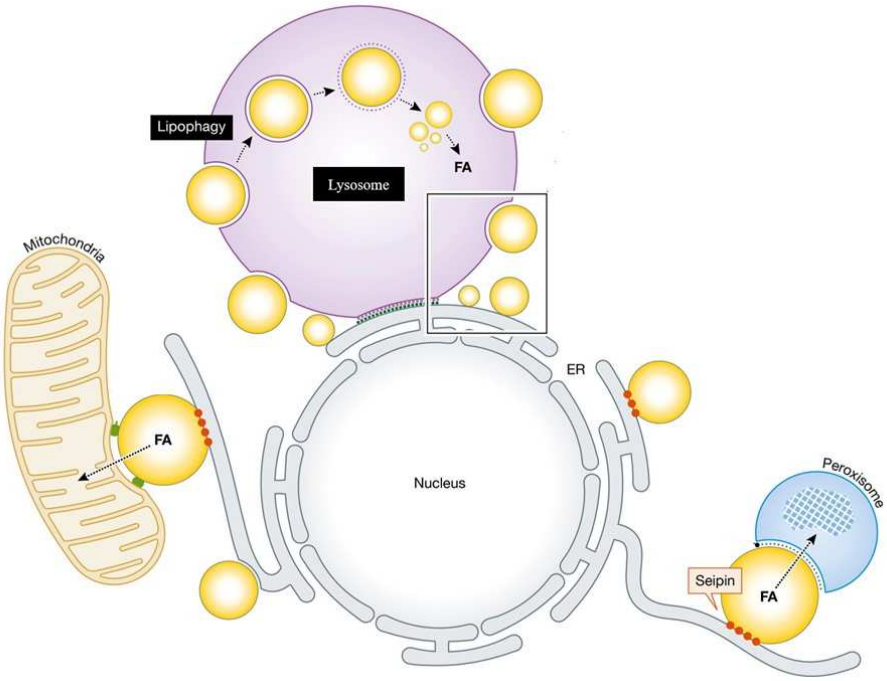

Figure 7. Lipid droplet contacts (Henne, 2019, image modified).

1.4 Autophagy and endolysosomal pathways in HSP

Autophagy is a catabolic process in which cellular contents such as proteins, lipids and entire organelles are degraded by lysosomal lytic enzymes (Fujikake et al., 2018). This cellular process is induced by different stressors such as nutrient deprivation (starvation), DNA damage, accumulation of abnormal proteins, ER stress and organelle impairment (Fujikake et al., 2018; Glick et al., 2010). There are three types of autophagy: macro-autophagy, micro-autophagy, and chaperone-mediated autophagy. All mechanisms promote proteolytic degradation of cytosolic components in the lysosomes. The macro-autophagy mechanism is characterized by three key steps: 1) induction, 2) autophagosome nucleation, and 3) membrane expansion and completion. The induction is due to the Tor pathway inhibition and is regulated by the complex containing autophagy-related genes (Atg) Atg1 and Atg13. The vesicle nucleation, that allows formation of an isolating membrane known as phagophore, is controlled by the III Phosphatidylinositol 3-kinase/Vps34 complex. The membrane expansion and completion of autophagosome are regulated from two ubiquitin-like conjugation proteins LC3-I (microtubule-associated protein light chain) and Atg12. Atg12 is conjugated to Atg5. The Atg12-Atg5 conjugate is activated by Atg7. Then the Atg12-Atg5 complex binds the Atg16 and they form the complex Atg12-Atg5-Atg16, that induces curvature into the growing phagophore. The protein LC3-I bound to phosphatidylethanolamine with phosphatidylethanolamine is cleaved by Atg4 and is associated with the autophagosome until it is transferred to the lysosome (Abounit et al., 2012; Glick et al., 2010; Zirin and Perrimon, 2010). The ER membrane appears to be essential for phagophore biogenesis and participate in ER-mediated endosomal tubule fission to maintain a

correct lysosomal function. The failure of ER-mediated endosomal tubule fission causes abnormal lysosomal morphology. Lysosomal abnormality and autophagy defects have already been described in several rare HSP subtypes, involving proteins that localize to endosomes, including SPG11, SPG15, and AP5 complex members (Hirst et al., 2018; Khundadze et al., 2013; Renvoisé et al., 2014; Varga et al., 2015). Moreover, the ER-localized isoform of spastin (M1-spastin) promotes endosomal tubule fission by modulating ER–endosome contacts; when this process fails due to loss of or abnormal spastin function, lysosomal enzyme trafficking is impaired and lysosomal morphology aberrant (Allison et al., 2017). The lysosomal alteration, in fact, was observed in primary cortical neurons from a spastin-HSP mouse model, in patient fibroblasts, and induced pluripotent stem cell (iPSC)-derived neurons (Allison et al., 2017; Rehbach et al., 2019). Similar phenotypes were present in mouse neurons lacking the ER-shaping HSP protein REEP1 (Allison et al., 2017).

1.5 *Drosophila melanogaster* as model organism

Drosophila melanogaster is a widely used and highly manageable genetic model organism to understand many molecular and developmental processes of human diseases. Many genetic, physiological and neurological properties are conserved between mammals and *D. melanogaster*. The UPR and autophagy pathways are highly conserved in flies and, *Drosophila melanogaster* reacts to ER stress by activating the same sensors (dPerk, Ire1 and Atf6) (Hetz, 2012) and possess most of the Atg proteins involved in mammalian autophagy (Lőrincz et al., 2017). The fruit fly genome is 60% homologous to that of humans and less redundant. Approximately the 75% of human disease-causing genes have a functional homolog in fruit flies and a significant fraction of these homologs are expressed in *Drosophila* tissues that perform the function of the equivalent human tissue. These features, together with a short generation time, low maintenance costs and the accessibility of powerful genetic tools and easy genetic manipulation, allow the fruit fly to be an appropriate animal model to study complex pathways in biomedical research (Allocca et al., 2018; Mirzoyan et al., 2019; Pandey and Nichols, 2011; Ugur et al., 2016).

Drosophila represents a good research tool for genetic and biological studies of different pathological conditions such as neurological, cardiac and metabolic diseases. The *Drosophila* body includes organ systems with comparable functions of mammalian lung, kidney, heart, liver and gonads. The fruit fly central nervous system (CNS) is simpler than that of vertebrates and the neurodevelopment pattern is conserved among the organisms. In the last decade, the *Drosophila* CNS has been used as a model for neurodegeneration studies. In order to characterize neuronal dysfunctions in *Drosophila*, many approaches are available, including testing motility, individual and social behaviors, hearing, learning, and memory. Fruit flies affected by neurodegeneration share

behavioral defects and reduced lifespan. *Drosophila* has been employed for studies in neurodegenerative diseases such as tauopathy, Alzheimer's disease (AD), Parkinson's disease (PD), fragile X syndrome, Spinocerabellar ataxia, Huntington's disease, and HSP (Allocca et al., 2018; Staats et al., 2018).

1.5.1 Drosophila melanogaster and drug discovery

Drosophila melanogaster offers a good background for genetic and biological studies of different pathological conditions such as neurological, cardiac, and metabolic disorders. Two main strategies to study human diseases using fly models have been developed: reverse and forward genetics.

Reverse genetic approach is a powerful tool for understanding novel genes and their functional role in human disorders. In this method, mutations are created in fly orthologs of human genes to study their phenotypes *in vivo*. There are many techniques to downregulate or abolish the gene expression in *Drosophila* flies: targeted gene disruption such as CRISPR/Cas9 (clustered regularly interspaced short palindromic repeats/Cas9), transposon-mediated mutagenesis and excision of existing transponable elements, and gene silencing using RNA interference (RNAi) or CRISPR/Cas9 (Ugur et al., 2016).

One of the most important genetic systems used in reverse approaches is the GAL4/UAS system, that allows driving the expression of a gene in a specific way. The yeast protein Gal4 is the transcriptional activator in GAL4/UAS system, the upstream activating sequence (UAS) is an enhancer and it is specific to the GAL4 protein. The *GAL4* gene has been inserted at random positions in the *Drosophila* genome to generate 'enhancer-trap' lines that express GAL4 under the control of nearby genomic enhancers. Therefore, the expression of *gene X* can be driven in any of these patterns by crossing the appropriate GAL4 enhancer trap line to flies that carry the *UAS–gene X* transgene. Many GAL4 driver lines including the glial promoter repo (reversed polarity), the pan-neuronal promoter elav (embryonal lethal, abnormal vision) and the eye-specific promoter GMR (Glass Multimer Reporter) are available in *Drosophila* (Allocca et al., 2018; Ugur et al., 2016).

The forward genetic approach is an impartial method for identifying previously unknown genes and understanding biological processes. Mutations are induced randomly, and flies are screened for a specific phenotype. Mutations are generated chemically using ethyl methanesulfonate (EMS) or by using insertional mutagenesis techniques such as Enhancer-Promoter (EP)-elements and RNAi lines. The unbiased strategy can help to identify uncharacterized mutations in known disease genes (phenotypic expansion) as well as in genes that have not been previously linked to a disease. Forward genetics can thus be a powerful driving force for identifying previously unknown genes and explaining biological phenomena (Allocca et al., 2018; Ugur et al., 2016).

In the past years, *Drosophila* has also successfully been used for drug discovery (Fernández-Hernández et al., 2016; Gao et al., 2014). Traditionally, drug-screening processes are based on *in vitro*, enzymatic or receptor binding assays, but lead compounds identified are often ineffective or toxic after *in vivo* test. Indeed, the lead compounds identified by traditional approaches often do not display the desirable pharmacokinetics and pharmacodynamics characteristics when administered to murine models. Furthermore, traditional animal models, such as rodents, are a poor choice for a whole-animal primary screening process due to the long time, high costs and difficulty in the manipulation. Moreover, the use of *Drosophila melanogaster* as model in drug screening has given important results on models of fragile X syndrome, intestinal stem cell-derived tumors, and lifespan(Allocca et al., 2018; Chattopadhyay et al., 2016; Pandey and Nichols, 2011). Recently, Drosophila has used as model in a screening of flavonoids (Fantin et al., 2019). These studies confirm that the fruit fly could be a valid alternative in the drug discovery process (Fernández-Hernández et al., 2016; Pandey and Nichols, 2011).

1.6 Flavonoids and human diseases

Flavonoids are a group of natural compounds characterized by phenolic structures and extracted from plants (Fantin et al., 2019; Panche et al., 2016). They are synthetized through phenyl propanoid pathway against microbial infection (Falcone Ferreyra et al., 2012). Numerous studies have shown that food and beverage-containing flavonoids, such as fruits, vegetables, cereals and red wine, can improve health and contribute in the prevention of numerous diseases. This protective mechanism seems to be related to their free radicals scavenging activity, inhibition of enzymes activity (such as aldose reductase, xanthine oxidase, lipoxygenase, and cyclic nucleotide phosphodiesterases [PDEs]), and modulation of protein kinase (e.g., AMP kinase), lipid kinase signaling, and peroxisome proliferator-activated receptor pathways (Assini et al., 2013). Several *in vivo* studies had revealed that flavonoids help to reduce body weight gain, food consumption, and fat accumulation. In mammals, fat is stored in the adipose tissue, which is made principally of white and brown adipocytes (Assini et al., 2013). It is well known that selected flavonoids can induce lipolysis in adipose tissue, likely through inhibition of PDEs and antagonism of cyclic adenosine monophosphate degradation (Janda et al., 2016).

Naringenin is a flavonoid belonging to flavanones subgroups. It is extracted from Citrus fruits and grapefruits, it is a molecule insoluble in water but soluble in organic solvents. Naringenin is able to traverse the blood-brain barrier (Yang et al., 2013), but it displays a low bioavailability (Salehi et al., 2019; Yang et al., 2013). Several studies have been conducted to improve naringenin's bioavailability. In the pharmaceutical industry, the polysaccharides cyclodextrins have been used for their capacity to enhance the drug solubility in aqueous solutions and to affect the chemical characteristic of the encapsulated drug (Salehi et al., 2019; Yang et al., 2013). Cyclodextrins are

polysaccharide compounds characterized by six to eight D-glucose monomers linked by α-1,4-glucose bonds. They possess a central hydrophobic cavity and a hydrophilic surface and they can encapsulate inorganic/organic molecules (Yang et al., 2013). The complexation with cyclodextrins enhances the water solubility and thermal stability of naringenin (Yang et al., 2013). Among the cyclodextrins, hydroxypropoyl -β-cyclodextrin (HPβCD) increased naringenin's solubility and transport across a Caco-2 model of the gut epitelium and, in rat models, oral administration of this complex improved its plasma concentrations (Shulman et al., 2011). Rats fed with the complex HPβCD and naringenin display an increase of the rate of glucose clearance and an up-regulation of expression of PPAR co-activator and PGC1 α in both liver and skeletal muscles (Shulman et al., 2011).

It is known that naringenin possesses the ability to modulate signaling pathways related to fatty acids metabolism. It favors fatty acids oxidation, impairs lipid accumulation in liver and thereby prevents fatty liver (Curti et al., 2017; Goldwasser et al., 2011; Harmon and Harp, 2001; Hegazy et al., 2016; Huong et al., 2006; Khan et al., 2012; Pellegrini et al., 2014; Salehi et al., 2019; Song et al., 2016; Tang et al., 2017; Zygmunt et al., 2010). *In vitro* studies reported that naringenin reverts ER stress condition due to the hypoxia/reoxygenation injury in myocardial cells (Tang et al., 2017). Recently, it has been demonstrated that flavonoid compounds are able to modulate the autophagy cellular process in many diseases included neurological disorders (Prieto-Domínguez et al., 2018).

2. RESEARCH AIMS

Hereditary spastic paraplegia (HSP) is a heterogeneous group of genetic diseases clinically characterized by progressive spasticity and weakness of lower limbs. Understanding the cellular mechanisms implicated in neurodegeneration is fundamental in order to develop new pharmacological approaches. The main purpose of this study was to investigate the pathological mechanisms underlying HSP by using *Drosophila melanogaster*, a favored organism for genetic, biological and pharmacological research. This approach is based on the high degree of evolutionary conservation of gene structure and function between *Drosophila* and human.

In this work, two fruit fly models were evaluated: ReepA (ortholog of REEP1/SPG31) and Dspastin (ortholog of Spastin/SPG4).

The main goal of this project was to understand the biological and functional role of ReepA and DSpastin in ER homeostasis, LD biogenesis and endolysosomal pathways as these processes represent important emerging cellular aspects of HSP mechanism. In order to characterize the phenotypes associated to the elimination of ReepA and Dspastin, we performed an *in vivo* analysis using loss-of-function alleles and RNAi approaches.

In order to reach our goal, we proposed the following specific aims:

1. Characterize the role of ReepA in endoplasmic reticulum (ER) morphology using a *Drosophila* ReepA null mutant line and generating a new ER marker for *in vivo* analysis
2. Examine the role of ReepA in ER stress conditions and in Unfolded Protein Response (UPR) by investigating the three mains signaling involved: IRE1, PERK and ATF6
3. Characterize the behavioral phenotypes of ReepA null mutant flies
4. Investigate the role of ReepA in lipid droplets (LDs) morphology by tissue specific analyses
5. Analyze the role of Spastin and ReepA in LD biogenesis quantifying the mRNA levels of the main genes involved in this process
6. Characterize the role of HSP proteins in endolysosomal pathway and autophagy by analyzing autophagosome maturation and fusion with lysosomes. The monomeric tandem GFP-mCherry-Atg8 (autophagosome maturation), the Lamp1-GFP (lysosomal morphology) markers and the transgenic line Lamp1-GFP; mCherry Atg8a (autophasome-lysosome fusion) were expressed in control, ReepA and Dspastin models and the associated phenotypes were analyzed.

The final part of this work was focused on naringenin ability to ameliorate *in vivo* phenotypes of *Drosophila* HSP models.

3.METHODS

3.1 *Drosophila* genetics

3.1.1 Fly strains and materials

Fly stocks were raised on standard medium (see appendix A) and in standard conditions at 25°C and 12:12 h light:dark cycle. The *Drosophila* strains used are shown in Table 1 (see appendix B). ReepA^{+C591} was used as a genetic background control. ReepA^{-541} mutant and ReepA^{+C591} flies were maintained on standard food at 25˚C and Gal4/UAS crossings were performed at 28˚C. All reagents, antibodies and compounds are listed in Table 2 (see appendix C).

3.1.2 Generation of constructs/transgenic flies

Full-length H-REEP1 cDNA (606 bp) was previously obtained from HeLa cells RNA extract followed by PCR reaction and cloned in the pUAST plasmid. The ReepA^{E} cDNA (867 bp) was obtained from *Drosophila* RNA extract and cloned in the pUAST plasmid. UAS-HNEU-GFP fly line was generated by cloning HNEU-GFP (Kassan et al., 2013) in pUASTattB, and transgenic lines were generated by BestGene Inc service (Chino Hills, CA, USA) (Napoli et al., 2019).

3.2 *Drosophila* life cycle

3.2.1 Drosophila life cycle

The first stage of fruit fly life cycle is represented by an embryo in an egg. This stage lasts for about one day. During this time, the embryo grows into a larva. The first instar larva comes out of the egg, crawls into a food source, and feed. After a day, the first instar larva sheds and converts in second instar larva. After two days in this stage, the larva molts again to become the third instar larva. After three days of eating in this stage, the larva crawls out of the food source and sheds again. Following this molt, the larva stops moving and forms a pupa. Drosophila stays in the pupa for about five days. During this period the metamorphosis from larva to adult is taking place. Adult structures like wings, legs, and eyes develop. When the adults emerge from the pupa they are fully formed. They become fertile after about ten hours, copulate, the females lay eggs, and the cycle begins again. The whole life cycle takes about 12-14 days.

3.2.2 Drosophila drug treatments

Tunicamycin previously dissolved in ethanol, naringenin complexed with hydroxylpropyl-β-cyclodextrin in a mole ratio of 1:1, chloroquine were added to standard *Drosophila* food at the final concentration of 0.024 mM, 0.5 mM and 2.5 mg/ml respectively.

3.2.3 Starvation assay

For starvation assay, third instar larvae were individually selected and placed in petri plates containing a solution of 20% sucrose in PBS for 4 hours.

3.3 Biochemal assays

3.3.1 RNA extraction and Real-time PCR

The relative expression levels of *Bip, Xbp1 total, Xbp1spliced, Ldh, Atf4, Gp93, Hrd3, Herp, ReepA Minotaur and Midway* were determined using quantitative real-time PCR. Total RNA was isolated from 5 third instar larvae and was extracted by Trizol reagent and purified using Direct-Zol TM RNA MiniPrep kit according to the manufacturer's instructions. The concentration and purity of RNA samples were determined using a NanoDrop 2000c spectrophotometer. Real-time PCR (qPCR) was performed on Eco Real-Time PCR System, using One Step SYBR® Prime Script TM RT-PCR Kit II. The real-time PCR cycling conditions were: reverse transcription 50°C for 15 minutes, polymerase activation 95°C for 2 minutes, followed by 40 cycles of 95°C for 15 seconds, 60 °C for a 1 minute; melting curve 95°C for 15 seconds, 55°C for 15 seconds and 95°C for 15 seconds for all target genes. The housekeeping *Rp49* gene was used as an internal control to normalize the data. Relative mRNA expression levels were calculated by the threshold cycle (Ct) value of each PCR product and normalized using comparative $2^{-\Delta\Delta Ct}$ method. Data represented are the result of five independent biological replicates. Each biological sample was loaded in triplicate. The gene specific primers used are shown in Table 3 (see appendix D) (Napoli et al., 2019).

3.3.2 Western Blotting

For western blots, total proteins were obtained from 10 adult flies using GRS FullSample purification kit. The protein levels were quantified using the Bradford proteins quantification kit (Sigma-Aldrich, MO, USA). Each sample was diluted 1:2 with standard 2X Laemmli buffer, boiled for 5 min a 95°C and 20-25 mg of proteins were separated on 5% stacking-10% separating SDS polyacrylamide gels. The resolved proteins were transferred electrophoretically transferred to polyvinylidene difluoride

(PVDF) membrane as described before. Membranes were blocked in 10% nonfat dried milk in Tris-Buffer Saline and 0.1% Tween 20 (TBST) and were incubated using primary antibody rabbit anti-phospho eIF2aS1 (1:1000) overnight at 4°C. Mouse anti-α-tubulin (1:2000) was used as loading control. Secondary polyclonal goat anti-rabbit and anti-mouse immunoglobulins HRP (1:2000) were used in all cases. The protein bands were detected using the C400 Azure chemiluminescence biosystem and band densities were quantified with ImageJ Fiji 1.52 software. The ratio of target protein to α-Tubulin was recorded and analyzed. At least three independent biological replicates were used for each genotype and condition (Napoli et al., 2019).

3.4 Behavioral assays

3.4.1 Lifespan assay

For lifespan assay, control ReepA^{+C591}, ReepA^{-541} mutant flies were collected after hatching and raised on standard medium or 0.5 mM naringenin enriched food at 25 °C in a 12:12 h light-dark cycle. Flies were kept in groups of 20 individuals and were maintained in a *Drosophila* vial. Flies were transferred to a fresh medium every three days and death events were scored daily. Experiment was repeated ten times for each genotype (Napoli et al., 2019).

3.4.2 Climbing assay

For climbing assays, 30 flies for each genotype (*ReepA^{+C591}/ ReepA^{+C591}, ReepA^{-541}/ ReepA^{-541}, Elav-Gal4/+ and UAS-RNAiDspastin/Elav-Gal4*) were collected after hatching and were transferred twice a week to tubes containing fresh standard or 0.5 mM naringenin enriched food. Climbing capability was tested six times along the life of these flies (5, 10, 15, 20, 25 and 30 days).
Drosophilae were placed in an empty plastic vial with a line drawn 2 centimeters from the bottom of the tube and allowed to recover from anesthesia for 1 hour. Flies were gently tapped to the bottom of the tube and the number of flies above the 2 cm mark at 20 seconds was recorded as a percentage of flies able to climb the vial. Ten separate and consecutive trials were performed, and the results were averaged. Experiment was repeated ten times for each genotype (Napoli et al., 2019).

3.5 Confocal microscopy

3.5.1 Immunohistochemistry

Third instar larvae raised at 25°C or 28°C were harvested, dissected in HL3, fixed in 4% paraformaldehyde for 10 min, and washed in PBS containing 0.3% Triton X-100 and mounted on glass slides using Mowiol 4-88. For live imaging, larvae were dissected in HL3 and acquired, as

described previously (D'Amore et al., 2016). For lipid droplets staining larvae were dissected and then incubated for 1 hour, at room temperature, using the LDs probe BODY PY 493/503 (1:100) and the probe HRP red anti Horseradish Peroxidase conjugated Cy3 (1:500) in PBS containing 0.3% Triton X-100. Then the larvae were washed in PBST 0.3% and mounted on glass slides using Mowiol 4-88 (Mushtaq et al., 2016). All confocal images were acquired using a confocal microscope (Nikon D-ECLIPSE C1) equipped with a Nikon 60x/1.40 oil Plan Apochromat objective using the Nikon EZ-C1 acquisition software.

3.5.2 ER marker HNEU-GFP fluorescence quantification

For ER morphological analysis, the fluorescence of the ER marker HNEU-GFP was quantified and analyzed with ImageJ Fiji 1.52 software. All quantitative analyses were performed on muscle 6/7 of abdominal segment A3 of ten third instar larvae. Fluorescence intensities were measured on maximum projections of confocal stacks (step size 0.55 µm) taken with a Nikon 60x/1.40 oil Plan Apochromat objective using the Nikon EZ-C1 acquisition software. For each sample, three Region of Interest (ROI) with a range of 800-1000 μm^2 were analyzed.
To quantify cisterna-like structures, an 8-bit ER image was requested. Image was processed with a manual threshold. Threshold values were 80–255 to eliminate the intensity distortion and 40–255 to preserve the continuity of tubules. Then a binary and open image was created and processed by erosion (subtract pixels) and dilation (add pixels) commands of ImageJ software. In the binary and opened image, tubules were eliminated, and cisterna-like structures were isolated. The sheet-like structures were analyzed with Analyze Particle tool and their number and size were quantified (Griffing, 2018; Napoli et al., 2019)

3.5.3 LD quantification

For lipid droplet (LDs) analysis, the BODIPY 493/503 dye staining was performed on muscles and proximal ventral ganglion nerves of ten third instar larvae, and the fluorescence was quantified and analyzed with ImageJ Fiji 1.52 software. All quantitative analyses were performed on muscle 6/7 of abdominal segment A3. LDs were measured using merged Z-stack images taken with a Nikon 60x/1.40 oil Plan Apochromat objective using the Nikon EZ-C1 acquisition software. The LDs were analyzed with Analyze Particle tool and their number and size were quantified (Fantin et al., 2019).

3.5.4 Autophagy's structure quantification

For autophagosomes, autolysosomes and lysosomes analysis, the fluorescence ubiquitously expressing the UAS mCherry-GFP Atg8a, the UAS-LAMP1-GFP and UAS-LAMP1-GFP;mCherry Atg8 a was quantified and analyzed with ImageJ Fiji 1.52 software. All quantitative analyses were

performed on muscle 6/7 of abdominal segment A3 of ten third instar larvae. Fluorescence intensities were measured on maximum projections of confocal stacks (step size 0.55 µm) taken with a Nikon 60x/1.40 oil Plan Apochromat objective using the Nikon EZ-C1 acquisition software. For each sample, three Region of Interest (ROI) with a range of 800-1000 μm^2 were analyzed. To quantify autophagic structure, an 8-bit image was requested. Image was processed with a manual threshold to eliminate the background signal. The autophagic structure were analyzed with Analyze Particle tool and their number and size were quantified.

3.6 Statistics

3.6.1 Statistical analysis

Statistic was performed with Microsoft Office Excel 2013 software and Prism version 6.00 for Windows (GraphPad Software, LaJolla, CA, USA). Survival data were analyzed using the log-rank test (Mantel-Cox method).
Significance was calculated using one-way or two way analysis of variance (ANOVA) followed by Dunnett's or Tukey's multiple comparison test. Student's t-test for unpaired variables (two-tailed) was used for real time PCR in young and old flies (Figure 2 B) and in climbing assay in Figure 2 D. Differences were considered statistically significant at $p<0.05$(*) and $p<0.01$ (**) and $p<0.001$ (***). Data are presented as mean and bars are s.e.m. (standard error of the mean).

APPENDIX A: Stocks and Solutions

Drosophila's food

Yeast extract	27 g/L
Agar	10 g/L
Corn meal	22 g/L
Molasses	66 ml/L
H_2O	to 1 L

Heat at 85° C for 20 minutes. Add the nipagin 2.5 ml/L dissolved in 12.5 ml/L of ethanol.

Phoshate Buffered Saline (PBS)

KH_2PO_4	15 g/L
NaCl	9 g/L
Na_2HPO_4	8 g/L

HL3

NaCl	70 mM
KCl	5 mM
CaCl2	1.5 mM
MgCl2	20 mM
NaHCO3	10 mM
Trealose	5 mM
Sucrose	115 mM
HEPES	5 mM

Adjust pH to 7.0 with 10N NaOH

Paraformaldeide 4% (PFA)

PFA 8%	10 ml
PBS 5x	4 ml
H_2O	6 ml

Running buffer 1X

Tris	25mM
Glycine	250mM
SDS	0.1%

In deionized H_2O

Transfer buffer 1X

Tris 25mM

Glycine 192mM

In deionized H_2O

TBS-T buffer 1X

Tris 100mM

NaCl 1,5M

Tween-20 1%

In deionized H2O

Mowiol 40-88 (Sigma-Aldrich)

Mowiol 2.4 g

Glicerolo 6 g

Shake for 10 min

Add 6 ml of H_2O

Shake for 4h at 50°C.

Add:

Tris/HCl pH 8.5 100 mM 12 ml

DABCO 0.1 %

Centrifuge at 6000 rpm for 15min. Store at -20°C.

APPENDIX B: Drosophila fly stocks

Genotype	Source	Reference	RRID
ReepA^{-541}/ ReepA^{-541}	O'Kane CJ (Department of Genetics, University of Cambridge, Cambridge, United Kingdom)	(Yalçın et al., 2017)	RRID:DGGR_123207
ReepA^{+C591}/ ReepA^{+C591}	O'Kane CJ (Department of Genetics, University of Cambridge, Cambridge, United Kingdom)	(Yalçın et al., 2017)	
ReepA^{E} myc	Generated in our laboratory	See Materials and Methods	
UAS H-Reep1	Generated in our laboratory	See Materials and Methods	
UAS HNEU-GFP	Generated in our laboratory	(Kassan et al., 2013) See Materials and Methods	
Tubulin-Gal4	Bloomington BL 5138		RRID:BDSC_5138
Elav-Gal4			
UAS-Lamp1-GFP	Helmut Krämer (Department of Neuroscience, University of Texas, Dallas, TX)	(Pulipparacharuvil et al., 2005)	
UAS-mCherry -GFP-Atg8a	Bloomington BL 37749		RRID:BDSC_37749
UAS-mCherry Atg8a	Bloomington BL 37750		RRID:BDSC_37750
UAS-Lamp1-GFP; mCherry-Atg8a	Generated in our laboratory		RRID:BDSC_38400
RNAiSpastin(III)	Generated in our laboratory	(Trotta et al., 2004)	
W^{1118}	Bloomington BL 5905		RRID:BDSC_5905

APPENDIX C: Reagents and antibodies

Reagent	Source	RRID	Catalogue number
Tunicamycin	Sigma-Aldrich		T7765
Ethanol	Carlo Erba Reagents		308640
Chloroquine diphosphate salt	Sigma-Aldrich		C6628
Naringenin	Sigma-Aldrich		W530098 Bacth Number MKBW8466
Hydroxylpropyl-β-cyclodextrin	Sigma-Aldrich		H107
Sucrose	Applichem		A 1125
Trizol	Euroclone		EMR507100
Direct-Zol TM RNA MiniPrep kit	Zymo Research, Tustin, CA, USA		R2052
One Step SYBR® Prime Script TM RT-PCR Kit II	Takara-Clontech		RR066A
GRS FullSample purification kit	Grisp Research Solutions		GK26.0050
Bradford proteins quantification kit	Sigma-Aldrich		B6916
Laemmli buffer	Sigma-Aldrich		S3401
Tween 20	Sigma-Aldrich		P1379
Rabbit anti-phospho eIF2aS1	Abcam	RRID:AB_732117	
Mouse anti-α-tubulin	Sigma-Aldrich	RRID:AB_477593	
Goat anti-rabbit immunoglobulins HRP	DakoCytomation	RRID:AB_2617138	
Rabbit anti-mouse immunoglobulins HRP	DakoCytomation	RRID:AB_2687969	
Triton X-100	Sigma-Aldrich		X100
BODYPY 493/503	Thermo Fisher Scientific, Waltham, MA		D3922
HRP red anti Horseradish Peroxidase coniujated Cy3	Jackson ImmunoResearch, Inc., West Grove,PA, USA		

APPENDIX D: List of primers used in Real time PCR

Gene	Primer sequence
Bip(Hsc3)	Fw: 5'-GATTTGGGCACCACGTATTCC-3' Rv: 5'-GGAGTGATGCGGTTACCCTG-3'
Xbp1 total	Fw: 5'-TCTAACCTGGGAGGAGAAAG-3' Rv: 5'-GTCCAGCTTGTGGTTCTTG-3'
Xbp1 spliced	Fw: 5'-CCGAACTGAAGCAGCAACAGC-3' Rv: 5'-GTATACCCTGCGGCAGATCC-3'
Atf4	Fw: 5'-TGCGAGTCTCAGGCG TCTTCATCTT-3' Rv: 5'-CTGCTCGATGGTTGTAGGAGCTGG-3'
Ldh	Fw: 5'-GTGTGACATCCGTGGTCAAG -3' Rv: 5'-CTACGATCCGTGGCATCTTT-3'
Gp93	Fw: 5'-TACCTGAGCTTCATTCGTGGCGTCG-3' Rv: 5'-GCGGACCAGCTTCTTCTTGATCACC-3'
Hrd3	Fw: 5'-GCTGTGAGAAGGCGCTGATCCACTA-3' Rv: 5'-CCAGCAGTCTTACCCGATGCACAAC-3'
Herp	Fw: 5'-CTTACGCGCAGTACATGCAGCAGTT-3' Rv: 5'-CAGCTGCTCCTGCCACTTGTTGTAC-3'
ReepA (s,p,j,h,g,e)	Fw: 5'-ATGATCAGCAGCCTGTTTTC -3' Rv: 5'-CAGTACATCATTCATTTAACATATTC-3'
Rp49	Fw: 5'-AGGCCCAAGATCGTGAAG AA-3' Rv: 5'-TCGATACCCTTGGGCTTGC-3'
Minotaur	Fw: 5' – CCC GAG AAG ATG GAA ACA TT – 3' Rv: 5' – GGA GGA GGT GGA CTG ATT GT – 3'
Midway	Fw: 5' – TGG TTA TGG CCT TGT TTC AA – 3' Rv: 5' – CAC GTC CAT ATT GGA GAA CG – 3'

4.RESULTS

4.1 ReepA regulates ER morphology

REEPs are endoplasmic reticulum (ER) resident proteins implicated in ER remodeling (Beetz et al., 2013; Zheng et al., 2018). To evaluate the function of *Drosophila* ReepA (firstly named DREEP1 in Appocher et al., 2014) in ER membrane shaping, we analyzed ER structure in *Drosophila* overexpressing the ReepA isoform E (here reported as ReepA^{E}), flies overexpressing the human *REEP1* cDNA, were also analyzed in order to identify a possible conservation of the REEP1 function across phylogenetically distant species (Figure 8). Besides the gain-of-function lines we analyzed the ReepA^{-541} *Drosophila* null mutant (Yalçın et al., 2017) for loss-of-function phenotypes. Two of the most used ER markers in *Drosophila* are: Lys-GFP-KDEL (Frescas et al., 2006) and BiP–sfGFP–HDEL (Summerville et al., 2016). Lys-GFP fails to recognize the complexity of ER and discriminate between tubules and cisternae (Figure 9). On the other hand, BiP–sfGFP–HDEL, defines better the ER structures but it results lethal at pupal stage when expressed with drivers as Elav-Gal4 and Mef2-Gal4 and at larval stage if expressed with Tubulin-Gal4 driver.

To overcome this problem, we used a recently published ER marker (HNEU-GFP) allowing us a finer visualization of ER structure in both living and fixed samples (Figure 10) (Forgiarini et al., 2019). The expression of HNEU-GFP transgene is not lethal, also with strong drivers and at relative high temperatures (28-29°C).

To determine if overexpression of DReepA or HREEP1 as well as loss of DReepA may cause morphological defects in the ER, we quantified the total cisternal area of the ER in muscles ubiquitously expressing UAS HNEU-GFP under the control of the Tubulin-Gal4 driver. The total area of the ER cisternae was measured along the muscle stacks and quantified as described by (Griffing, 2018). Both the ubiquitous overexpression of ReepA and HREEP1 and its absence in ReepA^{-541} induced evident morphological alteration of ER architecture, as shown by the HNEU-GFP marker profile (Figure 11A, 11B, 11C). In ReepA^{-541} mutant, the cisterna-like structures were increased, and peripheral tubular ER appears to lose its complexity (Figure 11B, 11C). In contrast, ubiquitous expression of ReepA^{E} induced a reduction of cisternae (Figure 11B, 11C), thus implying a direct role of ReepA in the modulation of ER structure in *Drosophila*. Interestingly, overexpression of human REEP1 also led to a reduction of cisternal structures, a phenotype similar to that of ReepA^{E} overexpression, suggesting a high conservation of Reep1 proteins function in ER remodeling. Therefore, our data confirmed that *Drosophila* ReepA, similarly to its ortholog REEP1, is involved in ER membrane shaping (Napoli et al., 2019)

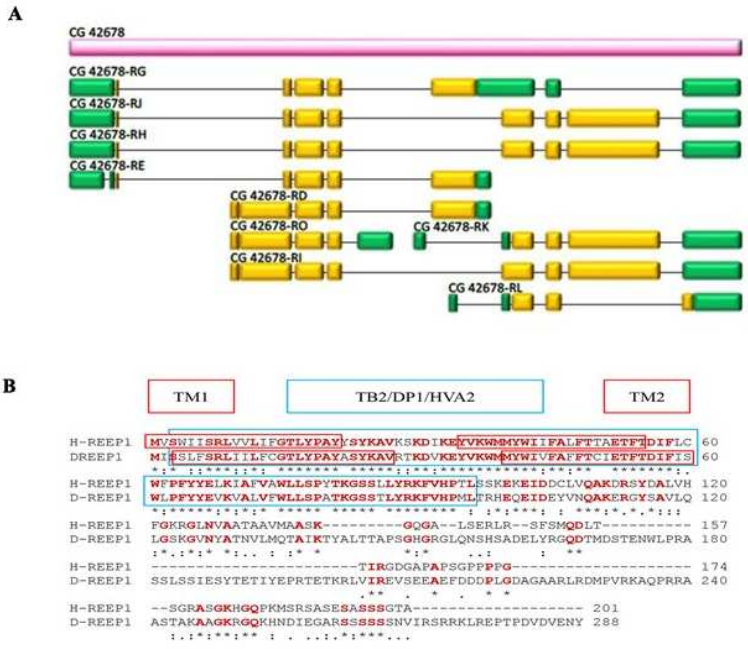

Figure 8. *Drosophila melanogaster* ReepA transcript map. (A) Schematic representation of D-*REEP1*(*ReepA)* gene. The *Drosophila* ortholog of H-*REEP1* gene localizes on the second chromosome and codifies nine transcript isoforms. **(B)** Alignment of human and *Drosophila* REEP1 protein sequence. The conserved amino acids are in red; blu and red boxes are the conserved domains of the protein (Napoli et al., 2019).

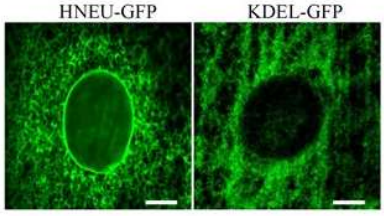

Figure 9. HNEU-GFP and Lys-GFP-KDEL ER marker fly lines. Representative confocal images of larval muscle 6/7 of abdominal segment A3 of wild type third instar larvae ubiquitously expressing the ER markers HNEU-GFP and Lys-GFP-KDEL (*Tubulin-Gal4/ UAS HNEU-GFP, Tubulin-Gal4/ UAS Lys-GFP-KDEL*). Scale bar=10 μm (Napoli et al., 2019).

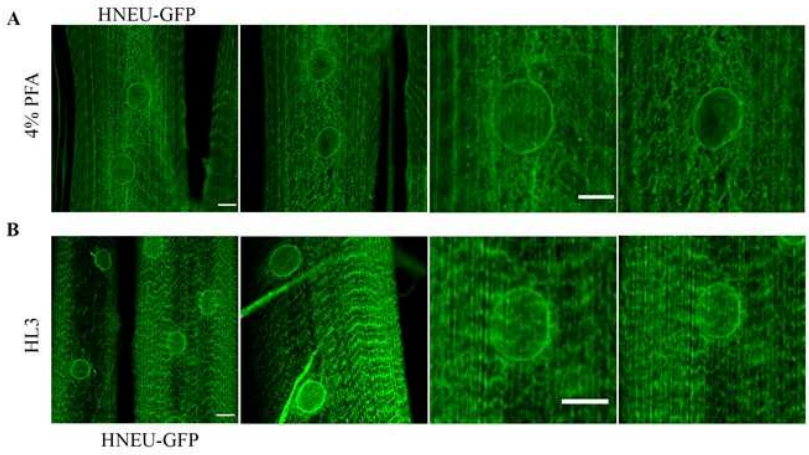

Figure 10. *In vivo* ubiquitous expression of ER-marker HNEU-GFP in control *Drosophila melanogaster*. Representative confocal images of larval muscle 6/7 of abdominal segment A3 of control larvae (*Tubulin-Gal4/ UAS HNEU-GFP*) acquired after PFA 4% fixation **(A)** or live **(B)** (Napoli et al., 2019).

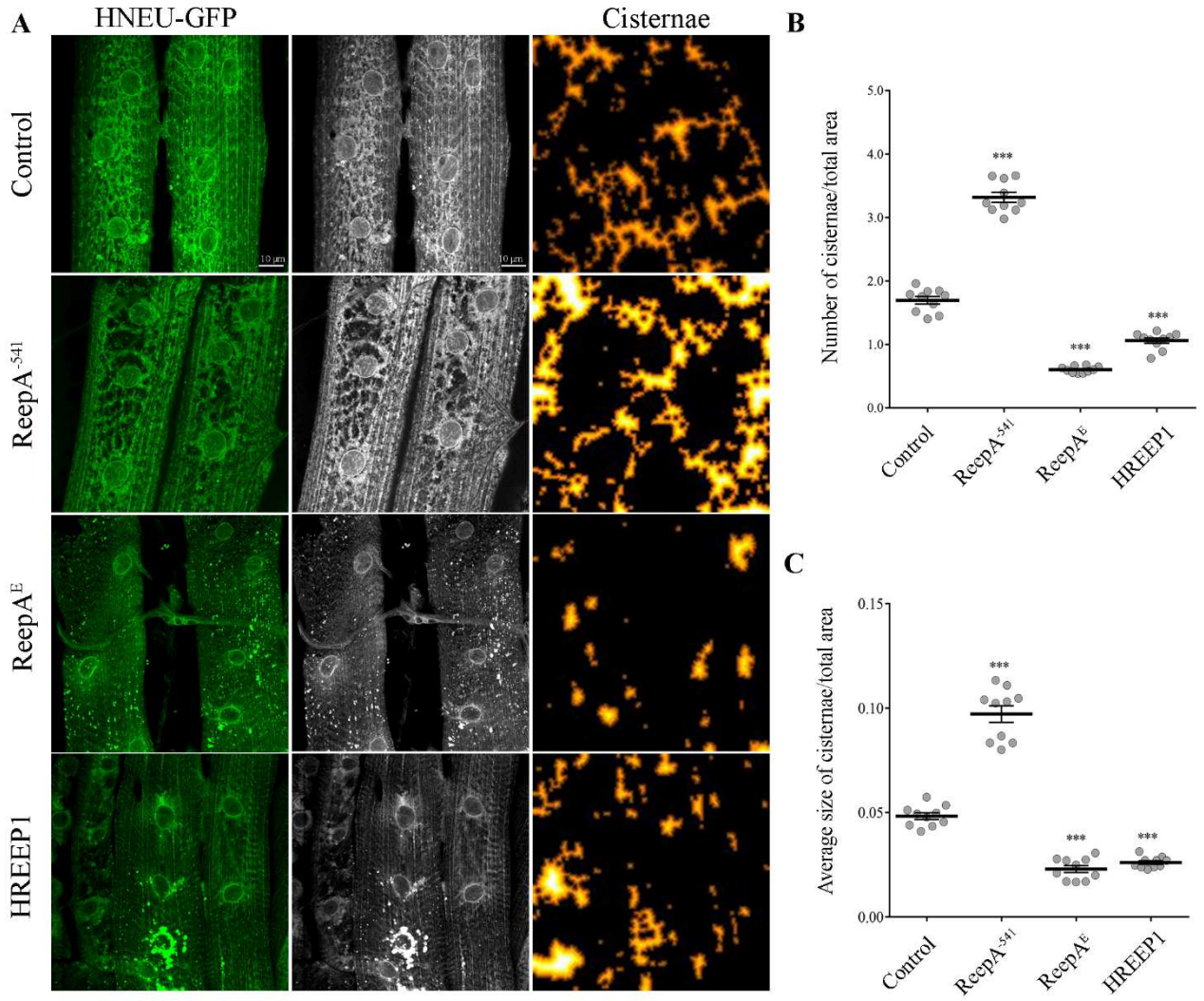

Figure 11. ***In vivo*** **ubiquitous expression of ER-marker HNEU-GFP in** ***Drosophila melanogaster*** **ReepA model. (A)** Representative confocal images of larval muscle 6/7 of abdominal segment A3 of control (*ReepA^{+C591}/ ReepA^{+C591} ; Tubulin-Gal4/ UAS HNEU-GFP*), ReepA^{-541} mutant (*ReepA^{-541}/ ReepA^{-541}; Tubulin-Gal4/ UAS HNEU-GFP*), ReepA^{E} (*UAS ReepA^{E} myc/+; UAS HNEU-GFP, Tubulin-Gal4/+*) and HREEP1 (*UAS HREEP1/ UAS HNEU-GFP, Tubulin-Gal4*) larvae, ubiquitously expressing UAS HNEU-GFP. Scale bar=10 µm. Quantification of cisterna-like structures number **(B)** and size **(C)** of ER-marker HNEU-GFP. Significance was calculated using one-way ANOVA followed by Dunnett's multiple comparison test. Significance vs ctr. (***P<0.001). The bars indicate s.e.m., n=10 larvae (Napoli et al., 2019).

4.2 ReepA is required during ageing and stress

A functional screening performed in *Drosophila melanogaster* demonstrated that ReepA promotes neuronal resistance to ER stress and prevents Tau toxicity (Appocher et al., 2014). Neuronal resistance was tested in adult flies against heat-shock stress and tunicamycin (TM) treatment, identifying ReepA as a new modulator of cellular response to stress. In spite of this, the molecular mechanism underlying such a response remains unclear. In attempt to elucidate this mechanism, we evaluated the expression levels of ReepA^{E} transcript after chronic TM treatment or starvation (Appocher et al., 2014; Lindström et al., 2016). We therefore compared ReepA^{E} transcription levels in wild type larvae before and after TM treatment or starvation. Our analysis shows that ReepA^{E} is upregulated both after starvation and chronic TM feeding (Figure 12A). We thus, investigated the role of ReepA during aging. We tested the expression level of ReepA^{E} in young versus old wild type flies and found that 30 day-old adults expressed higher levels of ReepA^{E} compared to one day-old adults (Figure 12B), indicating an upregulation of ReepA over adult lifespan. Furthermore, we found that ReepA^{-541} null mutant flies displayed a significant reduction of lifespan (Figure 12C) and climbing ability (Figure 12D), reinforcing the hypothesis that ReepA is required during aging. Our data confirmed a crucial role of ReepA in ageing and stress conditions (Napoli et al., 2019).

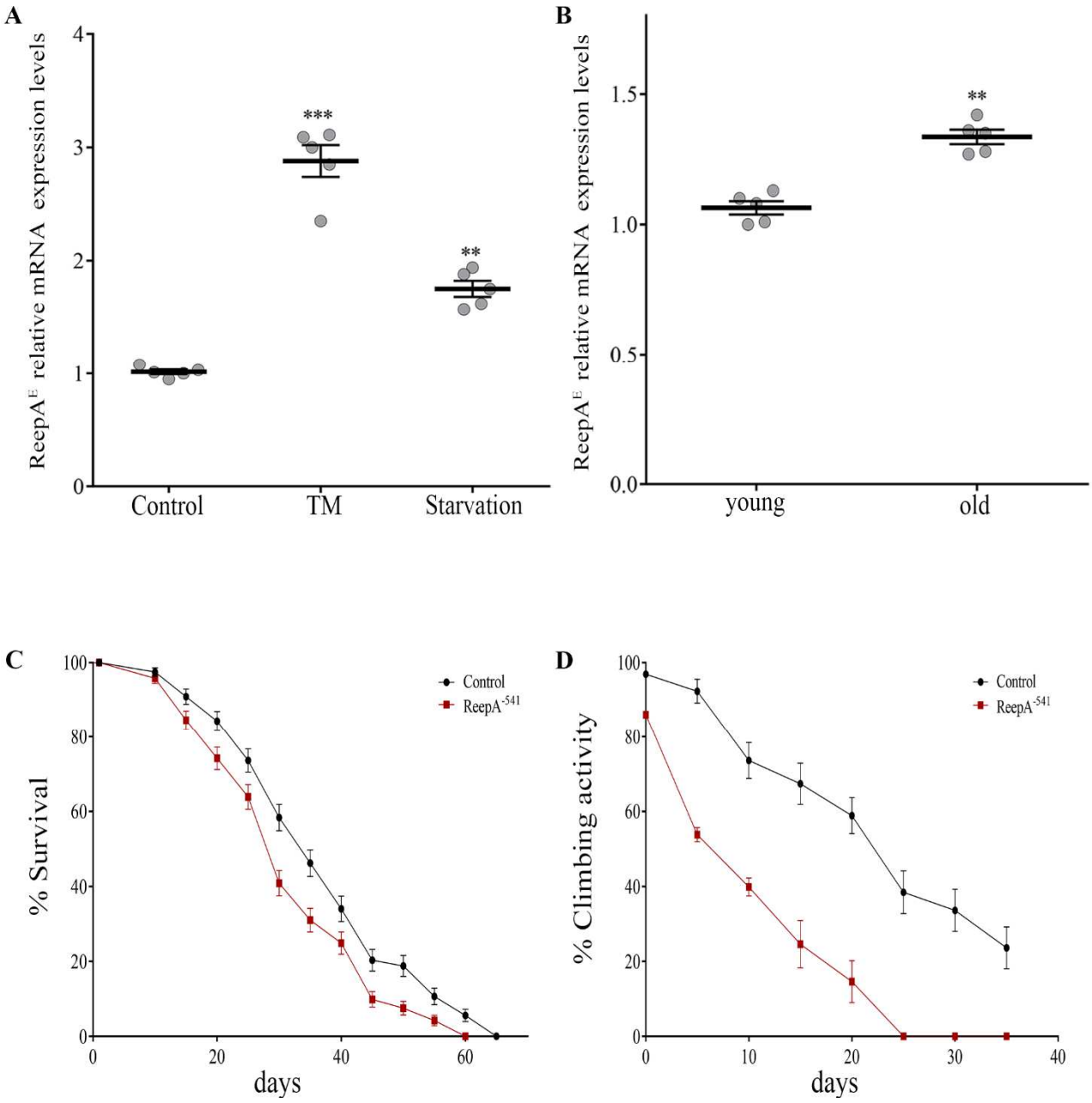
A
ReepA^E relative mRNA expression levels
4
3
2
1
0
***
**
Control
TM
Starvation
B
ReepA^E relative mRNA expression levels
1.5
1.0
0.5
0.0
**
young
old
C
% Survival
100
80
60
40
20
0
0
20
40
60
days
Control
ReepA-541
D
% Climbing activity
100
80
60
40
20
0
0
10
20
30
40
days
Control
ReepA-541

Figure 12. Loss of *ReepA* reduces *Drosophila* longevity and flies' climbing activity. **(A)** *ReepA*^{E} relative gene expression in control (*ReepA*$^{+C591}$/ *ReepA*$^{+C591}$) larvae raised on standard, TM 0.024 mM containing food, or on starvation conditions. Significance was calculated using one-way ANOVA followed by Dunnett's multiple comparison test. Significance vs ctr. (**P < 0.01*; ***P<0.001), n=5. **(B)** *ReepA*^{E} relative gene expression in young (1 day) and old (30 days) control (*ReepA*$^{+C591}$/ *ReepA*$^{+C591}$) flies raised on standard food. Significance was calculated by using two tailed T-test, **P <0.01, n=5. **(C)** Lifespan in control (*ReepA*$^{+C591}$/ *ReepA*$^{+C591}$) and ReepA^{-541} mutant (*ReepA*$^{-541}$/ *ReepA*$^{-541}$) raised on standard food. Significance was calculated by using log-rank Mantel-Cox test, P value: *** P<0.001. The bars indicate s.e.m., n= 10 (30 flies for each vial). **(D)** Climbing activity in control (*ReepA*$^{+C591}$/ *ReepA*$^{+C591}$) and ReepA^{-541} mutant (*ReepA*$^{-541}$/ *ReepA*$^{-541}$) raised on standard food and tested at 0, 5, 10, 15, 20, 25, 30 and 35 days. Significance was calculated by using two tailed T-test, P value: * P < 0.05. The bars indicate s.e.m., n= 10 (20 flies for each vial)(Napoli et al., 2019).

4.3 ReepA mutant flies triggered a selective activation of Atf6 and Ire1 branches

To elucidate the molecular mechanism underlying ReepA function in cellular stress we tested the effects of the loss of ReepA on UPR response, one of the main cellular signaling activated during of ER stress (Figure 13A) (Mandl et al., 2013; Rutkowski and Kaufman, 2007). We thus measured the activation of the three main branches of UPR signaling (Perk, Ire1 and Atf6) in *Drosophila* under normal or stress conditions induced by TM administration.

In order to identify the UPR branches activation, a qRT-PCR analysis on control and ReepA^{-541} third instar larvae, grown on standard or TM-containing food, was performed. Our data showed that the expression of *Hsc3,* the homologue of Bip/GPR94 chaperon, was significantly increased in control larvae treated with TM (Figure 13B), in agreement with previous *in vitro* studies (Lindström et al., 2016). Intriguingly, untreated ReepA^{-541} mutant larvae showed an increase of 1.5-fold in *Bip* transcript levels, that remained high even after TM treatment (Figure 13B). The activation of IRE1 pathway was quantified by measuring the levels of the unspliced (*Xbp1 total (Xbp1 t*)) and IRE1-dependent spliced forms of *Xbp1 (Xbp1 spliced* (*Xbp1 s*). Our analysis showed that the levels of spliced *Xbp1* mRNA were significantly increased in ReepA^{-541} mutant and in control larvae exposed to chronic TM feeding (Figure 13C), supporting the activation of IRE1 pathway in absence of ReepA. Similar data were obtained by analyzing Atf6 pathway. Specifically, we found that the Atf6 targets genes *Gp93*, *Herp* and *Hrd3* were upregulated in ReepA^{-541} mutant, mimicking again the response of control larvae treated with TM (Figure 13D). Finally, we evaluated the activation of Perk pathway by quantifying the expression levels of *Atf4*, but no statistically significant changes were observed in ReepA^{-541} mutant nor in TM treated larvae (Figure 13E). We then considered the expression levels of *Lactate Dehydrogenase* (*Ldh*), a marker of ER stress activation in *Drosophila*, mediated by Atf4 (Lee et al., 2015). Our results showed that *Ldh* expression was strongly increased in control and in

ReepA^{-541} mutant larvae fed with TM (3 and 2.5 folds as compared to untreated control, respectively), but was decreased in ReepA^{-541} mutant untreated larvae (Figure 13E), suggesting that loss of ReepA do not trigger Perk activation. This observation was further confirmed by western blot analysis showing that phosphorylated eIF2α is not upregulated in ReepA^{-541} mutant background flies (Figure 14A, B). Thus, our results suggest a selective role of ReepA in Atf6 and Ire1 pathways regulation (Napoli et al., 2019).

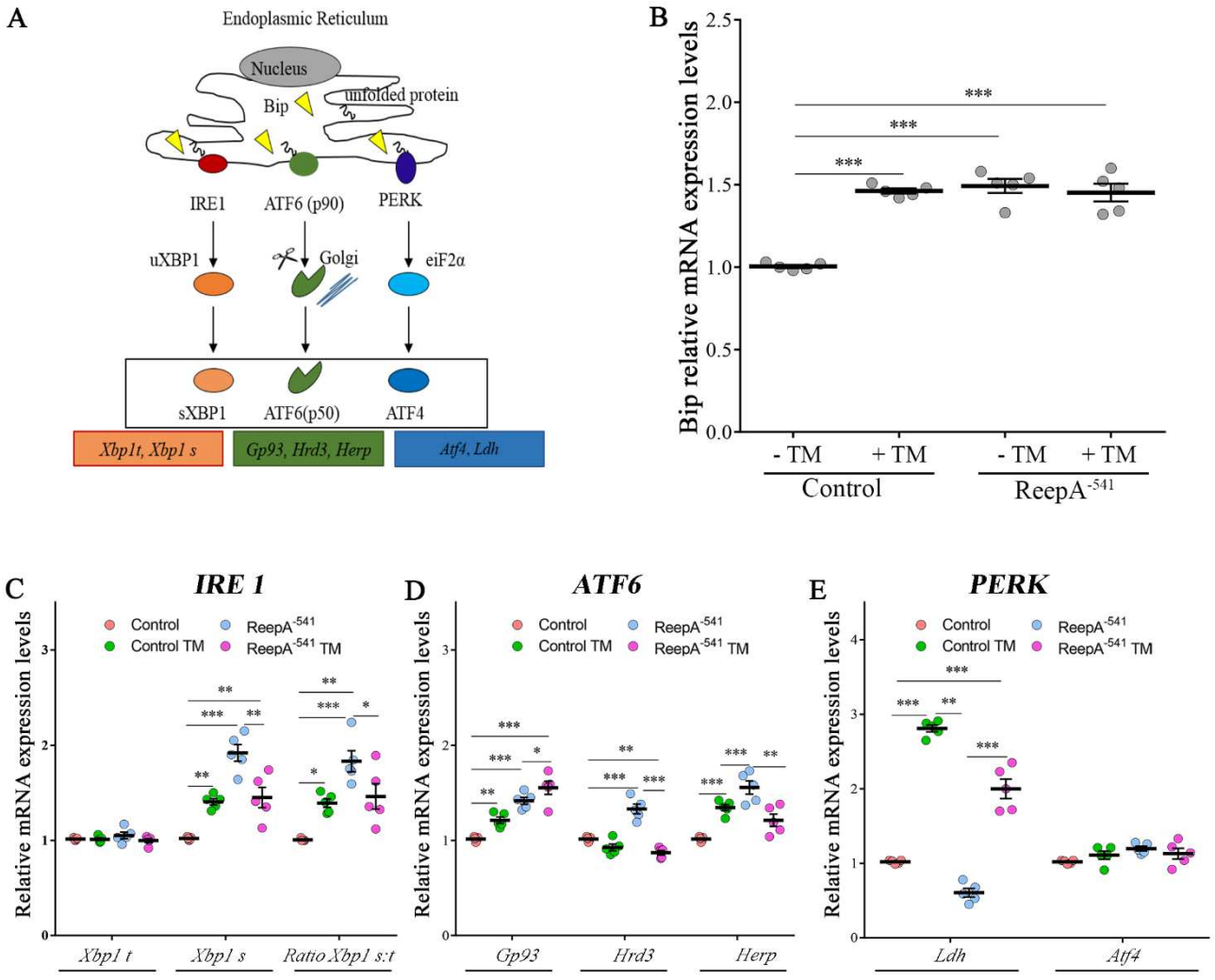

Figure 13. Loss of *ReepA* alters the expression levels of genes involved in Ire1/Xbp1, Atf6 and Perk-Atf4 pathways. **(A)** Schematic representation of the three branches of UPR: PERK, IRE1α, and ATF6. Boxes show the genes considered in our analyses. Relative mRNA expression levels of *Bip* **(B)**, *Xbp1 t* and *Xbp1 s* **(C)**; *Gp93, Hrd3* and *Herp* **(D)**; *Ldh* and *Atf4* **(E)** in control (*ReepA*$^{+C591}$/ *ReepA*$^{+C591}$) and ReepA^{-541} mutant (*ReepA*$^{-541}$/ *ReepA*$^{-541}$) larvae raised on standard food or TM 0.024 mM containing medium. Significance was calculated by using one-way ANOVA with Tukey's post-hoc test. *P < 0.05; **P <0.01; ***P<0.001. The bars indicate s.e.m., n=5 (Napoli et al., 2019).

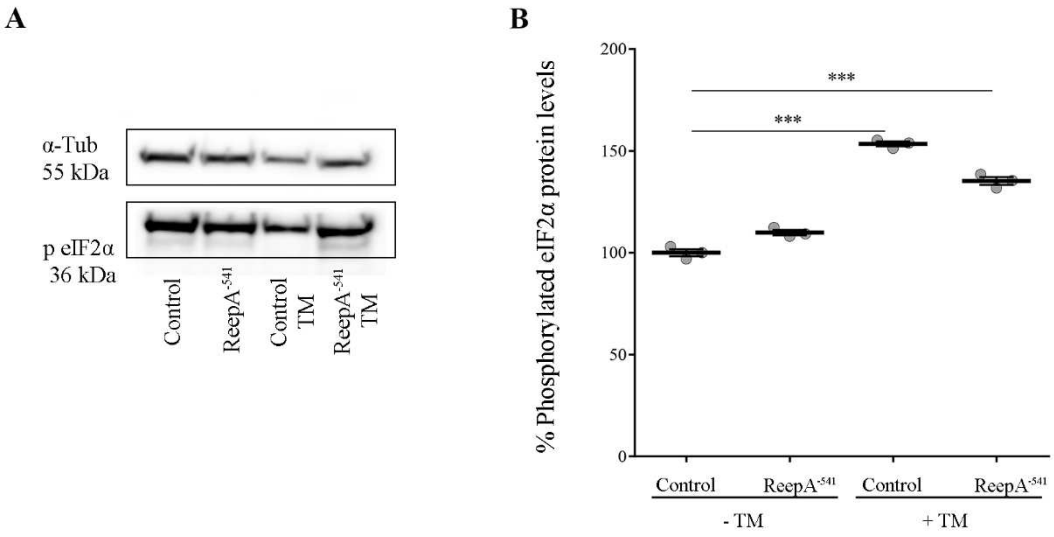

Figure 14. Phosphorylated eIF2α protein expression in ReepA^{-541} mutant and control adults. (A) Western blots showing the phosphorylated eIF2α and α-Tubulin (used as loading control) protein levels in control (*ReepA^{+C591}/ ReepA^{+C591}*) and ReepA^{-541} mutant (*ReepA^{-541}/ ReepA^{-541}*) raised on standard and TM 0.024 mM containing food. **(B)** eIF2α western blot band quantification. Significance was calculated by using one-way ANOVA test with Tukey's post-hoc test ***P<0.001. The bars indicate s.e.m., n=3 (Napoli et al., 2019).

4.4 Lipid droplet biogenesis defects in Drosophila ReepA and spastin HSP models

Lipid droplets (LDs) are specialized cellular organelles that store neutral lipids in all living organisms. LDs are composed by a core, containing mainly triacylglycerides (TAG) and sterol esters (SE), surrounded by a phospholipid monolayer (Ohsaki et al., 2014). Several *in vivo* and cell models of Hereditary Spastic Paraplegia (HSP) show alterations in lipid metabolism caused by a dysregulation of LD biogenesis. In *Drosophila*, D-Spastin downregulation causes a decrease of the LD number in nerves, skeletal muscles and fat bodies (Papadopoulos et al., 2015). REEP1 null mutant mice displays impairment of LDs and lipoatrophy, with significantly decreased visceral fat (Renvoisé et al., 2016). We therefore investigated if a LD phenotype was present in our ReepA^{-541} mutant *Drosophila*.

Third instar larvae were dissected and stained with BODIPY 493/505 probe to visualize lipid droplets in different tissues. We focused our studies on proximal axons departing from ventral nerve cord and quantified the number and size distribution of LDs in control and mutant larvae. We found that proximal axons of ReepA^{-541} mutants have a reduced number of LDs (0.02 LDs/μm2) compared to control flies (0.044 LDs/μm2) (Figure 15B). A similar decrease in LD number was observed in ReepA^{-}

^{541} mutant muscles (Figure 15E). To quantify change in LDs subpopulation, the diameter of LDs was classified into different classes: 0–0.50 µm, 0.51–1 µm and >1.01 µm for muscles quantification; 0–0.50 µm, 0.51–1 µm, 1.01–1.5 and >1.51 µm for neuronal analysis. The quantification of LD size distribution showed an increase of LDs in the range 0–0.50 µm and a simultaneous decrease of class >1.0 µm LDs in D-REEPA mutant in nervous (Figure 15C) and muscle (Figure 15F) tissues. These phenotypes are reminiscent of previous observations in Dspastin loss of function individuals (Papadopoulos et al., 2015).

We then quantified the expression of the two key enzymes, glycerol-3-phosphate acyltransferase (GPAT) and diacylglycerol O-acyltransferase 1 (DGAT1), of fatty acid metabolism, using a real-time RT-PCR approach. In *Drosophila*, GPAT and DGAT1 are encoded by the *Minotaur* (*Mino*) and *Midway* (*Mdy*) genes respectively (Cabirol-Pol et al., 2018). We found that *Mdy* and *Mino* expression levels were reduced in ReepA^{-541} mutant; Dspastin-RNAi decreased *Mino* to 0.70 and *Mdy* to 0.56 (Figure 16 A, B). Our data strongly suggest a functional conservation of ReepA and Spastin in LD biogenesis.

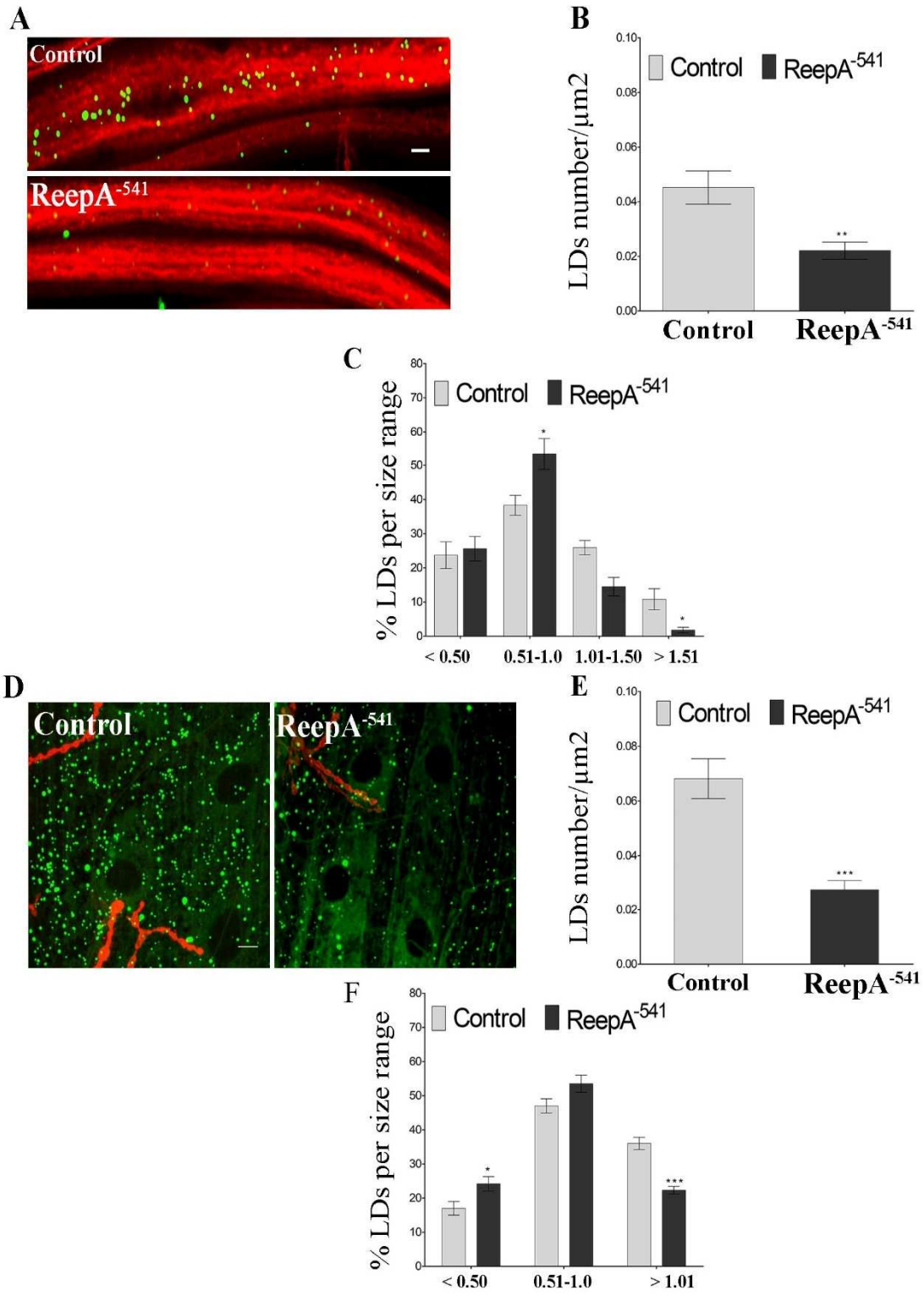
A
Control
ReepA-541
B
LDs number/µm2
Control
ReepA-541
0.10
0.08
0.06
0.04
0.02
0.00
**
Control
ReepA-541
C
% LDs per size range
Control
ReepA-541
80
70
60
50
40
30
20
10
0
*
*
< 0.50
0.51-1.0
1.01-1.50
> 1.51
D
Control
ReepA-541
E
LDs number/µm2
Control
ReepA-541
0.10
0.08
0.06
0.04
0.02
0.00
***
Control
ReepA-541
F
% LDs per size range
Control
ReepA-541
80
70
60
50
40
30
20
10
0
*
***
< 0.50
0.51-1.0
> 1.01

Figure 15. REEPA affects LDs number and size in nerves and skeletal muscles. (A) Representative confocal images of Drosophila REEPA mutant and control larval proximal ventral ganglion nerves labeled with BODIPY 493/503 (green) and HRP-Cy3 (red). Quantification of LD number **(B)** and size **(C)** distribution. **(D)** Representative confocal images of Drosophila D-REEPA mutant and control larval muscles labeled with BODIPY 493/503 (green) and HRP-Cy3(red). Quantification of LD number **(E)** and size **(F)** distribution. Scale bar = 10µm. Significance was calculated by using one way and two-way ANOVA followed by Dunnett's multiple comparison test. *P < 0.05; **P <0.01; ***P<0.001. The bars indicate s.e.m., n=10.

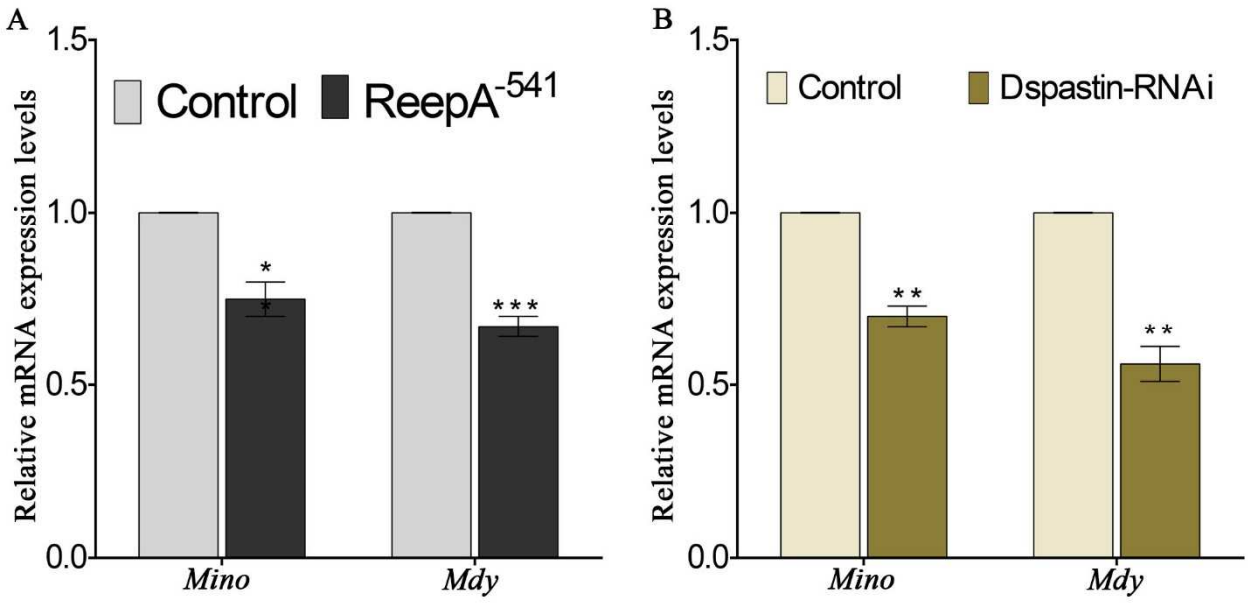

Figure 16. ReepA and Dspastin loss of function alter the expression levels of genes involved in LD synthesis. Relative mRNA expression levels of Mino and Mdy in D-REEPA mutant **(A)** and in UAS-Dspastin-RNAi/Tub-Gal4 **(B)** larvae raised on standard food. Significance was calculated by using one-way ANOVA followed by Dunnett's multiple comparison test. *P<0.05; **P <0.01; ***P<0.001. The bars indicate s.e.m., n=5.

4.5. Naringenin restores locomotor defects and lifespan of ReepA and spastin Drosophila models

In mice, the absence of REEP1 induced motor dysfunctions such as spasticity and weakness in hind limb (Renvoisé et al., 2016). In *Drosophila*, the expression of UAS-D-Spastin-RNAi in a pan-neuronal pattern using the Elav-Gal 4 driver induced behavioral impairments (locomotor and lifespan phenotypes) (Orso et al., 2005). Several *in vivo* studies have shown that naringenin ameliorates

behavioral dysfunctions linked to different neurodegenerative disorders such as Alzheimer, Parkinson, Huntington's disease and amyotrophic lateral sclerosis (Maher, 2019). We therefore tested if naringenin could restore lifespan alterations in Dspastin model.

Firstly, adult flies ubiquitously expressing Dspastin-RNAi (Tubulin-Gal4/RNAiDspastin) and control (Tubulin-Gal4) animals were raised on normal and naringenin containing food. Naringenin was added to the standard medium at final concentrations of 0.3 mM, 0.5 mM and 0.8 mM as within this range naringenin shows beneficial effect on wild type *Drosophila* lifespan (Chattopadhyay et al., 2016). As shown in Figure 17, the Dspastin-RNAi displayed an eclosion rate of 25% compared to control flies (84.5%) when raised on standard medium. While 0.3 mM naringenin had no obvious effects on the eclosion rate (30%). Naringenin 0.5mM showed a significant increase of eclosion rate to 38% and at 0.8mM naringenin has a seemingly detrimental effect with an eclosion rate of 20%. Our data suggest that naringenin at 0.5 mM partially suppress the lethality of Dspastin-RNAi.

In oral administration, naringenin (4',5,7-trihydroxy flavanone) has a low bioavailability. Different groups shown that the complexation with hydroxylpropyl-β-cyclodextrin (HPβCD) increases naringenin bioavailability (Shulman et al., 2011). In order to determine the dosage, we examined the eclosion rate and quantified the number of escapers of adult flies ubiquitously expressing Dspastin-RNAi (Tubulin-Gal4/RNAiDspastin) and control (Tubulin-Gal4) animals and raised on normal, 0.5 mM naringenin and 0.5 mM naringenin complexed with the HPβCD food. As shown in Figure 18, addition of HPβCD increased the eclosion rate of Dspastin-RNAi flies (57%) compared to naringenin alone (38%) thus showing that the naringenin-HPβCD is more effective than naringenin alone. We then performed the climbing assay in Dspastin-RNAi and control flies raised on normal and naringenin- HPβCD containing food. As shown in Figure 19, the flavonoid compound restored the locomotor defects in Dspastin-RNAi.

In order to identify the ideal concentration of naringenin, we conducted a pilot test on ReepA^{-541} mutant and quantified the expression levels of *Bip* transcript using the same range of naringenin-HPβCD complex tested for spastin (0.3 mM, 0.5 mM and 0.8 mM). As for spastin model, the minimum concentration with a complete rescue effect was 0.5 mM (Figure 20) (Napoli et al., 2019).

Finally, we tested the ability of naringenin 0.5 mM complexed with HPβCD to ameliorate climbing activity and lifespan of ReepA^{-541}null mutant flies. As shown in Figure 21 A naringenin extended D-REEPA null mutant lifespan to 75 ± 3 days compared to 60 ± 3 untreated flies. The figure also displayed that in ReepA^{-541} null mutant raised on naringenin containing food possess 33% of locomotor abilities at 30 days compared to the 0% at the same day in flies raised on standard medium (Figure 21 B) (Napoli et al., 2019). Our data suggest that naringenin is capable of reverting the behavioral phenotypes caused by REEP1 and Spastin loss of function.

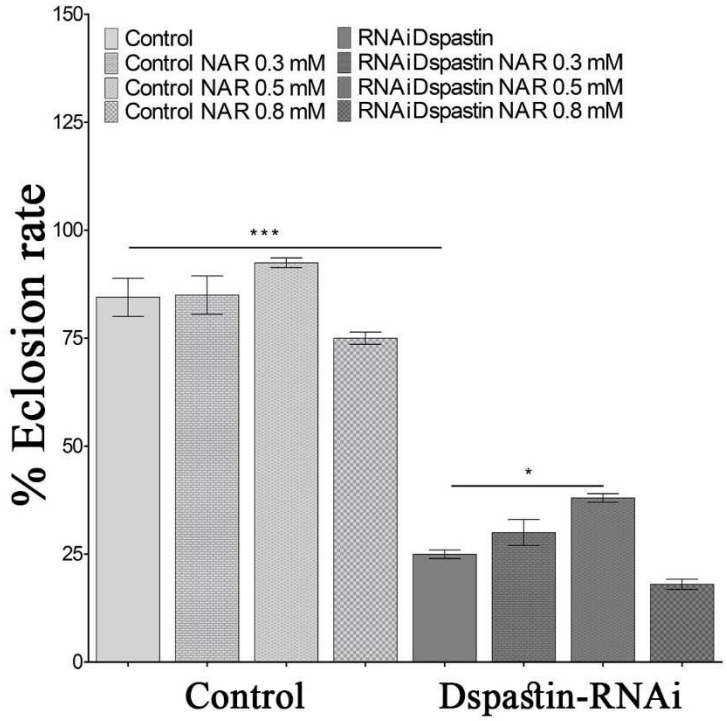

Figure 17. Effects of naringenin in Dspastin-RNAi flies' lifespan. Eclosion rate of neuronal transgenic expression of control and Dspastin-RNAi raised on standard or naringenin containing food. The concentrations used were 0.3 mM, 0.5 mM and 0.8mM. Significance was calculated by using one-way ANOVA Dunnett's multiple comparison test. *P < 0.05. The bars indicate s.e.m., n=10 (20 flies for each vial). Significance was calculated using one-way using one-way ANOVA test with Tukey's post-hoc test. * P <0.05; ***P<0.001. The bars indicate s.e.m. n=10 (20 flies for each vial).

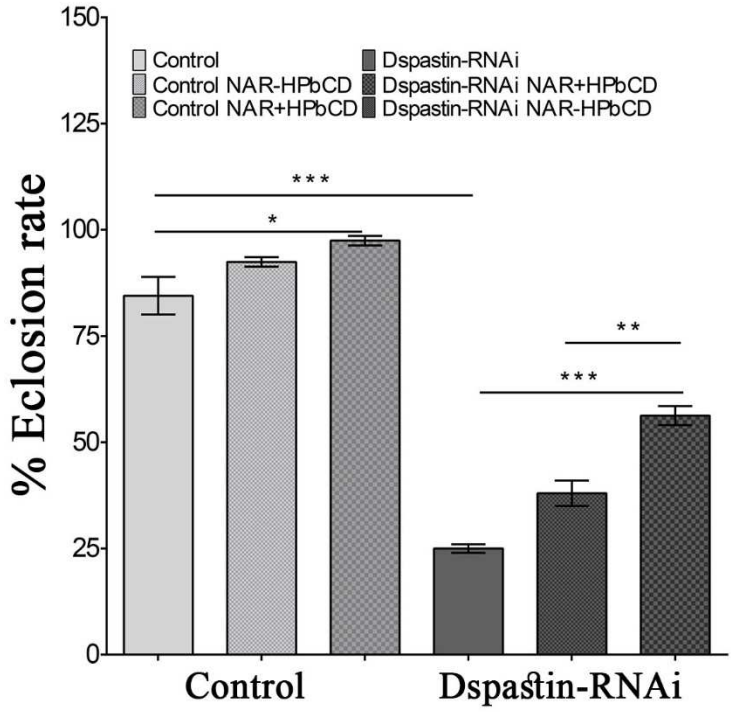

Figure 18. Effects of naringenin-HPβCD in Dspastin-RNAi flies' lifespan. Eclosion rate of neuronal transgenic expression of Dspastin-RNAi raised on NAR 0.5 mM alone or NAR 0.5 mM complexed (HPβCD) containing standard food. Significance was calculated using one-way using one-way ANOVA test with Tukey's post-hoc test. * P <0.05; **P<0.01; ***P<0.001. The bars indicate s.e.m. n=10 (20 flies for each vial).

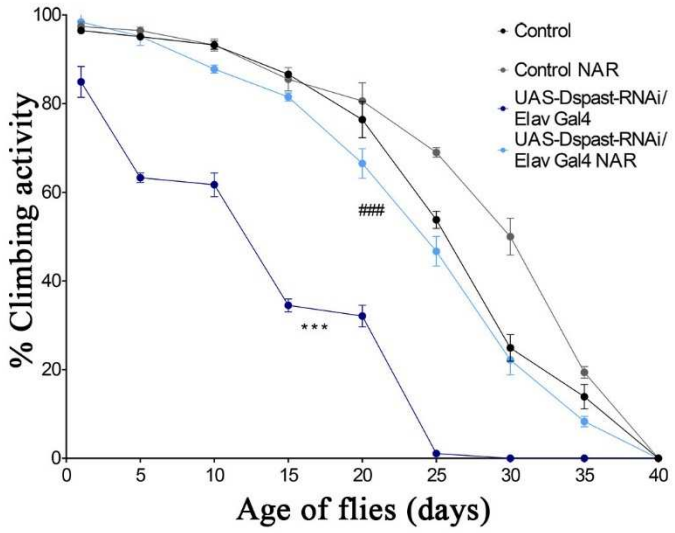

Figure 19. **Naringenin ameliorates Dspastin-RNAi flies' climbing activity.** Climbing activity in control and neuronal transgenic expression of Dspastin-RNAi raised on NAR containing standard food and tested at 0, 5, 10, 15, 20, 25, 30, 35 and 40 days. Significance was calculated using one-way using one-way ANOVA test with Tukey's post-hoc test. ***P<0.001 vs Control; ### P< 0.001 vs UAS-Dspastin RNAi/Elav-Gal4. The bars indicate s.e.m. n=10 (20 flies for each vial).

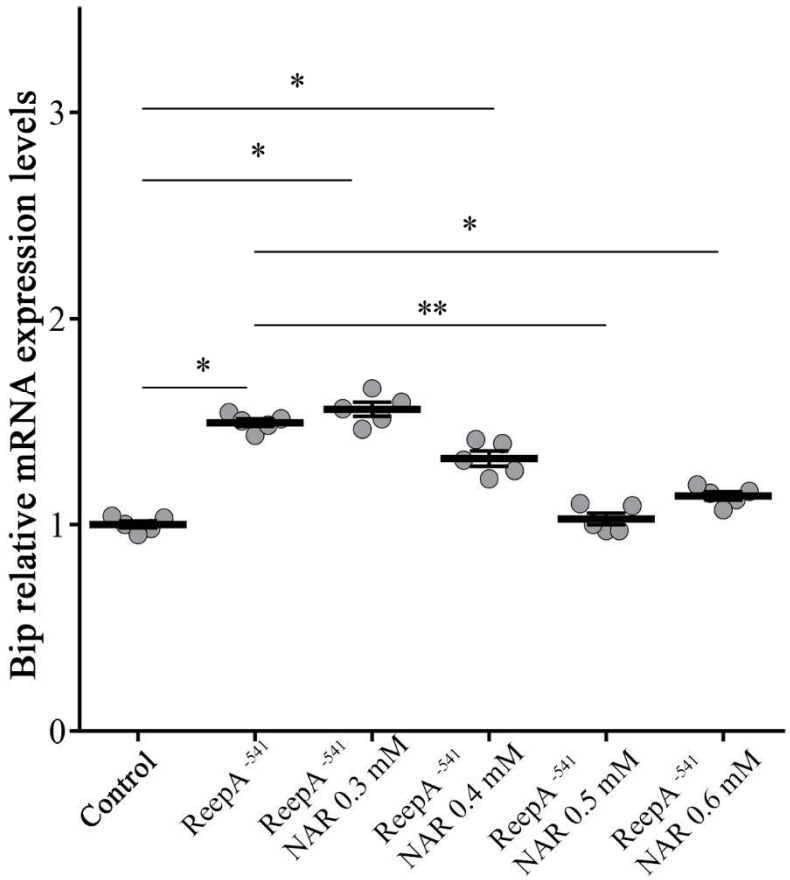

Figure 20. Real time PCR of *Bip* gene. Relative mRNA expression levels of *Bip* in control (*ReepA*$^{+C591}$/ *ReepA*$^{+C591}$) and ReepA^{-541} mutant (*ReepA*$^{-541}$/ *ReepA*$^{-541}$) larvae raised on standard food or NAR 0.3, 0.5 and 0.8 mM containing medium. Significance was calculated by using one-way ANOVA with Tukey's post-hoc test. *P < 0.05; **P <0.01. The bars indicate s.e.m., n=5 (Napoli et al., 2019).

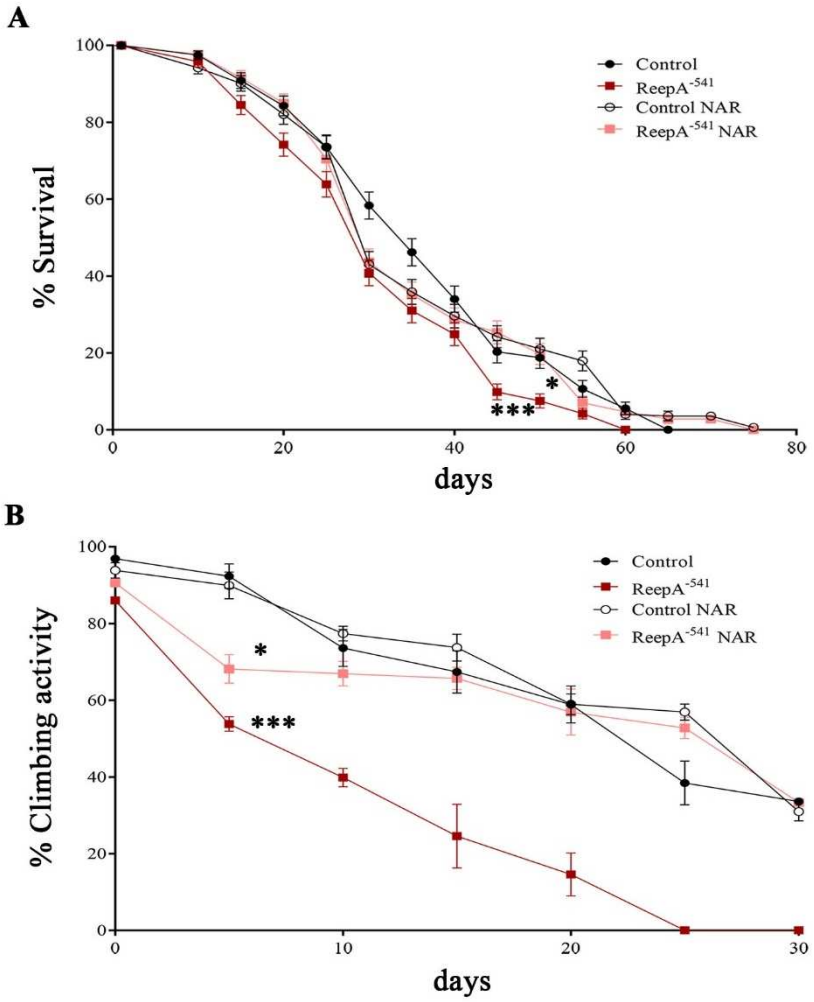

Figure 21. Naringenin ameliorates ReepA^{-541} flies' lifespan and climbing activity. (A) Lifespan in control (*ReepA^{+C591}/ ReepA^{+C591}*) and ReepA^{-541} mutant (*ReepA^{-541}/ ReepA^{-541}*) raised on NAR 0.05 mM enriched or standard food. Significance was calculated using log-rank Mantel-Cox test. P value: * P < 0.05 (ReepA^{-541} mutant NAR vs ReepA^{-541} mutant), P value: *** P<0.001 (ReepA^{-541} mutant vs control), n=10 (30 flies for each vial). **(B)** Climbing activity in control (*ReepA^{+C591}/ ReepA^{+C591}*) and ReepA^{-541} mutant (*ReepA^{-541}/ ReepA^{-541}*) raised on NAR 0.05 mM enriched or standard food and tested at 0, 5, 10, 15, 20, 25, 30 and 35 days. Significance was calculated using one-way ANOVA with Tukey's post-hoc test. P value: * P < 0.05 (ReepA^{-541} mutant NAR vs ReepA^{-541} mutant), * P < 0.05 (ReepA^{-541} mutant vs control). The bars indicate s.e.m., n=10 (20 flies for each vial) (Napoli et al., 2019).

4.6 ER homeostasis defects of ReepA^{-541} mutant are rescued by naringenin administration

We focused our experiments on testing the effects of naringenin on ReepA^{-541} mutant-associated ER phenotypes. Larvae were grown in 0.5 mM naringenin complexed with HPβCD and the UPR response levels were detected. Administration of naringenin totally rescued *Bip, Xbp1 s, Hrd3, Herp* and *Ldh* expression levels of ReepA^{-541} mutant (Figure 22). Of note, as shown in Figure 22, control larvae treated with the flavonoid displayed a transcription profile of UPR genes similar to that of untreated larvae. We also analyzed the effect of naringenin on ER morphology and we found that naringenin treatment was able to reduce the cisternae-like structures caused by the loss of ReepA (Figure 26 A, B, C) (Napoli et al., 2019).

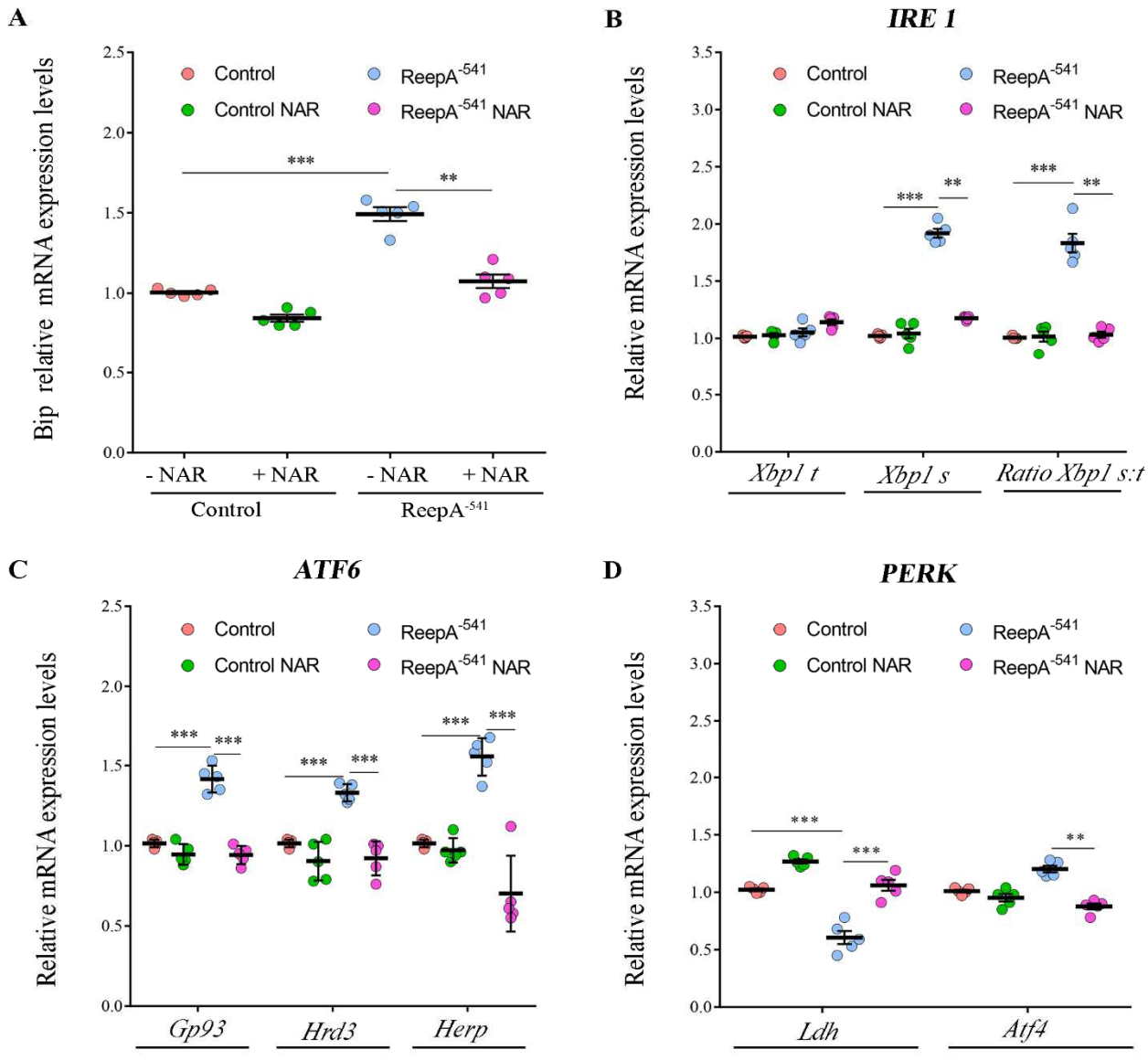

Figure 22. Naringenin restores the expression levels of the genes involved in Ire1/Xbp1, Atf6 and Perk-Atf4 pathways in ReepA^{-541} mutant. Relative mRNA levels of *Bip* **(A)**, *Xbp1 t* and *Xbp1 s* **(B)**, *Gp93, Hrd3* and *Herp* **(C)**, *Ldh* and *Atf4* **(D)** in control (*ReepA^{+C591}/ ReepA^{+C591}*) and ReepA^{-541} mutant (*ReepA^{-541}/ ReepA^{-541}*) larvae raised on NAR 0.5 mM enriched or standard food. Significance was calculated by using one-way ANOVA with Tukey's post-hoc test. **P < 0.01; ***P <0.001. The bars indicate s.e.m., n=5 (Napoli et al., 2019).

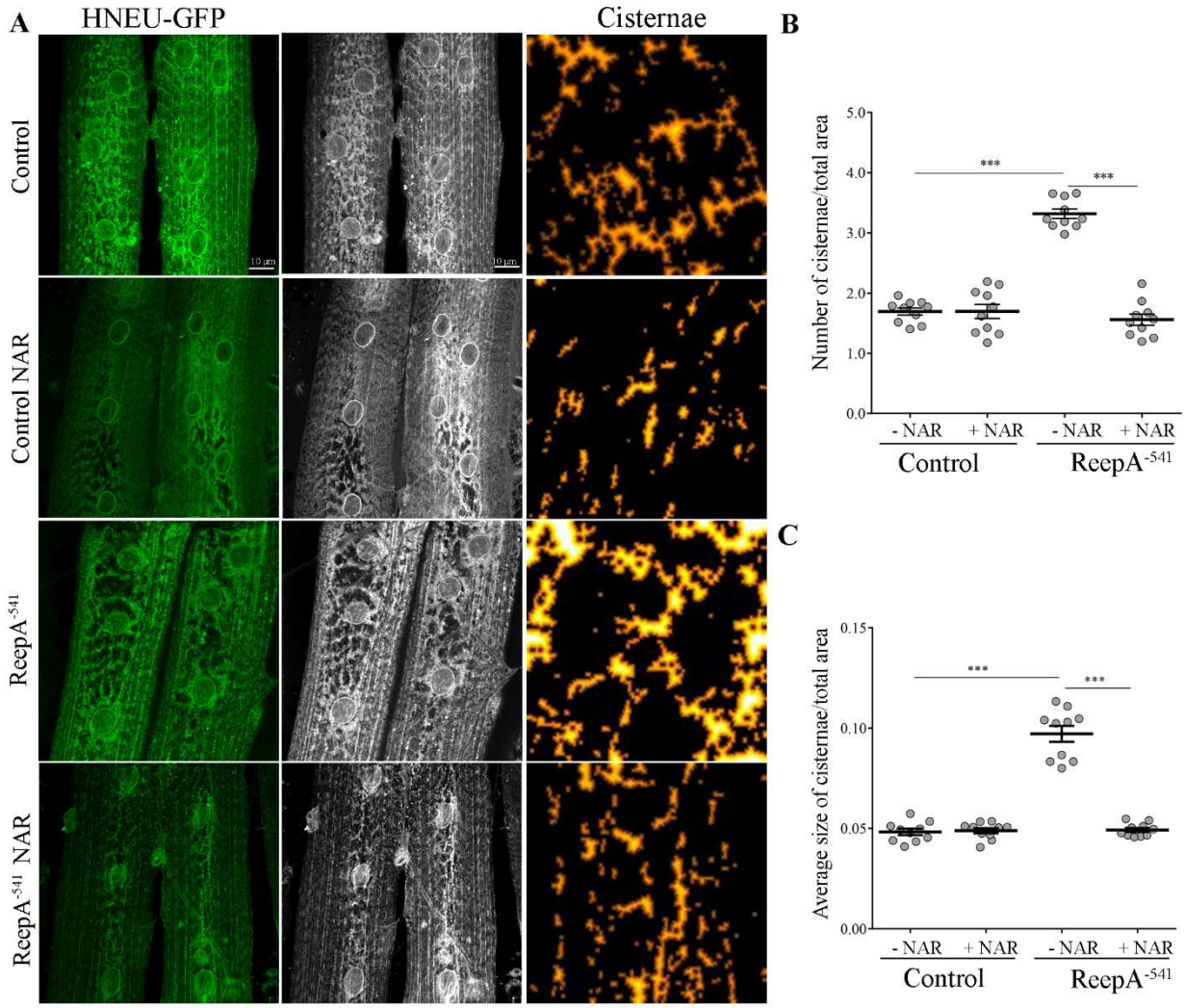

Figure 23. Naringenin rescues ReepA^{-541} mutant ER morphology defects. (A) Representative confocal images of muscle 6/7 of abdominal segment A3 of control (*ReepA^{+C591}/ ReepA^{+C591}; Tubulin-Gal4/ UAS HNEU-GFP*) and ReepA^{-541} mutant (*ReepA^{-541}/ ReepA^{-541}; Tubulin-Gal4/ UAS HNEU-GFP*) third instar larvae expressing ubiquitously UAS HNEU-GFP raised on standard or NAR 0.5 mM enriched food. Scale bar=10 µm. Quantification of cisterna-like structures number **(B)** and size **(C)** of ER- marker HNEU-GFP. Significance was calculated by using one-way ANOVA with Tukey's post-hoc test. ***P<0.001. The bars indicate s.e.m., n=10 larvae (Napoli et al., 2019).

4.7 Naringenin regulates lipid droplets biogenesis in Drosophila melanogaster

Flavonoids are natural phenolic compounds that exert beneficial effects on cardiovascular disorders, neuronal diseases, inflammation and obesity in animals as well as in humans (JOSEPH et al., 2007; Kawser Hossain et al., 2016; Mozaffarian and Wu, 2018). These protective properties are linked to their free radicals scavenger activity, inhibition of enzymes activity (lipoxygenase, xanthine oxidase); modulation of lipid kinase signaling (Janda et al., 2016; Panche et al., 2016). Several *in vivo* studies have shown that flavonoids play an important role in lipid metabolism reducing body weight gain, food consumption and fat accumulation (Assini et al., 2013; Liu et al., 2016). In mammals adipose tissue flavonoids induce lipolysis through inhibition of cyclic phosphodiesterases (PDEs) and antagonism of cyclic adenosine monophosphate degradation (Janda et al., 2016). In *Drosophila*, flavonoids display potent effects on LD biogenesis in a tissue-specific manner. Xhanthohumol (a prenilated flavonol) and isoquercetin (flavonol) induce an increase of LDs in nerves and muscles (Fantin et al., 2019). We therefore tested the effects of naringenin to investigate its role in LD biogenesis of wild type larvae.

Third instar larvae were grown in 0.5 mM naringenin complexed with HPβCD and were dissected and stained with BODIPY 493/505 probe to visualize lipid droplets in different tissues. We focused our studies on proximal axon departing from ventral nerve cord and on muscles and then we quantified the number and size of LDs in wild type larvae. Our data suggested that naringenin increased the number (0.058 LDs/μm^2) and the size (1.02 µm) of LDs compared to control larvae number 0.044 LDs/μm^2 and size 0.087 µm in nerves (Figure 24 B, C). In muscle tissues, naringenin treatment induces a robust increase in LD number (0.11 LDs/μm^2) and size (0. 074 µm) compared to control larvae (Figure 24 E, F).

We then quantified the expression of the two key enzymes of fatty acid metabolism *Mino* and *Mdy*, using a real-time RT-PCR approach. We found that *Mino* and *Mdy* mRNA levels were strongly up-regulated in naringenin to 1.30-fold and to 1.5-fold respectively compared to control larvae (Figure 25). Our data confirmed that naringenin acts as strong modulator of LDs biogenesis *in Drosophila.*

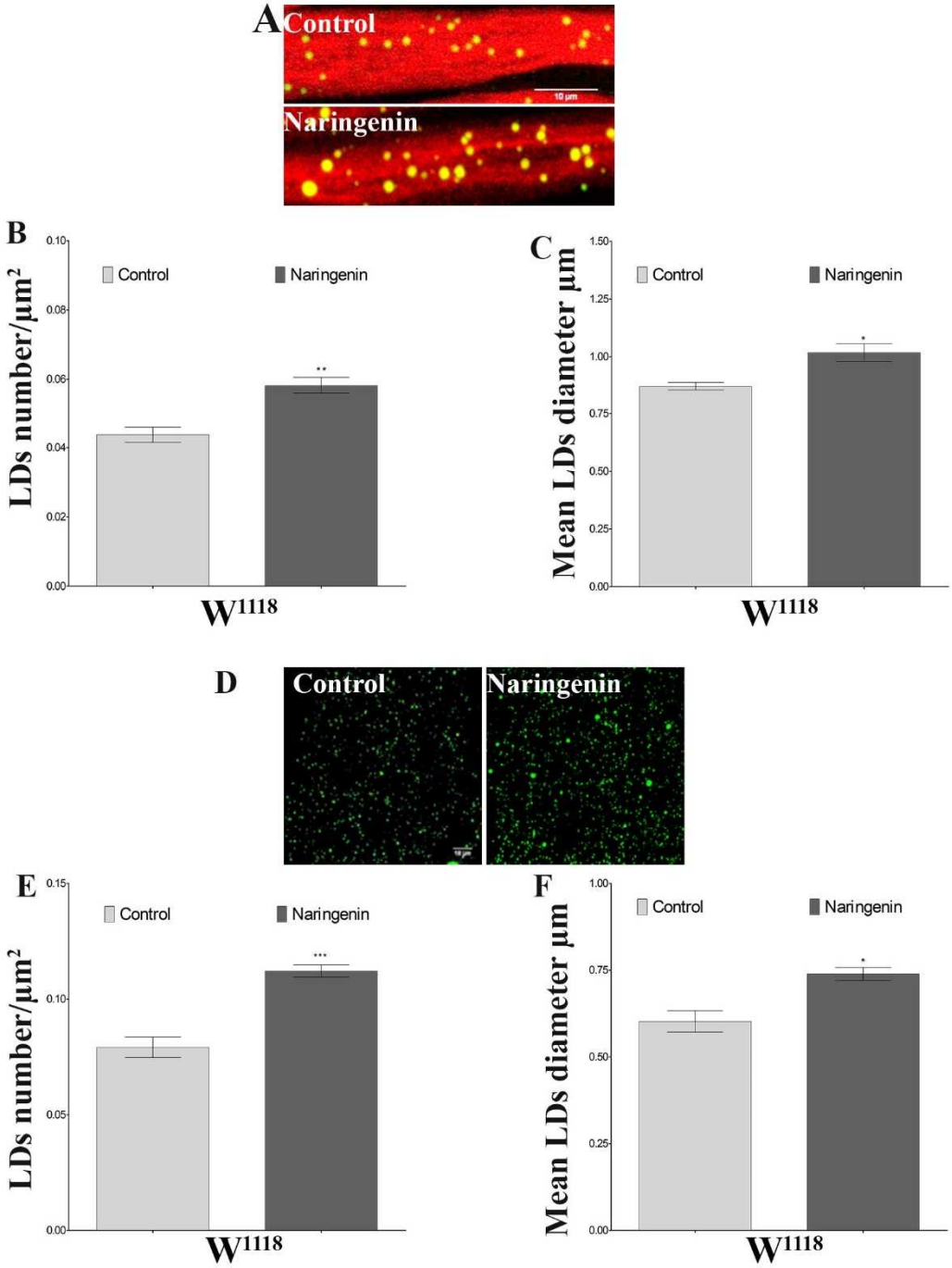

Figure 24. Naringenin modulates LDs number and size in nerves and skeletal muscles. (A) Representative confocal images of Drosophila control larval proximal ventral ganglion nerves labeled with BODIPY 493/503 (green) and HRP-Cy3 (red) and raised on standard and naringenin 0.5 mM complexed with HPβCD containing food. Quantification of LDs number **(B)** and size **(C)**. **(D)** Representative confocal images of Drosophila control larval muscles labeled with BODIPY 493/503 (green) and HRP-Cy3(red) and raised on standard and naringenin 0.05 mM enriched food. Quantification of LDs number **(E)** and size **(F)**. Scale bar = 10µm. Significance was calculated by using one-way ANOVA followed by Dunnett's multiple comparison test. *P < 0.05; **P <0.01; ***P<0.001. The bars indicate s.e.m., n=10.

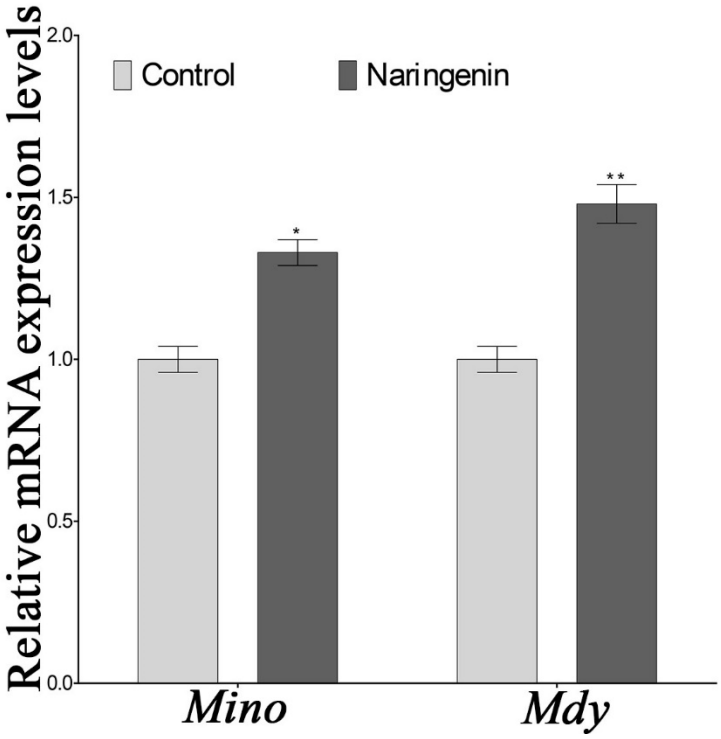

Figure 25. Flavonoids modulate positively the expression levels of the genes involved in LDs biogenesis in control larvae. Relative mRNA levels of Minotaur (Mino) and Midway (Mdy) in control larvae raised on standard or naringenin 0.5 mM- HPβCD containing food. Significance was calculated by using one-way ANOVA Dunnett's multiple comparison test. ***P <0.001. The bars indicate s.e.m., n=5.

4.8 Naringenin administration ameliorates ReepA and Dspastin LDs depletion

We tested the capacity of naringenin to rescue ReepA^{-541} and Dspastin loss of function associated LDs phenotypes. Naringenin administration restored LDs number in the muscles (Figure 26 B, C and Figure 27 B) and nervous system (Figure 26 E, F and Figure 27 D) of both HSP models. We also found that naringenin restored the transcript expression of *Mdy* and *Mino* in both SPG models (Figure 28 A, B).

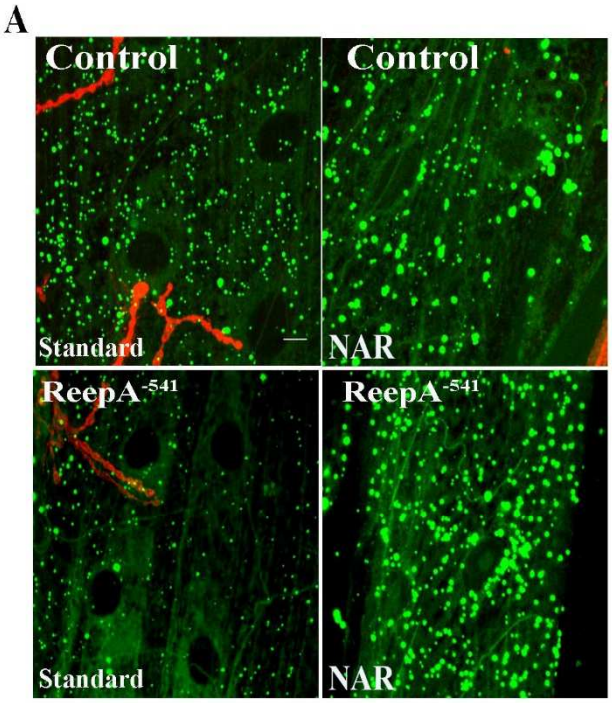
A
Control
Control
Standard
NAR
ReepA-541
ReepA-541
Standard
NAR

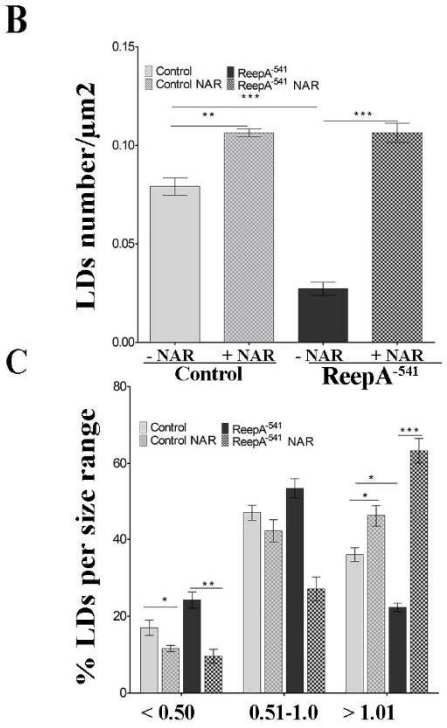
B
LDs number/µm2
Control
Control NAR
ReepA-541
ReepA-541 NAR
- NAR
+ NAR
- NAR
+ NAR
Control
ReepA-541
C
% LDs per size range
< 0.50
0.51-1.0
> 1.01

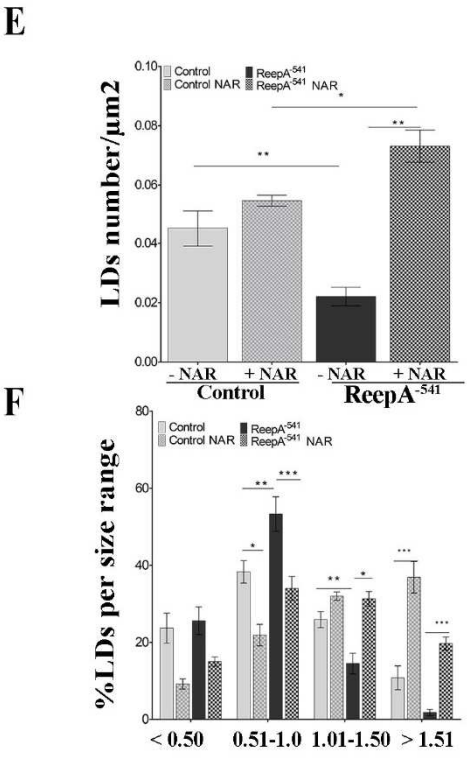
E
LDs number/µm2
Control
Control NAR
ReepA-541
ReepA-541 NAR
- NAR
+ NAR
- NAR
+ NAR
Control
ReepA-541
F
%LDs per size range
< 0.50
0.51-1.0
1.01-1.50
> 1.51

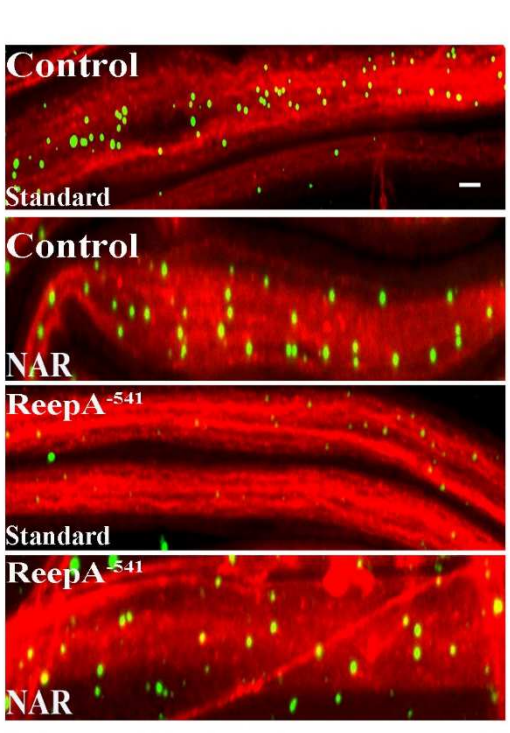
D
Control
Standard
Control
NAR
ReepA-541
Standard
ReepA-541
NAR

Figure 26. Naringenin restored the LDs number and size in D-REEPA mutant in skeletal muscles and nerves. **(A)** Representative confocal images of *Drosophila* REEPA mutant and control larval muscles labeled with BODIPY 493/503 (green) and HRP-Cy3 (red), raised on standard and 0.5 mM NAR enriched food. Quantification of LDs number **(B)** and size **(C)** distribution. **(D)** Representative confocal images of Drosophila REEPA mutant and control larval proximal ventral ganglion nerves labeled with BODIPY 493/503(green) and HRP-Cy3 (red), raised on standard and NAR 0.5 Mm enriched food. Quantification of LDs number **(E)** and size **(F)** distribution. Scale bar = 10µm. Significance was calculated by using one way and two way ANOVA. *P < 0.05, **P <0.01, ***P<0.001. The bars indicate s.e.m., n=10.

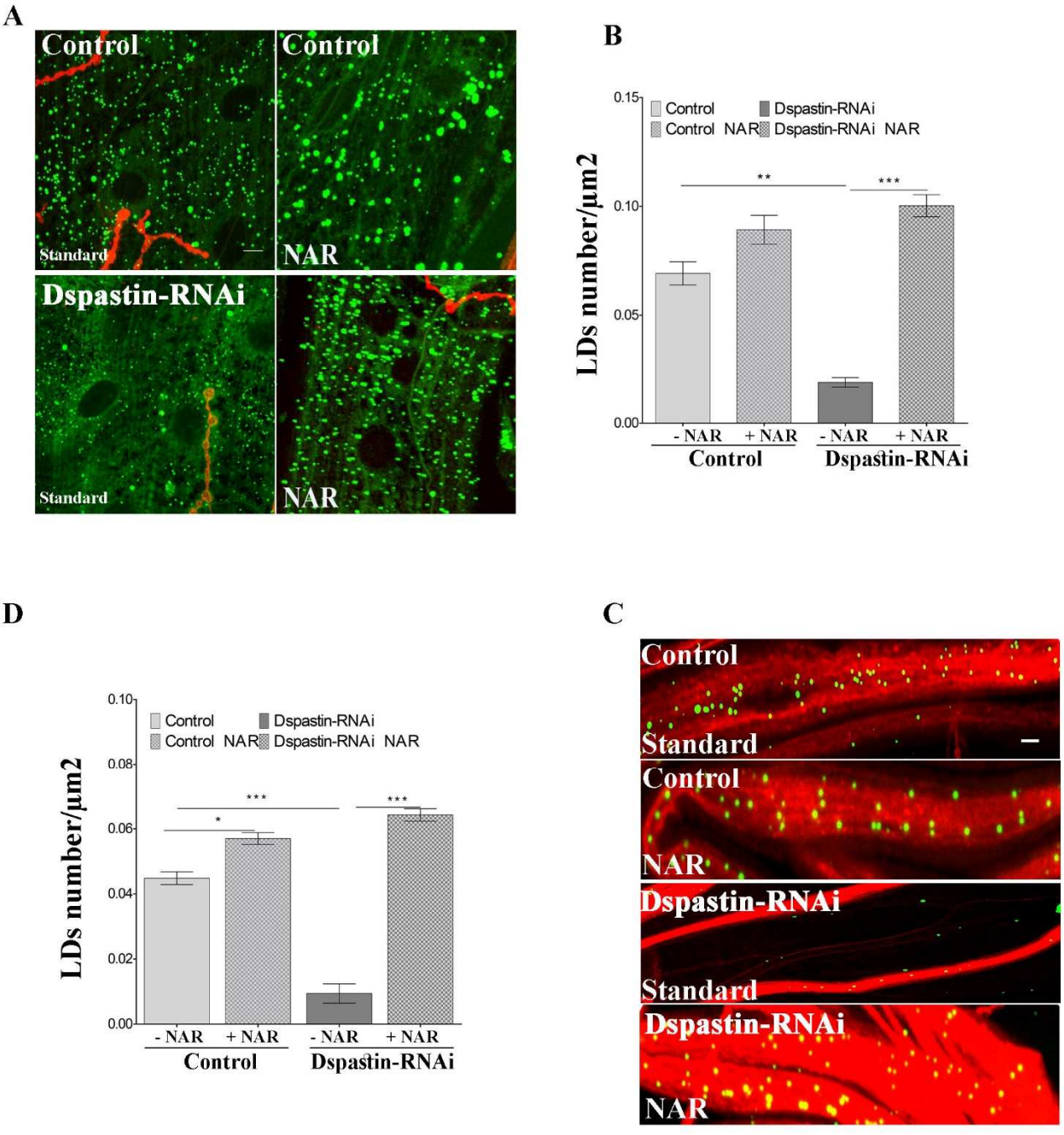

Figure 27. Naringenin restored the LDs number and size in Dspastin-RNAi in skeletal muscles and nerves. (A) Representative confocal images of Drosophila Spastin loss of function and control larval muscles labeled with BODIPY 493/503 (green) and HRP-Cy3 (red). Quantification of LDs number **(B)** and size **(C)** distribution. **(D)** Representative confocal images of Drosophila REEPA mutant and control larval proximal ventral ganglion nerves labeled with BODIPY 493/503 (green) and HRP-Cy3 (red). Quantification of LDs number **(E)** and size **(F)** distribution. Scale bar = 10µm. Significance was calculated by using one way and two-way ANOVA. *P<0.05, **P <0.01, ***P<0.001. The bars indicate s.e.m., n=10.

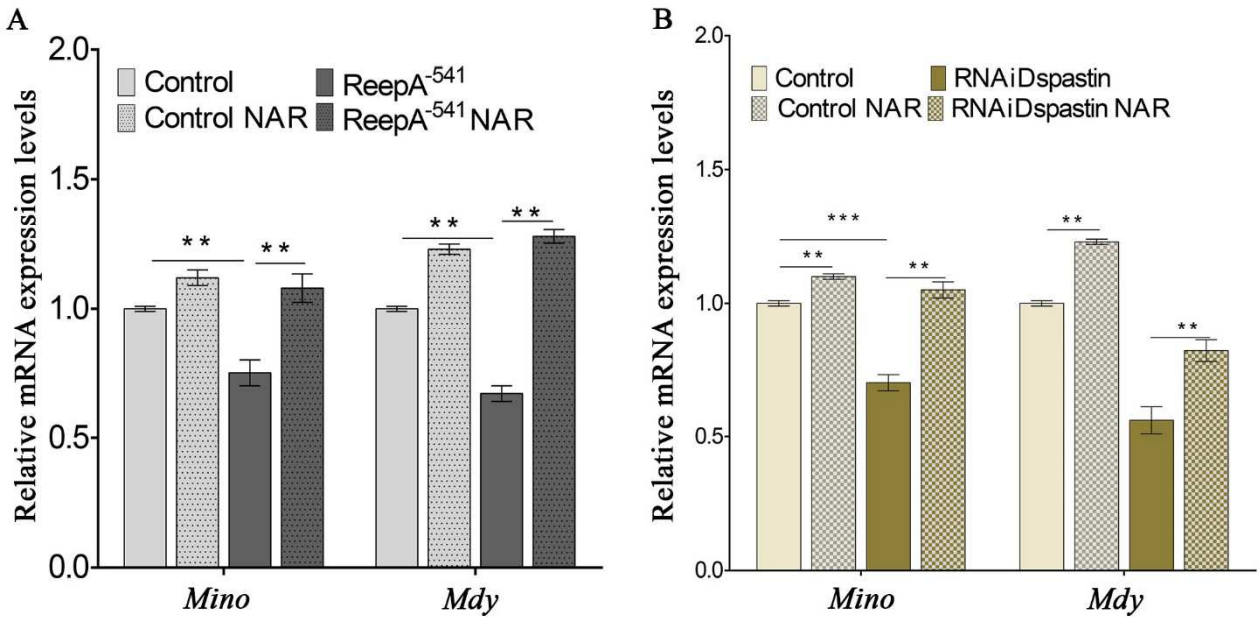

Figure 28. Naringenin restored the LDs the transcription levels of *Mino* and *Mdy*. Relative mRNA expression levels of *Mino* and *Mdy* in D-REEPA mutant **(A)** and in Dspastin-RNAi **(B)** larvae raised on standard food. Significance was calculated by using one way and two-way ANOVA. **P <0.01. The bars indicate s.e.m., n=4.

4.9 ReepA and Dspastin loss of function cause autophagic pathway and lysosomes alterations

Recently, *in vitro* experiments have shown that the interaction between Spastin and ESCRT protein IST1 at ER-endosome contacts drives endosomal tubule fission and the failure of fission caused disrupted lysosomal enzyme trafficking and abnormal lysosomal morphology. Consistent with a role for ER-mediated endosomal tubule fission in lysosome function, similar lysosomal abnormalities

were seen in cellular models lacking the WASH complex component strumpellin or in cortical neurons of REEP1 knockout mouse (Allison et al., 2017). Lysosomal abnormalities may alter many pathways in which these organelles are involved, including autophagy. These variations may reflect a connection between lipid metabolism alterations and organelle, i.e. the ER shaping thereby suggesting plausible links between the different cellular processes altered in HSP (Boutry et al., 2019). Several neurodegenerative disorders such as Alzheimer's disease, Parkinson disease, amyotrophic lateral sclerosis are often characterized by the formation of abnormal protein aggregates and dysregulation of autophagic pathway (Nah et al., 2015).

To study the role of Dspastin and D-ReepA in lysosomal function, we analyzed both the size and the number of lysosomes in control, Dspastin and D-ReepA loss of function larvae using an RNA interference approach (RNAi).

To visualize the lysosomes in *Drosophila* tissues, we ubiquitously expressed the Lamp1-GFP transgenic line, a GFP tagged version of the lysosome-associated membrane protein (Lamp) which is considered a useful marker to monitor lysosome morphology and biogenesis in *Drosophila* (Mauvezin et al., 2014). Down-regulation of Dspastin and D-ReepA affected lysosome number and size as shown in Figure 29 A, B, C causing accumulation of large lysosomes and suggesting a defective trafficking or functionality of lysosomes.

We then analyzed the effects of loss of Dspastin and D-ReepA on autophagy. To investigate the role of Dspastin and D-ReepA in the autophagic pathway, we firstly measured the autophagosomes formation and maturation in our models by expressing the monomeric tandem mCherry-GFP-Atg8 a marker. Formation of autophagosomes produces an increase of GFPpositive/mCherry-positive (yellow) puncta that become GFP-negative/mCherry-positive (red) when autophagosomes fuse with lysosomes. When autophagy is induced, as in starved condition, yellow and red puncta increase. Finally, when lysosomal acidification or lysosome fusion are blocked by chloroquine or bafilomycin the yellow puncta increase while red puncta decrease.

In order to analyze if autophagic flux was defective after down-regulation of Dspastin and D-ReepA, we quantified the number of mCherry positive/GFP negative, mCherry positive/ GFP positive vesicle and red/yellow ratio under standard food, during starvation and after chloroquine treatment (Figure 30 A, C, E).

As shown in Figure 30 B, both Dspastin and D-ReepA down-regulation caused the accumulation of yellow puncta and the decrease of red puncta compared to control larvae. Under starved condition, both ReepA-RNAi and Dspastin-RNAi displayed a strong reduction of ratio between red and yellow puncta compared to control larvae (Figure 30G), indicating a defective formation of acidic

autolysosomes vesicles. This result suggests that lysosomal acidification or lysosome fusion are blocked when Spastin and D-ReepA are absent.

Chloroquine, that neutralizes the lysosomal pH, is a potent inhibitor of autophagic pathway and the treatment with this drug increases the number of immature autophagosomes (yellow puncta) and decrease the number of red puncta for area (Figure 30 E, F) compared to the control in standard condition (Figure 30 A, B). When control flies were grown in chloroquine the yellow puncta increase and red puncta decrease as expected (Figure 30F). In Dspastin and D-ReepA loss of function flies grown in chloroquine the ratio red/yellow puncta is similar to the control indicating a complete block of authophagosomes/lysosomes fusion (Figure 30G).

To investigate the possible block of autophagosomes/lysosomes fusion, we co-expressed Lamp1-GFP and mCherry Atg8 transgenic lines with ReepA-RNAi and Dspastin-RNAi lines under the control of Tubulin-Gal4 driver line. Formation of autolysosomes produces an increase of GFPpositive/mCherry-positive (yellow) puncta indicating that autophagosome (red puncta) are fused with lysosomes (green puncta). Both HSP models presented a reduction of red puncta and yellow puncta under standard condition (Figure 31A, B). Induction of autophagy by starvation in control larvae causes an increase of yellow puncta and the yellow/red (autolysosomes/autophagosomes) ratio is strongly increased. Conversely, in both RNAiDspastin and RNAiREEPA the ratio is strongly reduced indicating a block of authophagosomes/lysosomes fusion compared to the control larvae. This hypothesis was confirmed from the data obtained by chloroquine treatment where the yellow/red ratio decreased in control as expected and both HSP models larvae displayed similar values (Figure 31G).

In several studies, flavonoids are used alone or in combination with other compounds as autophagy modulators in the treatment of many disorders such as cardiovascular, hepatic, diabetes and neurodegeneration diseases, all characterized by a deregulation of autophagic pathway (Prieto-Domínguez et al., 2018). We thus investigated the autophagosomes maturation and lysosomes morphology in D-ReepA and Dspastin loss of function raised on naringenin enriched food. Naringenin administration restored the autophagic defects in both HSP models. In D-ReepA and Dspastin loss of function ubiquitously expressing the tandem GFP-mCherry-Atg8a, the ratio red/yellow puncta is similar to control larvae raised under standard condition (Figure 32F). In DReepA-RNAi and Dspastin-RNAi ubiquitously co-expressing Lamp 1-GFP and mCherryAtg8, the ratio yellow/red puncta is similar to control larvae raised under standard condition (Figure 32 I). Finally, naringenin administration increased the number and the size of lysosomes in both HSP models. Our data suggested that naringenin could restore the autophagic deregulation-related to Drosophila HSP models (Figure 32 B, C).

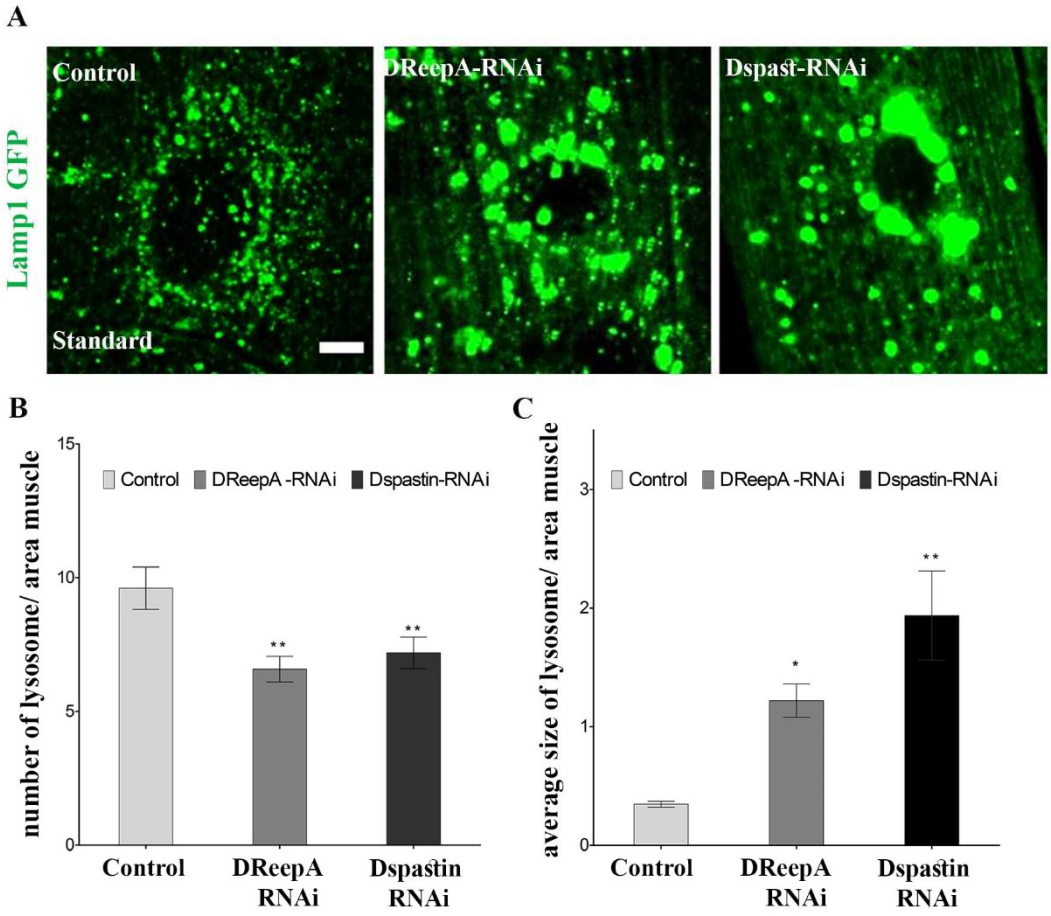
A
Control
DReepA-RNAi
Dspast-RNAi
Lamp1 GFP
Standard
B
number of lysosome/ area muscle
Control
DReepA -RNAi
Dspastin-RNAi
Control
DReepA RNAi
Dspastin RNAi
C
average size of lysosome/ area muscle
Control
DReepA -RNAi
Dspastin-RNAi
Control
DReepA RNAi
Dspastin RNAi

Figure 29. REEPA and Dspastin down regulation cause lysosomes morphology defects. **(A)** Representative confocal images of *Drosophila* REEPA loss of function and Dspastin loss of function larval muscles ubiquitously expressing Lamp1-GFP (Tub-Gal4 > UAS-Lamp1-GFP). Quantification of the number **(B)** and of the mean size **(C)** of Lamp1-GFP punctae. Scale bar = 10µm. Significance was calculated by using Student's t-test. *P <0.05. The bars indicate s.e.m., n=10.

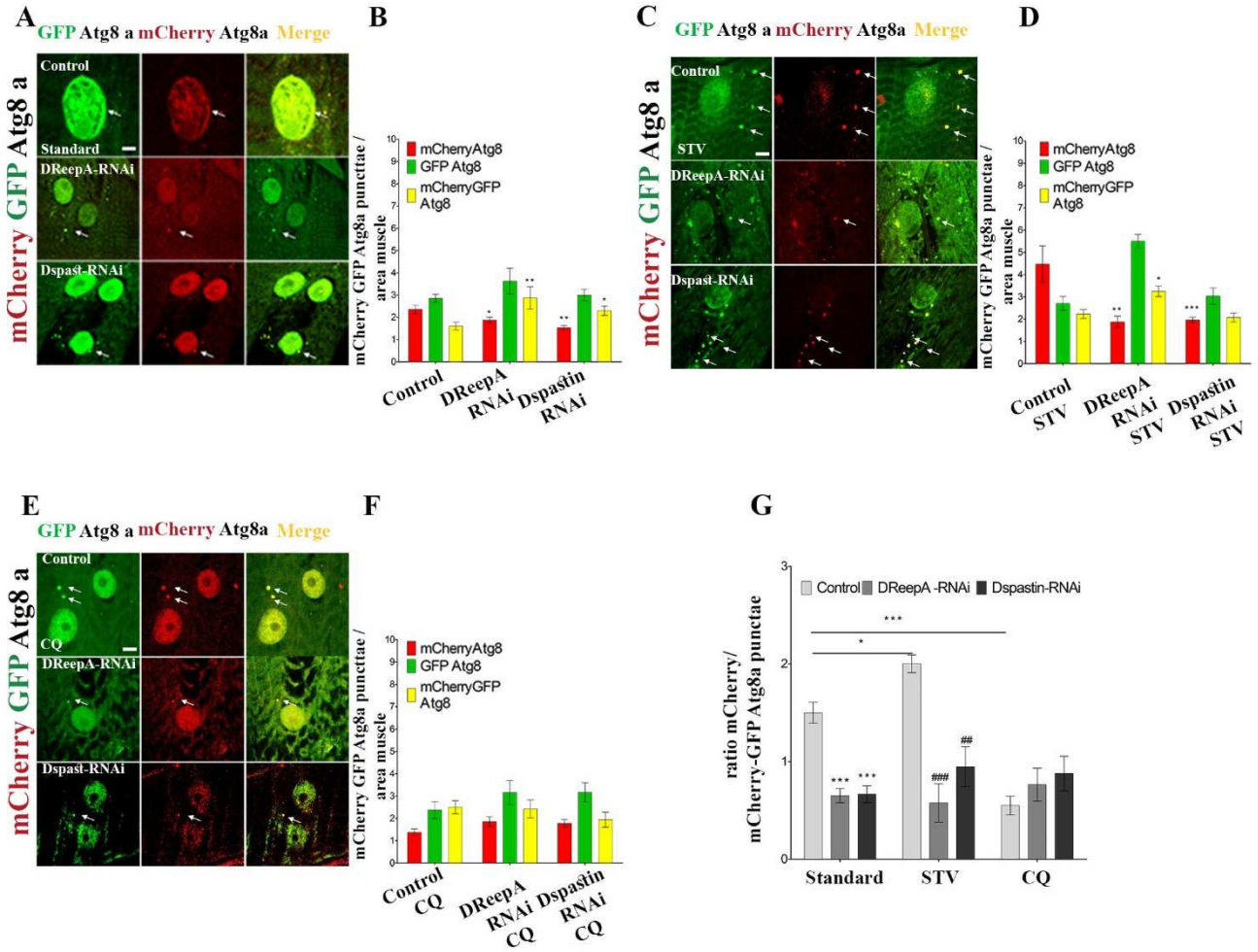

Figure 30. REEPA and Dspastin down regulation impairs the formation of acid autolysosomes. Representative confocal images of Drosophila REEPA-RNAi and Dspastin-RNAi larval muscles ubiquitously expressing the tandem mCherry-GFP-Atg8a (Tub-Gal4 > UAS-mCherry-GFP-Atg8a) in standard medium **(A)**, in stress condition (STV) **(C)** and in Chloroquine (CQ) **(E)**. Quantification of the number of mCherry-GFP-Atg8 puncta in standard medium **(B)**, in stress condition (STV) **(D)** and in Chloroquine (CQ) **(F)**. **(G)** Ratio of mCherry punctae to GFP-mCherry. Scale bar = 10µm. Significance was calculated by using one way and two way ANOVA. *P < 0.05, ***P <0.001 vs Control; ## P<0.01, ### P< 0.001 vs Control STV. The bars indicate s.e.m., n=10 larvae.

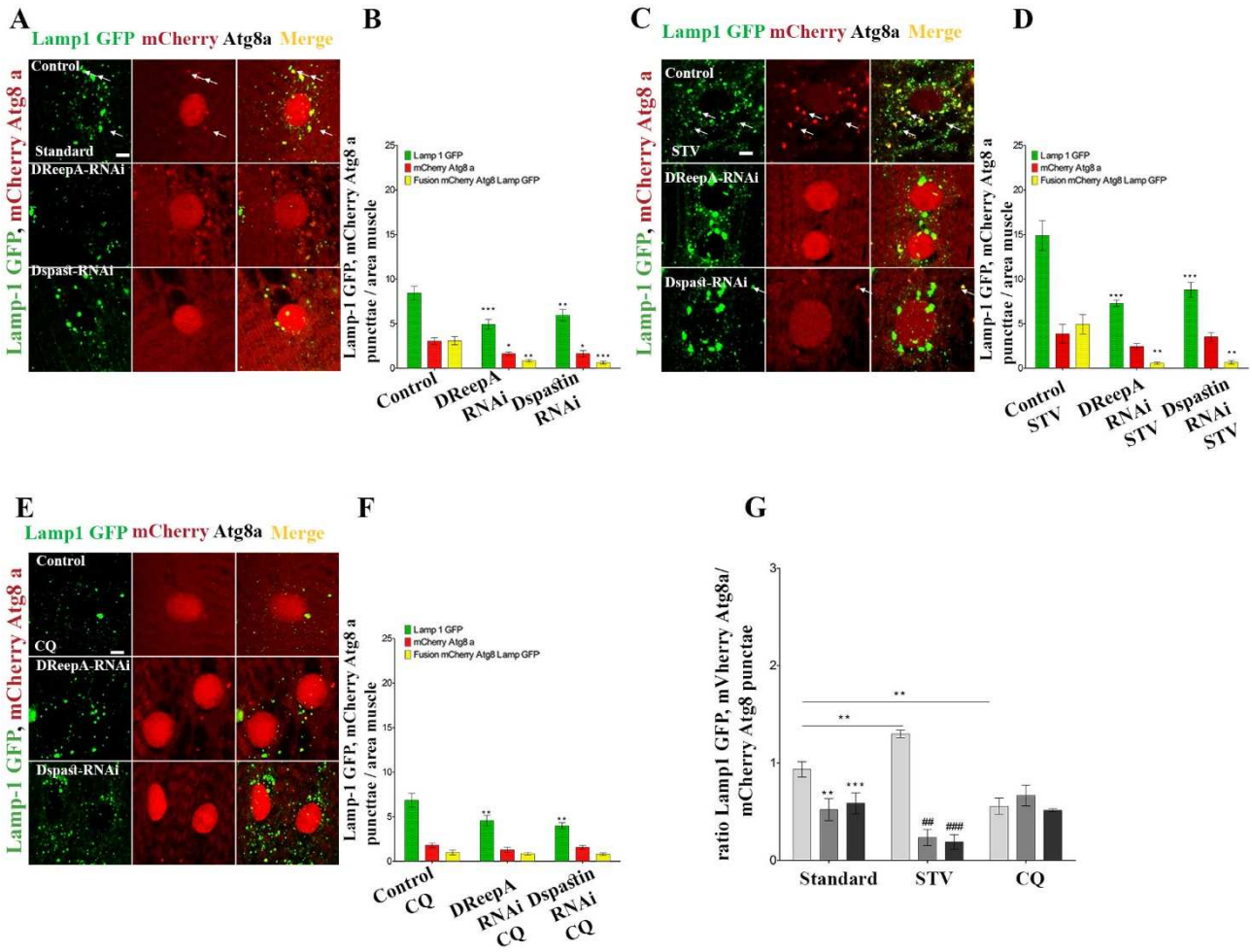

Figure 31. REEPA and Dspastin down regulation blocks the autophagosomes/lysosomes fusion. Representative confocal image of *Drosophila* REEPA-RNAi and Dspastin-RNAi larvae muscles ubiquitously expressing the recombinant Lamp1-GFP; mCherry Atg8a (Tub-Gal4 > UAS-mCherry-GFP-Atg8a) in standard medium **(A)**; in stress condition (STV) **(C)** and in Chloroquine (CQ) **(E)**. Quantification of the number of Lamp1-GFPmCherryAtg8a puncta in standard medium (B), in stress condition (STV) **(D)** and in Chloroquine (CQ) **(F)**. **(G)** Ratio of GFP-mCherry to mCherry punctae. Scale bar = 10µm. Significance was calculated by using one way and two-way ANOVA. *P < 0.05, **P <0.01 vs Control; ## P<0.01, ### P< 0.001 vs Control STV. The bars indicate s.e.m., n=10.

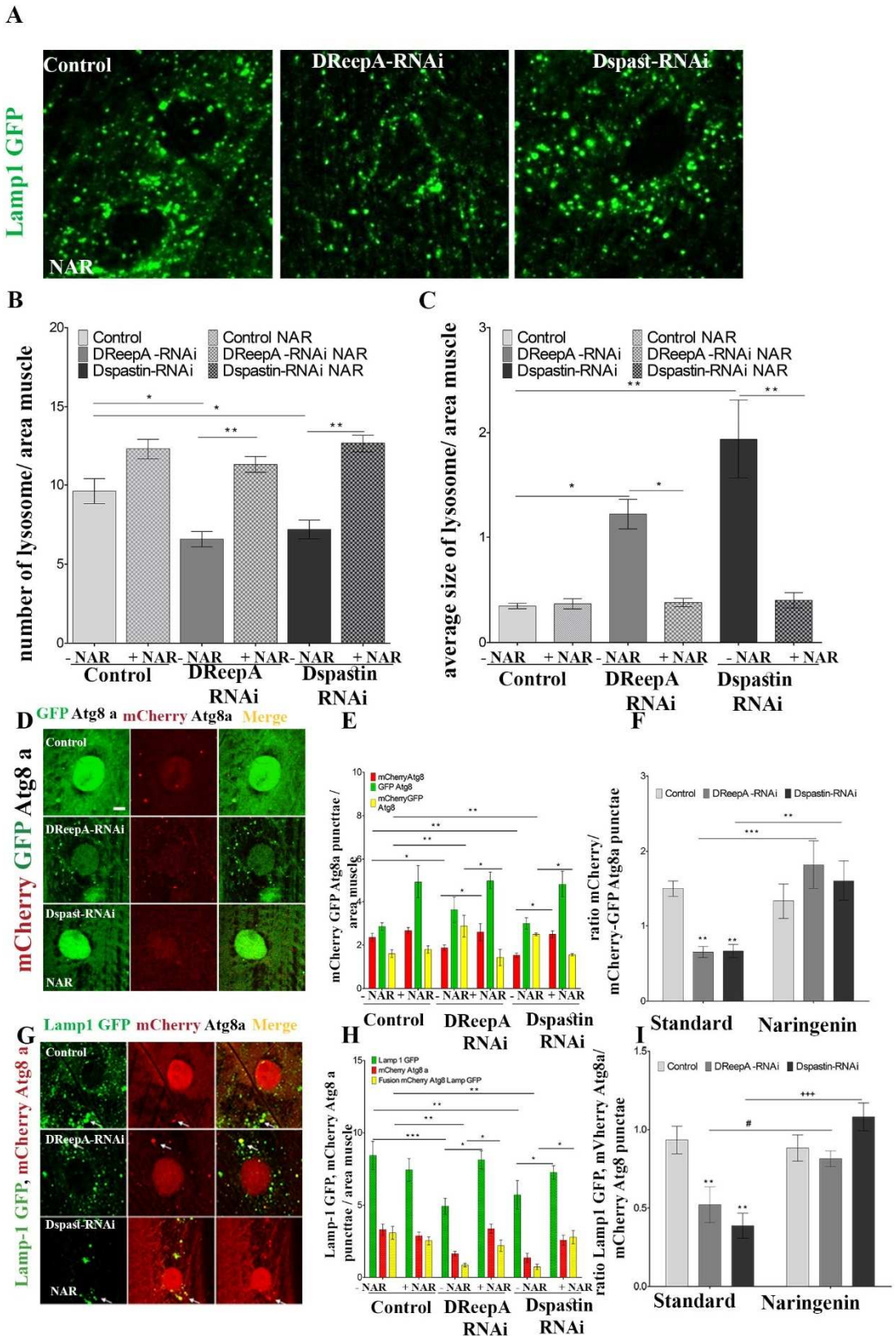
A
Control
DReepA-RNAi
Dspast-RNAi
Lamp1 GFP
NAR
B
number of lysosome/ area muscle
Control
DReepA -RNAi
Dspastin-RNAi
Control NAR
DReepA -RNAi NAR
Dspastin-RNAi NAR
- NAR + NAR - NAR + NAR - NAR + NAR
Control
DReepA RNAi
Dspastin RNAi
C
average size of lysosome/ area muscle
Control
DReepA -RNAi
Dspastin-RNAi
Control NAR
DReepA -RNAi NAR
Dspastin-RNAi NAR
- NAR + NAR - NAR + NAR - NAR + NAR
Control
DReepA RNAi
Dspastin RNAi
D
GFP Atg8 a
mCherry Atg8a
Merge
mCherry GFP Atg8 a
Control
DReepA-RNAi
Dspast-RNAi
NAR
E
mCherryAtg8
GFP Atg8
mCherryGFP Atg8
mCherry GFP Atg8a puncttae / area muscle
- NAR + NAR - NAR + NAR - NAR + NAR
Control
DReepA RNAi
Dspastin RNAi
F
Control
DReepA -RNAi
Dspastin-RNAi
ratio mCherry/ mCherry-GFP Atg8a punctae
Standard
Naringenin
G
Lamp1 GFP
mCherry Atg8a
Merge
Lamp-1 GFP, mCherry Atg8 a
Control
DReepA-RNAi
Dspast-RNAi
NAR
H
Lamp 1 GFP
mCherry Atg8 a
Fusion mCherry Atg8 Lamp GFP
Lamp-1 GFP, mCherry Atg8 a puncttae / area muscle
- NAR + NAR - NAR + NAR - NAR + NAR
Control
DReepA RNAi
Dspastin RNAi
I
Control
DReepA -RNAi
Dspastin-RNAi
ratio Lamp1 GFP, mVherry Atg8a/ mCherry Atg8 punctae
Standard
Naringenin

Figure 32. Naringenin ameliorated the autophagic defects in REEPA and Dspastin loss of function larvae. Representative confocal image of Drosophila REEPA-RNAi and Dspastin-RNAi larval muscles ubiquitously expressing Lamp1-GFP (Tub-Gal4 > UAS-Lamp1-GFP) **(A)**, the tandem mCherry-GFP-Atg8a (Tub-Gal4 > UAS-mCherry-GFP-Atg8a) **(D)** and the recombinant Lamp1-GFP; mCherry Atg8a (Tub-Gal4 > UAS-mCherry-GFP-Atg8a) **(G)**, raised on 0.5 mM NAR enriched food. Quantification of the lysosomes number **(B)** and size **(C)**; quantification of the number of mCherry-GFP-Atg8 puncta **(E)** and of mCherry punctae to GFP-mCherry ratio **(F)**; quantification of the Lamp1-GFP; mCherryAtg8a puncta **(H)** and the ratio of GFP-mCherry to mCherry punctae **(I)**. Scale bar= 10µm. Significance was calculated by using one way and two-wayNOVA. *P < 0.05; ** P< 0.01; ***P<0.001 vs Control; +++P <0.001 vs Dspastin-RNAi; # P <0.05 vs DReepA-RNAi. The bars indicate s.e.m., n=10.

5. DISCUSSION

To date, 56 disease-causing variants in REEP1 and over 300 mutations in Spastin, have been reported. HSP-associated REEP1 mutations are predominantly truncating mutations that have been proposed to act by a haploinsufficiency loss-of-function mechanism (Beetz et al., 2008; Goizet et al., 2011; Richard et al., 2017a; Schlang et al., 2008; Züchner et al., 2006). In Spastin mutations are missense, nonsense, splice site, deletions and insertions and frequently linked to a loss of protein expression (Allocca et al., 2018; Bürger et al., 2000; Harmon and Harp, 2001; Solowska et al., 2014a; Solowska and Baas, 2015). In the first part of this work, we explored the role of ReepA in ER homeostasis by investigating the consequences of its loss. Our data showed a functional link between the absence of ReepA and the corresponding activation of two specific branches of the UPR pathway: Ire1 and Atf6. Moreover, in loss-of-function ReepA animals we found a morphological change of the ER characterized by the increase of ER membrane sheet-like structures. The function of REEP proteins in cellular stress has been previously investigated by different groups. HVA22, the plant homolog of REEP1, is required to counteract stressful situations by inhibiting the activation of programmed cell death in plants (Chen et al., 2002); *Drosophila* ReepA downregulation enhances Tau aggregates, whereas its overexpression results protective, suggesting that ReepA is required to confer stress resistance against the accumulation of unfolded proteins induced by TM (Appocher et al., 2014); DNA damage in human cells triggers tubular ER extension via the p53-mediated expression of REEP1/2 and EI24, and this facilitates contacts between ER and mitochondria (Zheng et al., 2018). All these reports support a role of REEPs in response to stressors, but the molecular mechanism remains still to be elucidated. In our work we analyzed the activation of the three main pathways involved in UPR response and showed a peculiar selective induction of Atf6 and Ire1 in the absence of ReepA. Moreover, it has been demonstrated that the activation of Atf6 and Ire1, but not of Perk signaling, increases the synthesis of phosphatidylcholine, a key ER lipid, and induces ER expansion (Chiang et al., 2012; McQuiston and Diehl, 2017). When a constitutively active form of ATF6α or Xbp1 is expressed in culture cells, the ER appears enlarged and distended. On the contrary, PERK pathway has not been implicated in ER biogenesis. Modulation of UPR after the disruption of optimal membrane rearrangements has already been reported: in *Drosophila*, downregulation of the ER-shaping protein *Rtln1,* causes partial loss of tubular ER and a significant increase of the ER stress response in epidermal cells and neurons (O'Sullivan et al., 2012). Although the mechanism by which these ER-shaping proteins regulate UPR is not clear, a link between tubular ER structure and ER stress exists. Indeed, recent findings indicate that the UPR can be directly activated by altering ER lipid composition (Halbleib et al., 2017; Hapala et al., 2011; Volmer et al., 2013). *Reep1*$^{-/-}$ mice that presents ER sheet expansion showed an impairment of LDs and lipoatrophy, with significantly decreased visceral fat (Beetz et al., 2013; Falk et al., 2014; Lim et al., 2015; Park et al., 2010; Renvoisé et al., 2016). Our Drosophila model of REEPA shows similar defects on LD biogenesis, thus highlighting the role of ER structure in lipid metabolism. The

biogenesis of LDs takes place in the ER by a mechanism that starts with the deposition of neutral lipids between the leaflets of the ER and the following emersion of LD from the outer leaflet of the ER into the cytoplasm, with a final separation phase (Park et al., 2010; Wilfling et al., 2014). LDs are a convenient lipid storage supplier during conditions of nutrient deprivation and result critical to buffer the levels of toxic lipid species (Liu et al., 2017; Nguyen et al., 2017; Shpilka et al., 2015). Dysfunctional lipid droplet biogenesis can result in the activation of UPR signaling. ER proteins such as REEP1, Atlastin and Spastin can affect LD biogenesis (Falk et al., 2014; Papadopoulos et al., 2015; Renvoisé et al., 2016; Rong et al., 2018).

Even if the mechanism connecting impaired lipid droplet biogenesis to UPR activation is not clear, some hypothesis can be formulated, also in the light of the data presented in this work. REEPs can modify ER structure, influencing the ER membrane physicochemical properties (such as changes in membrane thickness and lipid packing density) and modulating the response of the luminal sensing domains of yeast Ire1 and mammalian IRE1 and PERK, implicated in sensing unfolded proteins (Koh et al., 2018). Very recently, a study conducted on *C. elegans* demonstrated that the abnormal ER morphology caused by loss of atalstin 1 led to defects in mitochondria attachment and fission at dendritic branch points and abnormalities in protein homeostasis when the unfolded protein response (UPR) was compromised (Byrne et al., 2019) . Alternatively, assuming that REEPs could regulate the ER-LDs contact or curvature, the consequent impaired fatty acid sequestration could result in an aberrant ER membrane lipid composition that directly activates the UPR, independently of alterations in protein folding.

Moreover, when lipid droplets are lost, the ER phospholipid composition is altered and result in impaired autophagosome biogenesis (Velázquez et al., 2016b; Vevea et al., 2015).

Our HSP models displayed lysosome morphology defects. Similar phenotypes have been observed in a study, where depletion of spastin disrupted the ER-endosome contact, impaired endosomal tubule fission and induced lysosome morphology defects (Allison et al., 2017) This phenotype was reported also in REEP1 loss-of-function cell and mouse model, supporting the idea that ER morphogenesis play an important role in ER-mediated endosomal fission and lysosome function and morphology (Allison et al., 2017). These defects have been described in other HSP forms such as SPG11 and SPG15 (Renvoisé et al., 2014).

In addition, we found that loss of ReepA resulted in a decline of motor ability and a reduction of lifespan similarly to Dspastin-RNAi, confirming that our *Drosophila* models display the classical hallmarks of HSP disease.

Finally, we explored the pharmacological effects of the flavonoid naringenin on ReepA and Spastin *Drosophila* models. In *Drosophila*, the ability of naringenin, but not of chrysin and lutein, to activate the Nrf2/Keap1 signalling pathway is consistent with a hormesis-mediated mechanism of this

compound (Lashmanova et al., 2017). Nrf2, an antioxidant transcription factor that modulates ER stress response and autophagy and mediates the crosstalk between lipid metabolism and antioxidant defence, has gained attention in the last years as a target for certain neurodegenerative disorders such as Alzheimer's and Parkinson's disease (Barone et al., 2011; Jain et al., 2015; Jiang et al., 2015; Misra et al., 2011; Murphy and Park, 2017; Speciale et al., 2011; Tsakiri et al., 2018). Naringenin, as other flavonoids are able to modulate LDs biogenesis/turnover even if the mechanism is under investigation (Fantin et al., 2019; Harmon and Harp, 2001).

Besides the efficacy of naringenin in pathological models of liver diseases, obesity and diabetes, a potential role of naringenin in the treatment of neurological disorders has emerged in the past few years. The protective effects of naringenin in cellular and animal Parkinson's models is demonstrated by its ability to restore dopaminergic function, neuro-inflammation and locomotor deficit (Hegazy et al., 2016; Khan et al., 2012; Wang et al., 2019). Naringenin protects motor neuron against methylglyoxal-induced neurotoxicity *in vitro* (Lo et al., 2017). The relative recent interest in the molecule, the few data on pharmacokinetic and metabolic aspects, as well as the chemical instability of this compound have prevented the development of clinical trial activity, at least for now. The increasing attention to naringenin, in fact, has stimulated the researchers to work on delivering systems (Joshi et al., 2018). In this study, we tested the effects of naringenin after the complexation with β-cyclodextrin, an FDA approved excipient that enhances its solubility and increases the adsorption rate, as previously reported (Salehi et al., 2019; Sangpheak et al., 2015).
All the phenotypes elicited in the ReepA and Spastin loss-of-function models reported in this work were greatly ameliorated by administration of naringenin that rescues not only the defects at the molecular and cellular levels, but also restores the climbing behavior and increases flies' lifespan. Overall, our *in vivo* data strongly support the beneficial effects of the natural compound naringenin and open the way for future studies devoted to pharmacotherapy in HSP. We propose a possible protective role of naringenin in HSP neurodegeneration and, therefore, the testing of this compound in additional HSP models (Napoli et al., 2019).

6.REFERENCES

Abounit, K., Scarabelli, T. M., and McCauley, R. B. (2012). Autophagy in mammalian cells. *World J. Biol. Chem.* 3, 1–6. doi:10.4331/wjbc.v3.i1.1.

Alberts, P., and Rotin, D. (2010). Regulation of lipid droplet turnover by ubiquitin ligases. *BMC Biol.* 8, 94. doi:10.1186/1741-7007-8-94.

Allison, R., Edgar, J. R., Pearson, G., Rizo, T., Newton, T., Günther, S., et al. (2017). Defects in ER–endosome contacts impact lysosome function in hereditary spastic paraplegia. *J Cell Biol* 216, 1337–1355. doi:10.1083/JCB.201609033.

Allocca, M., Zola, S., and Bellosta, P. (2018). "The Fruit Fly, Drosophila melanogaster: Modeling of Human Diseases (Part II)," in *Drosophila melanogaster - Model for Recent Advances in Genetics and Therapeutics* doi:10.5772/intechopen.73199.

Appocher, C., Klima, R., and Feiguin, F. (2014). Functional screening in Drosophila reveals the conserved role of REEP1 in promoting stress resistance and preventing the formation of Tau aggregates. *Hum. Mol. Genet.* 23, 6762–6772. Available at: http://dx.doi.org/10.1093/hmg/ddu393.

Assini, J. M., Mulvihill, E. E., and Huff, M. W. (2013). Citrus flavonoids and lipid metabolism. *Curr. Opin. Lipidol.* 24. Available at: https://journals.lww.com/co-lipidology/Fulltext/2013/02000/Citrus_flavonoids_and_lipid_metabolism.7.aspx.

Barone, M. C., Sykiotis, G. P., and Bohmann, D. (2011). Genetic activation of Nrf2 signaling is sufficient to ameliorate neurodegenerative phenotypes in a Drosophila model of Parkinson's disease. *Dis. Model. {&} Mech.* 4, 701–707. doi:10.1242/dmm.007575.

Beetz, C., Koch, N., Khundadze, M., Zimmer, G., Nietzsche, S., Hertel, N., et al. (2013). A spastic paraplegia mouse model reveals REEP1-dependent ER shaping. *J. Clin. Invest.* 123, 4273–4282. doi:10.1172/JCI65665.

Beetz, C., Schüle, R., Deconinck, T., Tran-Viet, K.-N., Zhu, H., Kremer, B. P. H., et al. (2008). REEP1 mutation spectrum and genotype/phenotype correlation in hereditary spastic paraplegia type 31. *Brain* 131, 1078–1086. doi:10.1093/brain/awn026.

Bellofatto, M., De Michele, G., Iovino, A., Filla, A., and Santorelli, F. M. (2019). Management of Hereditary Spastic Paraplegia: A Systematic Review of the Literature. *Front. Neurol.* 10, 3. doi:10.3389/fneur.2019.00003.

Belzil, V. V, and Rouleau, G. A. (2012). Endoplasmic reticulum lipid rafts and upper motor neuron degeneration. *Ann. Neurol.* 72, 479–80. doi:10.1002/ana.23678.

Boutry, M., Morais, S., and Stevanin, G. (2019). Update on the Genetics of Spastic Paraplegias. *Curr. Neurol. Neurosci. Rep.* 19, 18. doi:10.1007/s11910-019-0930-2.

Bravo, R., Parra, V., Gatica, D., Rodriguez, A. E., Torrealba, N., Paredes, F., et al. (2013). “Chapter Five - Endoplasmic Reticulum and the Unfolded Protein Response: Dynamics and Metabolic Integration,” in *International Review of Cell and Molecular Biology*, ed. K. W. B. T.-I. R. of C. and M. B. Jeon (Academic Press), 215–290. doi:https://doi.org/10.1016/B978-0-12-407704-1.00005-1.

Bürger, J., Fonknechten, N., Hoeltzenbein, M., Neumann, L., Bratanoff, E., Hazan, J., et al. (2000). Hereditary spastic paraplegia caused by mutations in the SPG4 gene. *Eur. J. Hum. Genet.* 8, 771–776. doi:10.1038/sj.ejhg.5200528.

Byrne, J. J., Soh, M. S., Chandhok, G., Vijayaraghavan, T., Teoh, J.-S., Crawford, S., et al. (2019). Disruption of mitochondrial dynamics affects behaviour and lifespan in Caenorhabditis elegans. *Cell. Mol. Life Sci.* 76, 1967–1985. doi:10.1007/s00018-019-03024-5.

Cabirol-Pol, M.-J., Khalil, B., Rival, T., Faivre-Sarrailh, C., and Besson, M. T. (2018). Glial lipid droplets and neurodegeneration in a Drosophila model of complex I deficiency. *Glia* 66, 874–888. doi:doi:10.1002/glia.23290.

Calfon, M., Zeng, H., Urano, F., Till, J. H., Hubbard, S. R., Harding, H. P., et al. (2002). IRE1 couples endoplasmic reticulum load to secretory capacity by processing the XBP-1 mRNA. *Nature* 415, 92–96. doi:10.1038/415092a.

Chang, C.-L., Weigel, A. V, Ioannou, M. S., Pasolli, H. A., Xu, C. S., Peale, D. R., et al. (2019). Spastin tethers lipid droplets to peroxisomes and directs fatty acid trafficking through ESCRT-III. *J. Cell Biol.* 218, 2583 LP – 2599. doi:10.1083/jcb.201902061.

Chattopadhyay, D., Sen, S., Chatterjee, R., Roy, D., James, J., and Thirumurugan, K. (2016). Context- and dose-dependent modulatory effects of naringenin on survival and development of Drosophila melanogaster. *Biogerontology* 17, 383–393. doi:10.1007/s10522-015-9624-6.

Chen, C.-N., Chu, C.-C., Zentella, R., Pan, S.-M., and David Ho, T.-H. (2002). AtHVA22 gene family in Arabidopsis: phylogenetic relationship, ABA and stress regulation, and tissue-specific expression. *Plant Mol. Biol.* 49, 631–642. doi:10.1023/A:1015593715144.

Chen, R., Jin, R., Wu, L., Ye, X., Yang, Y., Luo, K., et al. (2011). Reticulon 3 attenuates the clearance of cytosolic prion aggregates via inhibiting autophagy. *Autophagy* 7, 205–216. doi:10.4161/auto.7.2.14197.

Chen, S., Novick, P., and Ferro-Novick, S. (2013). ER structure and function. *Curr. Opin. Cell Biol.* 25, 428–33. doi:10.1016/j.ceb.2013.02.006.

Chiang, W.-C., Hiramatsu, N., Messah, C., Kroeger, H., and Lin, J. H. (2012). Selective Activation of ATF6 and PERK Endoplasmic Reticulum Stress Signaling Pathways Prevent Mutant Rhodopsin Accumulation. *Investig. Opthalmology {&} Vis. Sci.* 53, 7159. doi:10.1167/iovs.12-10222.

Chitraju, C., Mejhert, N., Haas, J. T., Diaz-Ramirez, L. G., Grueter, C. A., Imbriglio, J. E., et al. (2017). Triglyceride Synthesis by DGAT1 Protects Adipocytes from Lipid-Induced ER Stress during Lipolysis. *Cell Metab.* 26, 407-418.e3. doi:10.1016/j.cmet.2017.07.012.

Credle, J. J., Finer-Moore, J. S., Papa, F. R., Stroud, R. M., and Walter, P. (2005). On the mechanism of sensing unfolded protein in the endoplasmic reticulum. *Proc. Natl. Acad. Sci. U. S. A.* 102, 18773 LP--18784. doi:10.1073/pnas.0509487102.

Curti, V., Di Lorenzo, A., Rossi, D., Martino, E., Capelli, E., Collina, S., et al. (2017). Enantioselective Modulatory Effects of Naringenin Enantiomers on the Expression Levels of miR-17-3p Involved in Endogenous Antioxidant Defenses. *Nutrients* 9. doi:10.3390/nu9030215.

D'Amore, C., Orso, G., Fusi, F., Pagano, M. A., Miotto, G., Forgiarini, A., et al. (2016). An NBD Derivative of the Selective Rat Toxicant Norbormide as a New Probe for Living Cell Imaging. *Front. Pharmacol.* 7. doi:10.3389/fphar.2016.00315.

English, A. R., and Voeltz, G. K. (2013). Endoplasmic reticulum structure and interconnections with other organelles. *Cold Spring Harb. Perspect. Biol.* 5, a013227–a013227. doi:10.1101/cshperspect.a013227.

English, A. R., Zurek, N., and Voeltz, G. K. (2009). Peripheral ER structure and function. *Curr. Opin. Cell Biol.* 21, 596–602. doi:10.1016/j.ceb.2009.04.004.

Errico, A., Claudiani, P., D'Addio, M., and Rugarli, E. I. (2004). Spastin interacts with the centrosomal protein NA14, and is enriched in the spindle pole, the midbody and the distal axon. *Hum. Mol. Genet.* 13, 2121–2132. doi:10.1093/hmg/ddh223.

Evans, K., Keller, C., Pavur, K., Glasgow, K., Conn, B., and Lauring, B. (2006). Interaction of two hereditary spastic paraplegia gene products, spastin and atlastin, suggests a common pathway for axonal maintenance. *Proc. Natl. Acad. Sci. U. S. A.* 103, 10666–10671. doi:10.1073/pnas.0510863103.

Falcone Ferreyra, M. L., Rius, S. P., and Casati, P. (2012). Flavonoids: biosynthesis, biological functions, and biotechnological applications. *Front. Plant Sci.* 3, 222. doi:10.3389/fpls.2012.00222.

Falk, J., Rohde, M., Bekhite, M. M., Neugebauer, S., Hemmerich, P., Kiehntopf, M., et al. (2014). Functional mutation analysis provides evidence for a role of REEP1 in lipid droplet biology. *Hum. Mutat.* 35, 497–504. doi:10.1002/humu.22521.

Fantin, M., Garelli, F., Napoli, B., Forgiarini, A., Gumeni, S., De Martin, S., et al. (2019). Flavonoids Regulate Lipid Droplets Biogenesis in *Drosophila melanogaster*. *Nat. Prod. Commun.* 14, 1934578X1985243. doi:10.1177/1934578X19852430.

Fernández-Hernández, I., Scheenaard, E., Pollarolo, G., and Gonzalez, C. (2016). The translational relevance of Drosophila in drug discovery. *EMBO Rep.* 17, 471–472. doi:10.15252/embr.201642080.

Fink, J. K. (2013). Hereditary spastic paraplegia: clinico-pathologic features and emerging molecular mechanisms. *Acta Neuropathol.* 126, 307–328. doi:10.1007/s00401-013-1115-8.

Forgiarini, A., Wang, Z., D'Amore, C., Jay-Smith, M., Li, F. F., Hopkins, B., et al. (2019). Live applications of norbormide-based fluorescent probes in Drosophila melanogaster. *PLoS One* 14, e0211169. doi:10.1371/journal.pone.0211169.

Frescas, D., Mavrakis, M., Lorenz, H., DeLotto, R., and Lippincott-Schwartz, J. (2006). The secretory

membrane system in the Drosophila syncytial blastoderm embryo exists as functionally compartmentalized units around individual nuclei. *J. Cell Biol.* 173, 219 LP – 230. Available at: http://jcb.rupress.org/content/173/2/219.abstract.

Fujikake, N., Shin, M., and Shimizu, S. (2018). Association Between Autophagy and Neurodegenerative Diseases. *Front. Neurosci.* 12, 255. doi:10.3389/fnins.2018.00255.

Fujimoto, T., Ohsaki, Y., Cheng, J., Suzuki, M., and Shinohara, Y. (2008). Lipid droplets: a classic organelle with new outfits. *Histochem. Cell Biol.* 130, 263–279. doi:10.1007/s00418-008-0449-0.

Gao, G., Chen, L., and Huang, C. (2014). Anti-cancer drug discovery: update and comparisons in yeast, Drosophila, and zebrafish. *Curr. Mol. Pharmacol.* 7, 44–51. Available at: https://www.ncbi.nlm.nih.gov/pubmed/24993385.

Glick, D., Barth, S., and Macleod, K. F. (2010). Autophagy: cellular and molecular mechanisms. *J. Pathol.* 221, 3–12. doi:10.1002/path.2697.

Goizet, C., Depienne, C., Benard, G., Boukhris, A., Mundwiller, E., Solé, G., et al. (2011). REEP1 mutations in SPG31: Frequency, mutational spectrum, and potential association with mitochondrial morpho-functional dysfunction. *Hum. Mutat.* 32, 1118–1127. doi:10.1002/humu.21542.

Goldwasser, J., Cohen, P. Y., Lin, W., Kitsberg, D., Balaguer, P., Polyak, S. J., et al. (2011). Naringenin inhibits the assembly and long-term production of infectious hepatitis C virus particles through a PPAR-mediated mechanism. *J. Hepatol.* 55, 963–971. doi:10.1016/J.JHEP.2011.02.011.

Goyal, U., and Blackstone, C. (2013). Untangling the web: Mechanisms underlying ER network formation. *Biochim. Biophys. Acta* 1833, 2492–2498. doi:10.1016/j.bbamcr.2013.04.009.

Griffing, L. R. (2018). “Dancing with the Stars: Using Image Analysis to Study the Choreography of the Endoplasmic Reticulum and Its Partners and of Movement Within Its Tubules,” in (Humana Press, New York, NY), 75–102. doi:10.1007/978-1-4939-7389-7_7.

Grumati, P., Morozzi, G., Hölper, S., Mari, M., Harwardt, M.-L. I. E., Yan, R., et al. (2017). Full length RTN3 regulates turnover of tubular endoplasmic reticulum via selective autophagy. *Elife* 6, e25555. doi:10.7554/eLife.25555.

Gumeni, S., Evangelakou, Z., Gorgoulis, V. G., and Trougakos, I. P. (2017). Proteome Stability as a Key Factor of Genome Integrity. *Int. J. Mol. Sci.* 18. doi:10.3390/ijms18102036.

Halbleib, K., Pesek, K., Covino, R., Hofbauer, H. F., Wunnicke, D., Hänelt, I., et al. (2017). Activation of the Unfolded Protein Response by Lipid Bilayer Stress. *Mol. Cell* 67, 673--684.e8. doi:10.1016/J.MOLCEL.2017.06.012.

Hapala, I., Marza, E., and Ferreira, T. (2011). Is fat so bad? Modulation of endoplasmic reticulum stress by lipid droplet formation. *Biol. Cell* 103, 271–285. doi:10.1042/BC20100144.

Harmon, A. W., and Harp, J. B. (2001). Differential effects of flavonoids on 3T3-L1 adipogenesis and lipolysis. *Am. J. Physiol. Physiol.* 280, C807--C813. doi:10.1152/ajpcell.2001.280.4.C807.

Hegazy, H. G., Ali, E. H. A., and Sabry, H. A. (2016). The neuroprotective action of naringenin on oseltamivir (Tamiflu) treated male rats. *J. Basic Appl. Zool.* 77, 83–90. doi:10.1016/j.jobaz.2016.12.006.

Henne, W. M. (2019). Spastin joins LDs and peroxisomes in the interorganelle contact ballet. *J. Cell Biol.* 218, 2439 LP – 2441. doi:10.1083/jcb.201906025.

Hetz, C. (2012). The unfolded protein response: controlling cell fate decisions under ER stress and beyond. *Nat. Rev. Mol. Cell Biol.* 13, 89. Available at: https://doi.org/10.1038/nrm3270.

Hirst, J., Itzhak, D. N., Antrobus, R., Borner, G. H. H., and Robinson, M. S. (2018). Role of the AP-5 adaptor protein complex in late endosome-to-Golgi retrieval. *PLoS Biol.* 16, e2004411–e2004411. doi:10.1371/journal.pbio.2004411.

Hooper, C., Puttamadappa, S. S., Loring, Z., Shekhtman, A., and Bakowska, J. C. (2010). Spartin activates atrophin-1-interacting protein 4 (AIP4) E3 ubiquitin ligase and promotes ubiquitination of adipophilin on lipid droplets. *BMC Biol.* 8, 72. doi:10.1186/1741-7007-8-72.

Hu, J., Shibata, Y., Voss, C., Shemesh, T., Li, Z., Coughlin, M., et al. (2008). Membrane proteins of the endoplasmic reticulum induce high-curvature tubules. *Science* 319, 1247–1250. doi:10.1126/science.1153634.

Huong, D. T. T., Takahashi, Y., and Ide, T. (2006). Activity and mRNA levels of enzymes involved in hepatic fatty acid oxidation in mice fed citrus flavonoids. *Nutrition* 22, 546–552. doi:10.1016/J.NUT.2005.11.006.

Inagi, R., Ishimoto, Y., and Nangaku, M. (2014). Proteostasis in endoplasmic reticulum—new mechanisms in kidney disease. *Nat. Rev. Nephrol.* 10, 369. Available at: https://doi.org/10.1038/nrneph.2014.67.

Ito, J., Ishii, N., Akihara, R., Lee, J., Kurahashi, T., Homma, T., et al. (2017). A high-fat diet temporarily renders Sod1-deficient mice resistant to an oxidative insult. *J. Nutr. Biochem.* 40, 44–52. doi:https://doi.org/10.1016/j.jnutbio.2016.10.018.

Jain, A., Rusten, T. E., Katheder, N., Elvenes, J., Bruun, J.-A., Sjøttem, E., et al. (2015). p62/Sequestosome-1, Autophagy-related Gene 8, and Autophagy in Drosophila Are Regulated by Nuclear Factor Erythroid 2-related Factor 2 (NRF2), Independent of Transcription Factor TFEB. *J. Biol. Chem.* 290, 14945–14962. doi:10.1074/jbc.M115.656116.

Janda, E., Lascala, A., Martino, C., Ragusa, S., Nucera, S., Walker, R., et al. (2016). Molecular mechanisms of lipid- and glucose-lowering activities of bergamot flavonoids. *PharmaNutrition* 4, S8--S18. doi:10.1016/J.PHANU.2016.05.001.

Jiang, T., Harder, B., Rojo de la Vega, M., Wong, P. K., Chapman, E., and Zhang, D. D. (2015). p62 links autophagy and Nrf2 signaling. *Free Radic. Biol. Med.* 88, 199–204. doi:10.1016/J.FREERADBIOMED.2015.06.014.

JOSEPH, J. A., SHUKITT-HALE, B., and LAU, F. C. (2007). Fruit Polyphenols and Their Effects on Neuronal Signaling and Behavior in Senescence. *Ann. N. Y. Acad. Sci.* 1100, 470–485. doi:doi:10.1196/annals.1395.052.

Joshi, R., Kulkarni, Y. A., and Wairkar, S. (2018). Pharmacokinetic, pharmacodynamic and formulations aspects of Naringenin: An update. *Life Sci.* 215, 43–56. doi:10.1016/J.LFS.2018.10.066.

Kassan, A., Herms, A., Fernández-Vidal, A., Bosch, M., Schieber, N. L., Reddy, B. J. N., et al. (2013). Acyl-CoA synthetase 3 promotes lipid droplet biogenesis in ER microdomains. *J. Cell Biol.* 203, 985–1001. doi:10.1083/jcb.201305142.

Kaushik, S., Rodriguez-Navarro, J. A., Arias, E., Kiffin, R., Sahu, S., Schwartz, G. J., et al. (2011). Autophagy in Hypothalamic AgRP Neurons Regulates Food Intake and Energy Balance. *Cell Metab.* 14, 173–183. doi:https://doi.org/10.1016/j.cmet.2011.06.008.

Kawser Hossain, M., Abdal Dayem, A., Han, J., Yin, Y., Kim, K., Kumar Saha, S., et al. (2016). Molecular Mechanisms of the Anti-Obesity and Anti-Diabetic Properties of Flavonoids. *Int. J. Mol. Sci.* 17, 569. doi:10.3390/ijms17040569.

Khan, M. B., Khan, M. M., Khan, A., Ahmed, M. E., Ishrat, T., Tabassum, R., et al. (2012). Naringenin ameliorates Alzheimer's disease (AD)-type neurodegeneration with cognitive impairment (AD-TNDCI) caused by the intracerebroventricular-streptozotocin in rat model. *Neurochem. Int.* 61, 1081–1093. doi:10.1016/j.neuint.2012.07.025.

Khundadze, M., Kollmann, K., Koch, N., Biskup, C., Nietzsche, S., Zimmer, G., et al. (2013). A hereditary spastic paraplegia mouse model supports a role of ZFYVE26/SPASTIZIN for the endolysosomal system. *PLoS Genet.* 9, e1003988–e1003988. doi:10.1371/journal.pgen.1003988.

Klemm, R. W., Norton, J. P., Cole, R. A., Li, C. S., Park, S. H., Crane, M. M., et al. (2013). A conserved role for atlastin GTPases in regulating lipid droplet size. *Cell Rep.* 3, 1465–75. doi:10.1016/j.celrep.2013.04.015.

Koh, J. H., Wang, L., Beaudoin-Chabot, C., and Thibault, G. (2018). Lipid bilayer stress-activated IRE-1 modulates autophagy during endoplasmic reticulum stress. *J. Cell Sci.* 131, jcs217992. doi:10.1242/JCS.217992.

Lai, Y.-S., Stefano, G., and Brandizzi, F. (2014). ER stress signaling requires RHD3, a functionally conserved ER-shaping GTPase. *J. Cell Sci.* 127, 3227–32. doi:10.1242/jcs.147447.

Lashmanova, E., Zemskaya, N., Proshkina, E., Kudryavtseva, A., Volosnikova, M., Marusich, E., et al. (2017). The Evaluation of Geroprotective Effects of Selected Flavonoids inDrosophila melanogasterandCaenorhabditis elegans. *Front. Pharmacol.* 8, 884. doi:10.3389/fphar.2017.00884.

Lavie, J., Serrat, R., Bellance, N., Courtand, G., Dupuy, J.-W., Tesson, C., et al. (2017). Mitochondrial morphology and cellular distribution are altered in SPG31 patients and are linked to DRP1 hyperphosphorylation. *Hum. Mol. Genet.* 26, 674–685. Available at: http://dx.doi.org/10.1093/hmg/ddw425.

Lee, J. E., Oney, M., Frizzell, K., Phadnis, N., and Hollien, J. (2015). Drosophila melanogaster Activating Transcription Factor 4 Regulates Glycolysis During Endoplasmic Reticulum Stress. *G3 Genes|Genomes|Genetics* 5, 667–675. doi:10.1534/g3.115.017269.

Lee, J., Homma, T., and Fujii, J. (2017). Mice in the early stage of liver steatosis caused by a high fat diet are resistant to thioacetamide-induced hepatotoxicity and oxidative stress. *Toxicol. Lett.* 277, 92–103. doi:https://doi.org/10.1016/j.toxlet.2017.06.005.

Li, D., Zhao, Y. G., Li, D., Zhao, H., Huang, J., Miao, G., et al. (2019). The ER-Localized Protein DFCP1 Modulates ER-Lipid Droplet Contact Formation. *Cell Rep.* 27, 343-358.e5. doi:https://doi.org/10.1016/j.celrep.2019.03.025.

Lim, Y., Cho, I.-T., Schoel, L. J., Cho, G., and Golden, J. A. (2015). Hereditary spastic paraplegia-linked REEP1 modulates endoplasmic reticulum/mitochondria contacts. *Ann. Neurol.* 78, 679–696. doi:10.1002/ana.24488.

Lindström, R., Lindholm, P., Kallijärvi, J., Palgi, M., Saarma, M., and Heino, T. I. (2016). Exploring the conserved role of MANF in the unfolded protein response in Drosophila melanogaster. *PLoS One*. doi:10.1371/journal.pone.0151550.

Liu, L., MacKenzie, K. R., Putluri, N., Maletić-Savatić, M., and Bellen, H. J. (2017). The Glia-Neuron Lactate Shuttle and Elevated ROS Promote Lipid Synthesis in Neurons and Lipid Droplet Accumulation in Glia via APOE/D. *Cell Metab.* 26, 719-737.e6. doi:10.1016/j.cmet.2017.08.024.

Liu, T. Y., Bian, X., Sun, S., Hu, X., Klemm, R. W., Prinz, W. A., et al. (2012). Lipid interaction of the C terminus and association of the transmembrane segments facilitate atlastin-mediated homotypic endoplasmic reticulum fusion. *Proc. Natl. Acad. Sci.* 109, E2146 LP-E2154. doi:10.1073/pnas.1208385109.

Liu, X., Wang, N., Fan, S., Zheng, X., Yang, Y., Zhu, Y., et al. (2016). The citrus flavonoid naringenin confers protection in a murine endotoxaemia model through AMPK-ATF3-dependent negative regulation of the TLR4 signalling pathway. *Sci. Rep.* 6, 39735. doi:10.1038/srep39735.

Lo, Y. C., Tseng, Y. T., Hsu, H. T., Liu, C. M., and Wu, S. N. (2017). Naringenin protects motor neuron against methylglyoxal-induced neurotoxicity through activatinG IGF-1R-related neuroprotection. *J. Neurol. Sci.* 381, 616–617. doi:10.1016/j.jns.2017.08.1737.

Lőrincz, P., Mauvezin, C., and Juhász, G. (2017). Exploring Autophagy in Drosophila. *Cells* 6, 22. doi:10.3390/cells6030022.

Maher, P. (2019). The Potential of Flavonoids for the Treatment of Neurodegenerative Diseases. *Int. J. Mol. Sci.* 20, 3056. doi:10.3390/ijms20123056.

Mandl, J., Mészáros, T., Bánhegyi, G., and Csala, M. (2013). Minireview: Endoplasmic Reticulum Stress: Control in Protein, Lipid, and Signal Homeostasis. *Mol. Endocrinol.* 27, 384–393. doi:10.1210/me.2012-1317.

Mauvezin, C., Ayala, C., Braden, C. R., Kim, J., and Neufeld, T. P. (2014). Assays to monitor autophagy in Drosophila. *Methods* 68, 134–139. doi:10.1016/j.ymeth.2014.03.014.

McDermott, C. J., and Shaw, P. J. (2002). Hereditary spastic paraplegia. *Int. Rev. Neurobiol.* 53, 191–204. doi:10.1016/S0074-7742(02)53008-7.

McQuiston, A., and Diehl, J. A. (2017). Recent insights into PERK-dependent signaling from the stressed endoplasmic reticulum. *F1000Research* 6, 1897. doi:10.12688/f1000research.12138.1.

Mirzoyan, Z., Sollazzo, M., Allocca, M., Valenza, A. M., Grifoni, D., and Bellosta, P. (2019). Drosophila melanogaster: A Model Organism to Study Cancer. *Front. Genet.* 10, 51. doi:10.3389/fgene.2019.00051.

Misra, J. R., Horner, M. A., Lam, G., and Thummel, C. S. (2011). Transcriptional regulation of xenobiotic detoxification in Drosophila. *Genes Dev.* 25, 1796–806. doi:10.1101/gad.17280911.

Morales, P. E., Bucarey, J. L., and Espinosa, A. (2017). Muscle Lipid Metabolism: Role of Lipid Droplets and Perilipins. *J. Diabetes Res.* 2017, 1–10. doi:10.1155/2017/1789395.

Moreno, J. A., and Tiffany-Castiglioni, E. (2015). The Chaperone Grp78 in Protein Folding Disorders of the Nervous System. *Neurochem. Res.* 40, 329–335. doi:10.1007/s11064-014-1405-0.

Mozaffarian, D., and Wu, J. H. Y. (2018). Flavonoids, Dairy Foods, and Cardiovascular and Metabolic Health: A Review of Emerging Biologic Pathways. *Circ. Res.* 122, 369–384. doi:10.1161/CIRCRESAHA.117.309008.

Murphy, K., and Park, J. (2017). Can Co-Activation of Nrf2 and Neurotrophic Signaling Pathway Slow Alzheimer's Disease? *Int. J. Mol. Sci.* 18, 1168. doi:10.3390/ijms18061168.

Mushtaq, Z., Choudhury, S. D., Gangwar, S. K., Orso, G., and Kumar, V. (2016). Human senataxin modulates structural plasticity of the neuromuscular junction in drosophila through a neuronally conserved TGF$β$ signalling pathway. *Neurodegener. Dis.* 16. doi:10.1159/000445435.

Nah, J., Yuan, J., and Jung, Y.-K. (2015). Autophagy in neurodegenerative diseases: from mechanism to therapeutic approach. *Mol. Cells* 38, 381–389. doi:10.14348/molcells.2015.0034.

Napoli, B., Gumeni, S., Forgiarini, A., Fantin, M., De Filippis, C., Panzeri, E., et al. (2019). Naringenin Ameliorates Drosophila ReepA Hereditary Spastic Paraplegia-Linked Phenotypes. *Front. Neurosci.* 13, 1202. doi:10.3389/fnins.2019.01202.

Nguyen, T. B., Louie, S. M., Daniele, J. R., Tran, Q., Dillin, A., Zoncu, R., et al. (2017). DGAT1-Dependent Lipid Droplet Biogenesis Protects Mitochondrial Function during Starvation-Induced Autophagy. *Dev. Cell* 42, 9-21.e5. doi:10.1016/j.devcel.2017.06.003.

O'Sullivan, N. C., Jahn, T. R., Reid, E., and O'Kane, C. J. (2012). Reticulon-like-1, the Drosophila orthologue of the Hereditary Spastic Paraplegia gene reticulon 2, is required for organization of endoplasmic reticulum and of distal motor axons. *Hum. Mol. Genet.* 21, 3356–3365. doi:10.1093/hmg/dds167.

Ohsaki, Y., Suzuki, M., and Fujimoto, T. (2014). Review Open Questions in Lipid Droplet Biology. *Chem. Biol.* 21, 86–96. doi:10.1016/j.chembiol.2013.08.009.

Olzmann, J. A., and Carvalho, P. (2019). Dynamics and functions of lipid droplets. *Nat. Rev. Mol. Cell Biol.* 20, 137–155. doi:10.1038/s41580-018-0085-z.

Onal, G., Kutlu, O., Gozuacik, D., and Dokmeci Emre, S. (2017). Lipid Droplets in Health and Disease. *Lipids*

Health Dis. 16, 128. doi:10.1186/s12944-017-0521-7.

Orso, G., Martinuzzi, A., Rossetto, M. G., Sartori, E., Feany, M., and Daga, A. (2005). Disease-related phenotypes in a Drosophila model of hereditary spastic paraplegia are ameliorated by treatment with vinblastine. *J. Clin. Invest.* 115, 3026–34. doi:10.1172/JCI24694.

Orso, G., Pendin, D., Liu, S., Tosetto, J., Moss, T. J., Faust, J. E., et al. (2009). Homotypic fusion of ER membranes requires the dynamin-like GTPase atlastin. *Nature* 460, 978–983. doi:10.1038/nature08280.

Panche, A. N., Diwan, A. D., and Chandra, S. R. (2016). Flavonoids: an overview. *J. Nutr. Sci.* 5, e47. doi:10.1017/jns.2016.41.

Pandey, U. B., and Nichols, C. D. (2011). Human disease models in Drosophila melanogaster and the role of the fly in therapeutic drug discovery. *Pharmacol. Rev.* 63, 411–436. Available at: http://dx.doi.org/10.1124/pr.110.003293.

Papadopoulos, C., Orso, G., Mancuso, G., Herholz, M., Gumeni, S., Tadepalle, N., et al. (2015). Spastin Binds to Lipid Droplets and Affects Lipid Metabolism. *PLOS Genet.* 11, e1005149. doi:10.1371/journal.pgen.1005149.

Park, S. H., Zhu, P.-P., Parker, R. L., and Blackstone, C. (2010). Hereditary spastic paraplegia proteins REEP1, spastin, and atlastin-1 coordinate microtubule interactions with the tubular ER network. *J. Clin. Invest.* 120, 1097–1110. doi:10.1172/JCI40979.

Parodi, L., Fenu, S., Stevanin, G., and Durr, A. (2017). Hereditary spastic paraplegia: More than an upper motor neuron disease. *Rev. Neurol. (Paris).* 5204, 243 YP – 360. doi:http://dx.doi.org/10.1016/j.neurol.2017.03.034.

Pellegrini, M., Bulzomi, P., Galluzzo, P., Lecis, M., Leone, S., Pallottini, V., et al. (2014). Naringenin modulates skeletal muscle differentiation via estrogen receptor $α$ and $β$ signal pathway regulation. *Genes {&} Nutr.* 9, 425. doi:10.1007/s12263-014-0425-3.

Pendin, D., Tosetto, J., Moss, T. J., Andreazza, C., Moro, S., McNew, J. A., et al. (2011). GTP-dependent packing of a three-helix bundle is required for atlastin-mediated fusion. *Proc. Natl. Acad. Sci.* 108, 16283 LP – 16288. doi:10.1073/pnas.1106421108.

Prieto-Domínguez, N., Garcia-Mediavilla, M. V, Sanchez-Campos, S., and Gonzalez-Gallego*, J. L. M. and J. (2018). Autophagy as a Molecular Target of Flavonoids Underlying their Protective Effects in Human Disease. *Curr. Med. Chem.* 25, 814–838. doi:http://dx.doi.org/10.2174/0929867324666170918125155.

Puhka, M., Joensuu, M., Vihinen, H., Belevich, I., and Jokitalo, E. (2012). Progressive sheet-to-tubule transformation is a general mechanism for endoplasmic reticulum partitioning in dividing mammalian cells. *Mol. Biol. Cell* 23, 2424–2432. doi:10.1091/mbc.E10-12-0950.

Puhka, M., Vihinen, H., Joensuu, M., and Jokitalo, E. (2007). Endoplasmic reticulum remains continuous and undergoes sheet-to-tubule transformation during cell division in mammalian cells. *J. Cell Biol.* 179, 895 LP – 909. doi:10.1083/jcb.200705112.

Pulipparacharuvil, S., Akbar, M. A., Ray, S., Sevrioukov, E. A., Haberman, A. S., Rohrer, J., et al. (2005). Drosophila Vps16A is required for trafficking to lysosomes and biogenesis of pigment granules. *J. Cell Sci.* 118, 3663 LP – 3673. doi:10.1242/jcs.02502.

Rehbach, K., Kesavan, J., Hauser, S., Ritzenhofen, S., Jungverdorben, J., Schüle, R., et al. (2019). Multiparametric rapid screening of neuronal process pathology for drug target identification in HSP patient-specific neurons. *Sci. Rep.* 9, 9615. doi:10.1038/s41598-019-45246-4.

Reid, E., Dearlove, A. M., Rhodes, M., and Rubinsztein, D. C. (1999). A New Locus for Autosomal Dominant "Pure" Hereditary Spastic Paraplegia Mapping to Chromosome 12q13, and Evidence for Further Genetic Heterogeneity. *Am. J. Hum. Genet.* 65, 757–763. doi:https://doi.org/10.1086/302555.

Renvoisé, B., Chang, J., Singh, R., Yonekawa, S., FitzGibbon, E. J., Mankodi, A., et al. (2014). Lysosomal abnormalities in hereditary spastic paraplegia types SPG15 and SPG11. *Ann. Clin. Transl. Neurol.* 1, 379–389. doi:10.1002/acn3.64.

Renvoisé, B., Malone, B., Falgairolle, M., Munasinghe, J., Stadler, J., Sibilla, C., et al. (2016). Reep1 null mice reveal a converging role for hereditary spastic paraplegia proteins in lipid droplet regulation. *Hum. Mol. Genet.* 25, 5111–5125. Available at: http://dx.doi.org/10.1093/hmg/ddw315.

Richard, S., Lavie, J., Banneau, G., Voirand, N., Lavandier, K., and Debouverie, M. (2017a). Hereditary spastic paraplegia due to a novel mutation of the REEP1 gene: Case report and literature review. *Medicine (Baltimore).* 96, e5911. doi:10.1097/MD.0000000000005911.

Richard, S., Lavie, J., Banneau, G., Voirand, N., Lavandier, K., and Debouverie, M. (2017b). Hereditary spastic paraplegia due to a novel mutation of the REEP1 gene: Case report and literature review. *Medicine (Baltimore).* 96, e5911. doi:10.1097/MD.0000000000005911.

Rong, X., Liang-liang, F., Hao, H., Ya-qin, C., Wanxia, H., Shuai, G., et al. (2018). Increased Reticulon 3 (RTN3) Leads to Obesity and Hypertriglyceridemia by Interacting With Heat Shock Protein Family A (Hsp70) Member 5 (HSPA5). *Circulation* 138, 1828–1838. doi:10.1161/CIRCULATIONAHA.117.030718.

Rutkowski, D. T., and Kaufman, R. J. (2007). That which does not kill me makes me stronger: adapting to chronic ER stress. *Trends Biochem. Sci.* 32, 469–476. doi:10.1016/J.TIBS.2007.09.003.

Salehi, B., Fokou, P., Sharifi-Rad, M., Zucca, P., Pezzani, R., Martins, N., et al. (2019). The Therapeutic Potential of Naringenin: A Review of Clinical Trials. *Pharmaceuticals* 12, 11. doi:10.3390/ph12010011.

Salinas, S., Carazo-Salas, R. E., Proukakis, C., Schiavo, G., and Warner, T. T. (2007). Spastin and microtubules: Functions in health and disease. *J. Neurosci. Res.* 85, 2778–2782. doi:10.1002/jnr.21238.

Salinas, S., Proukakis, C., Crosby, A., and Warner, T. T. (2008). Hereditary spastic paraplegia: clinical features and pathogenetic mechanisms. *Lancet Neurol.* 7, 1127–1138. doi:https://doi.org/10.1016/S1474-4422(08)70258-8.

Sanderson, C. M., Connell, J. W., Edwards, T. L., Bright, N. A., Duley, S., Thompson, A., et al. (2006). Spastin and atlastin, two proteins mutated in autosomal-dominant hereditary spastic paraplegia, are binding

partners. *Hum. Mol. Genet.* 15, 307–318. doi:10.1093/hmg/ddi447.

Sangpheak, W., Kicuntod, J., Schuster, R., Rungrotmongkol, T., Wolschann, P., Kungwan, N., et al. (2015). Physical properties and biological activities of hesperetin and naringenin in complex with methylated β-cyclodextrin. *Beilstein J. Org. Chem.* 11, 2763–2773. doi:10.3762/bjoc.11.297.

Scheper, W., and Hoozemans, J. J. M. (2015). The unfolded protein response in neurodegenerative diseases: a neuropathological perspective. *Acta Neuropathol.* 130, 315–331. doi:10.1007/s00401-015-1462-8.

Schlang, K. J., Arning, L., Epplen, J. T., and Stemmler, S. (2008). Autosomal dominant hereditary spastic paraplegia: Novel mutations in the REEP1 gene (SPG31). *BMC Med. Genet.* 9, 71. doi:10.1186/1471-2350-9-71.

Schuck, S., Prinz, W. A., Thorn, K. S., Voss, C., and Walter, P. (2009). Membrane expansion alleviates endoplasmic reticulum stress independently of the unfolded protein response. *J. Cell Biol.* 187, 525–536. doi:10.1083/jcb.200907074.

Schwarz, D. S., and Blower, M. D. (2016). The endoplasmic reticulum: structure, function and response to cellular signaling. *Cell. Mol. Life Sci.* 73, 79–94. doi:10.1007/s00018-015-2052-6.

Shibata, Y., Shemesh, T., Prinz, W. A., Palazzo, A. F., Kozlov, M. M., and Rapoport, T. A. (2010). Mechanisms determining the morphology of the peripheral ER. *Cell* 143, 774–788. doi:10.1016/j.cell.2010.11.007.

Shpilka, T., Welter, E., Borovsky, N., Amar, N., Mari, M., Reggiori, F., et al. (2015). Lipid droplets and their component triglycerides and steryl esters regulate autophagosome biogenesis. *EMBO J.* 34, 2117–2131. doi:doi:10.15252/embj.201490315.

Shulman, M., Cohen, M., Soto-Gutierrez, A., Yagi, H., Wang, H., Goldwasser, J., et al. (2011). Enhancement of Naringenin Bioavailability by Complexation with Hydroxypropoyl-$β$-Cyclodextrin. *PLoS One* 6, e18033. doi:10.1371/journal.pone.0018033.

Singh, R., Kaushik, S., Wang, Y., Xiang, Y., Novak, I., Komatsu, M., et al. (2009). Autophagy regulates lipid metabolism. *Nature* 458, 1131–1135. doi:10.1038/nature07976.

Solowska, J. M., and Baas, P. W. (2015). Hereditary spastic paraplegia SPG4: what is known and not known about the disease. *Brain* 138, 2471–2484. doi:10.1093/brain/awv178.

Solowska, J. M., D'Rozario, M., Jean, D. C., Davidson, M. W., Marenda, D. R., and Baas, P. W. (2014a). Pathogenic Mutation of Spastin Has Gain-of-Function Effects on Microtubule Dynamics. *J. Neurosci.* 34, 1856–1867. doi:10.1523/JNEUROSCI.3309-13.2014.

Solowska, J. M., D'Rozario, M., Jean, D. C., Davidson, M. W., Marenda, D. R., and Baas, P. W. (2014b). Pathogenic Mutation of Spastin Has Gain-of-Function Effects on Microtubule Dynamics. *J. Neurosci.* 34, 1856 LP – 1867. doi:10.1523/JNEUROSCI.3309-13.2014.

Song, H. M., Park, G. H., Eo, H. J., and Jeong, J. B. (2016). Naringenin-Mediated ATF3 Expression Contributes to Apoptosis in Human Colon Cancer. *Biomol. {&} Ther.* 24, 140–146. doi:10.4062/biomolther.2015.109.

Speciale, A., Chirafisi, J., Saija, A., and Cimino, F. (2011). Nutritional antioxidants and adaptive cell responses: an update. *Curr. Mol. Med.* 11, 770–789. Available at: http://www.ncbi.nlm.nih.gov/pubmed/21999148.

Staats, S., Lüersen, K., Wagner, A. E., and Rimbach, G. (2018). *Drosophila melanogaster* as a Versatile Model Organism in Food and Nutrition Research. *J. Agric. Food Chem.* doi:10.1021/acs.jafc.7b05900.

Summerville, J. B., Faust, J. F., Fan, E., Pendin, D., Daga, A., Formella, J., et al. (2016). The effects of ER morphology on synaptic structure and function in Drosophila melanogaster. *J. Cell Sci.* 129, 1635–48. doi:10.1242/jcs.184929.

Suzuki, M., Shinohara, Y., Ohsaki, Y., and Fujimoto, T. (2011). Lipid droplets: size matters. *J. Electron Microsc. (Tokyo).* 60 Suppl 1, S101-16. doi:10.1093/jmicro/dfr016.

Tan, J. S. Y., Seow, C. J. P., Goh, V. J., and Silver, D. L. (2014). Recent Advances in Understanding Proteins Involved in Lipid Droplet Formation, Growth and Fusion. *J. Genet. Genomics* 41, 251–259. doi:10.1016/j.jgg.2014.03.003.

Tang, J.-Y., Jin, P., He, Q., Lu, L.-H., Ma, J.-P., Gao, W.-L., et al. (2017). Naringenin ameliorates hypoxia/reoxygenation-induced endoplasmic reticulum stress-mediated apoptosis in H9c2 myocardial cells: involvement in ATF6, IRE1$α$ and PERK signaling activation. *Mol. Cell. Biochem.* 424, 111–122. doi:10.1007/s11010-016-2848-1.

Terasaki, M., Shemesh, T., Kasthuri, N., Klemm, R. W., Schalek, R., Hayworth, K. J., et al. (2013). Stacked Endoplasmic Reticulum Sheets Are Connected by Helicoidal Membrane Motifs. *Cell* 154, 285–296. doi:https://doi.org/10.1016/j.cell.2013.06.031.

Tolley, N., Sparkes, I., Craddock, C. P., Eastmond, P. J., Runions, J., Hawes, C., et al. (2010). Transmembrane domain length is responsible for the ability of a plant reticulon to shape endoplasmic reticulum tubules in vivo. *Plant J.* 64, 411–418. doi:doi:10.1111/j.1365-313X.2010.04337.x.

Trotta, N., Orso, G., Rossetto, M. G., Daga, A., and Broadie, K. (2004). The Hereditary Spastic Paraplegia Gene, spastin, Regulates Microtubule Stability to Modulate Synaptic Structure and Function. *Curr. Biol.* 14, 1135–1147. doi:https://doi.org/10.1016/j.cub.2004.06.058.

Tsakiri, E. N., Gumeni, S., Iliaki, K. K., Benaki, D., Vougas, K., Sykiotis, G. P., et al. (2018). Hyperactivation of Nrf2 increases stress tolerance at the cost of aging acceleration due to metabolic deregulation. *Aging Cell* 18, e12845. doi:10.1111/acel.12845.

Ugur, B., Chen, K., and Bellen, H. J. (2016). Drosophila tools and assays for the study of human diseases. *Dis. Model. Mech.* 9, 235–244. doi:10.1242/DMM.023762.

Varga, R.-E., Khundadze, M., Damme, M., Nietzsche, S., Hoffmann, B., Stauber, T., et al. (2015). In Vivo Evidence for Lysosome Depletion and Impaired Autophagic Clearance in Hereditary Spastic Paraplegia Type SPG11. *PLoS Genet.* 11, e1005454–e1005454. doi:10.1371/journal.pgen.1005454.

Velázquez, A. P., Tatsuta, T., Ghillebert, R., Drescher, I., and Graef, M. (2016a). Lipid droplet-mediated ER homeostasis regulates autophagy and cell survival during starvation. *J. Cell Biol.* 212, 621–31.

doi:10.1083/jcb.201508102.

Velázquez, A. P., Tatsuta, T., Ghillebert, R., Drescher, I., and Graef, M. (2016b). Lipid droplet–mediated ER homeostasis regulates autophagy and cell survival during starvation. *J. Cell Biol.* 212, 621–631. doi:10.1083/jcb.201508102.

Vevea, J. D., Garcia, E. J., Chan, R. B., Zhou, B., Schultz, M., Di Paolo, G., et al. (2015). Role for Lipid Droplet Biogenesis and Microlipophagy in Adaptation to Lipid Imbalance in Yeast. *Dev. Cell* 35, 584–599. doi:10.1016/j.devcel.2015.11.010.

Voeltz, G. K., Rolls, M. M., and Rapoport, T. A. (2002). Structural organization of the endoplasmic reticulum. *EMBO Rep.* 3, 944–950. doi:10.1093/embo-reports/kvf202.

Volmer, R., van der Ploeg, K., and Ron, D. (2013). Membrane lipid saturation activates endoplasmic reticulum unfolded protein response transducers through their transmembrane domains. *Proc. Natl. Acad. Sci. U. S. A.* 110, 4628–4633. doi:10.1073/pnas.1217611110.

Walther, T. C., and Farese Jr, R. V (2012). Lipid droplets and cellular lipid metabolism. *Annu. Rev. Biochem.* 81, 687–714. doi:10.1146/annurev-biochem-061009-102430.

Wang, C.-W. (2016). Lipid droplets, lipophagy, and beyond. *Biochim. Biophys. Acta - Mol. Cell Biol. Lipids* 1861, 793–805. doi:10.1016/J.BBALIP.2015.12.010.

Wang, G.-Q., Zhang, B., He, X.-M., Li, D.-D., Shi, J.-S., and Zhang, F. (2019). Naringenin targets on astroglial Nrf2 to support dopaminergic neurons. *Pharmacol. Res.* 139, 452–459. doi:10.1016/j.phrs.2018.11.043.

Ward, C., Martinez-Lopez, N., Otten, E. G., Carroll, B., Maetzel, D., Singh, R., et al. (2016). Autophagy, lipophagy and lysosomal lipid storage disorders. *Biochim. Biophys. Acta - Mol. Cell Biol. Lipids* 1861, 269–284. doi:https://doi.org/10.1016/j.bbalip.2016.01.006.

Wilfling, F., Thiam, A. R., Olarte, M.-J., Wang, J., Beck, R., Gould, T. J., et al. (2014). Arf1/COPI machinery acts directly on lipid droplets and enables their connection to the ER for protein targeting. *Elife* 3, e01607–e01607. doi:10.7554/eLife.01607.

Xu, D., Li, Y., Wu, L., Li, Y., Zhao, D., Yu, J., et al. (2018). Rab18 promotes lipid droplet (LD) growth by tethering the ER to LDs through SNARE and NRZ interactions. *J. Cell Biol.* 217, 975 LP – 995. doi:10.1083/jcb.201704184.

Yalçın, B., Zhao, L., Stofanko, M., O'Sullivan, N. C., Kang, Z. H., Roost, A., et al. (2017). Modeling of axonal endoplasmic reticulum network by spastic paraplegia proteins. *Elife* 6, e23882. doi:10.7554/eLife.23882.

Yamamoto, K., Sato, T., Matsui, T., Sato, M., Okada, T., Yoshida, H., et al. (2017). Transcriptional Induction of Mammalian ER Quality Control Proteins Is Mediated by Single or Combined Action of ATF6α and XBP1. *Dev. Cell* 13, 365–376. doi:10.1016/j.devcel.2007.07.018.

Yamanaka, T., and Nukina, N. (2018). ER Dynamics and Derangement in Neurological Diseases. *Front. Neurosci.* 12, 91. doi:10.3389/fnins.2018.00091.

Yang, L.-J., Ma, S.-X., Zhou, S.-Y., Chen, W., Yuan, M.-W., Yin, Y.-Q., et al. (2013). Preparation and characterization of inclusion complexes of naringenin with β-cyclodextrin or its derivative. *Carbohydr. Polym.* 98, 861–869. doi:10.1016/J.CARBPOL.2013.07.010.

Yoshida, H., Matsui, T., Yamamoto, A., Okada, T., and Mori, K. (2001). XBP1 mRNA Is Induced by ATF6 and Spliced by IRE1 in Response to ER Stress to Produce a Highly Active Transcription Factor. *Cell* 107, 881–891. doi:10.1016/S0092-8674(01)00611-0.

Zheng, P., Chen, Q., Tian, X., Qian, N., Chai, P., Liu, B., et al. (2018). DNA damage triggers tubular endoplasmic reticulum extension to promote apoptosis by facilitating ER-mitochondria signaling. *Cell Res.* 28, 833–854. doi:10.1038/s41422-018-0065-z.

Zheng, P., Xie, Z., Yuan, Y., Sui, W., Wang, C., Gao, X., et al. (2017). Plin5 alleviates myocardial ischaemia/reperfusion injury by reducing oxidative stress through inhibiting the lipolysis of lipid droplets. *Sci. Rep.* 7, 42574. doi:10.1038/srep42574.

Zirin, J., and Perrimon, N. (2010). Drosophila as a model system to study autophagy. *Semin. Immunopathol.* 32, 363–372. doi:10.1007/s00281-010-0223-y.

Züchner, S., Wang, G., Tran-Viet, K.-N., Nance, M. A., Gaskell, P. C., Vance, J. M., et al. (2006). Mutations in the Novel Mitochondrial Protein REEP1 Cause Hereditary Spastic Paraplegia Type 31. *Am. J. Hum. Genet.* 79, 365–369. Available at: http://www.ncbi.nlm.nih.gov/pmc/articles/PMC1559498/.

Zurek, N., Sparks, L., and Voeltz, G. (2011). Reticulon short hairpin transmembrane domains are used to shape ER tubules. *Traffic* 12, 28–41. doi:10.1111/j.1600-0854.2010.01134.x.

Zygmunt, K., Faubert, B., MacNeil, J., and Tsiani, E. (2010). Naringenin, a citrus flavonoid, increases muscle cell glucose uptake via AMPK. *Biochem. Biophys. Res. Commun.* 398, 178–183. doi:10.1016/j.bbrc.2010.06.048.